AD-A171 522 DEVELOPMENT OF AN ATMOSPHERIC DISPERSION MODEL FOR HEAVIER-THAN-AIR GAS M (U) ARKANSAS UNIV FAYETTEVILLE DEPT OF CHEMICAL ENGINEERING J A HAVENS ET AL MAY 85 1/2

UNCLASSIFIED USCG-D-22-85 DTCG23-80-C-20029 F/G 20/4 NL

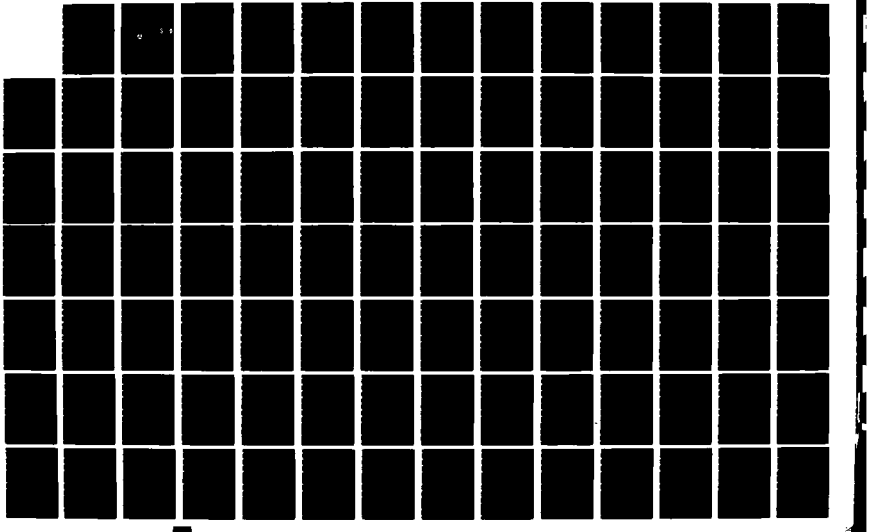

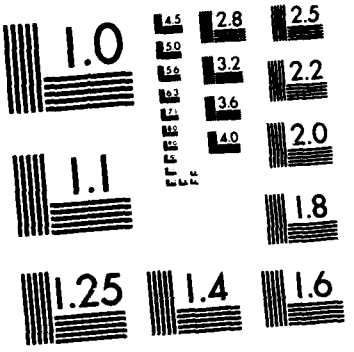

(2)

Report No. CG-D-22-85

AD-A171 522

DEVELOPMENT OF AN ATMOSPHERIC DISPERSION MODEL FOR HEAVIER-THAN-AIR GAS MIXTURES

Volume I

JERRY A. HAVENS

THOMAS O. SPICER

FINAL REPORT
MAY 1985

Prepared for:

U.S. Department of Transportation
United States Coast Guard

Office of Research and Development
Washington, D.C. 20593

NOTICE

This document is disseminated under the sponsorship of the Department of Transportation in the interest of information exchange. The United States Government assumes no liability for its contents or use thereof.

The contents of this report do not necessarily reflect the official view or policy of the Coast Guard; and they do not constitute a standard, specification, or regulation.

This report, or portions thereof may not be used for advertising or sales promotion purposes. Citation of trade names and manufacturers does not constitute endorsement or approval of such products.

Technical Report Documentation Page

1. Report No.	2. Government Accession No.	3. Recipient's Catalog No.
CG-D-22-85	AD A171522	

4. Title and Subtitle	5. Report Date
DEVELOPMENT OF AN ATMOSPHERIC DISPERSION MODEL FOR HEAVIER-THAN-AIR GAS MIXTURES	May 1985
	6. Performing Organization Code
7. Author(s) Jerry A. Havens and Thomas O. Spicer	8. Performing Organization Report No. Final Report
9. Performing Organization Name and Address Chemical Engineering Department University of Arkansas Fayetteville, Arkansas 72701	10. Work Unit No. (TRAIS)
	11. Contract or Grant No. DT-CG-23-80-C-20029
12. Sponsoring Agency Name and Address U.S. Coast Guard Commandant (G-FCP-22F/TP64) 2100 Second Street, SW Washington DC 20593	13. Type of Report and Period Covered Final Report Sept. 1980-May 1985
	14. Sponsoring Agency Code

15. Supplementary Notes
Final Report is in three volumes. Volumes II, "Laboratory Calm Air Heavy Gas Dispersion Experiments", and III, "DEGADIS Computer Program and Flow Chart", are bound separately.

16. Abstract

The mathematical modeling techniques ~~which have been~~ used to predict atmospheric dispersion of heavy gases are reviewed and critiqued. These dispersion processes are characterized by three ~~regimes or~~ phases: (1) near-field, negative buoyancy-dominated flow regime; (2) intermediate-field, stably stratified shear flow regime; and (3) far-field, passive turbulent diffusion regime.

Mathematical models of laboratory and natural gravity currents are used to describe the negative buoyancy-dominated regime flow and dilution processes. A laboratory investigation of instantaneous heavy gas releases in calm air demonstrates scaling from small release volumes (0.5 m^3) to large field (2000 m^3) field releases, and is used to develop a mathematical model for the buoyancy-dominated regime. Laboratory data from stratified shear flow mixing experiments are used to develop a model for vertical diffusion of heavy gases in the atmospheric surface layer. The model concepts are consistent with the limiting passive behavior of demonstrated air pollution models. An interactive computer model for heavy gas dispersion (DEGADIS) is developed. The DEGADIS model accounts for the three regimes of heavy gas dispersion processes and can be used to simulate instantaneous, steady state, and transient releases. The model provides predictions of downwind concentration decay which are in good agreement with the full range of field experimental data currently available, and is recommended for incorporation in the Coast Guard Hazard Assessment Computer System (HACS).

17. Key Words		18. Distribution Statement
Heavy Gas Dispersion	Gravity-Spreading Flows	
Turbulent Mixing	Density Currents	
Atmospheric Dispersion	Dispersion Models	
Buoyancy-Driven Flows	Risk Assessment	
Stratified Flows		

19. Security Classif. (of this report)	20. Security Classif. (of this page)	21. No. of Pages	22. Price
		184	

Form DOT F 1700.7 (8-72) Reproduction of completed page authorized

METRIC CONVERSION FACTORS

Approximate Conversions to Metric Measures

Symbol	When You Know	Multiply by	To Find	Symbol
	LENGTH			
in	inches	*2.5	centimeters	cm
ft	feet	30	centimeters	cm
yd	yards	0.9	meters	m
mi	miles	1.6	kilometers	km
	AREA			
in^2	square inches	6.5	square centimeters	cm^2
ft^2	square feet	0.09	square meters	m^2
yd^2	square yards	0.8	square meters	m^2
mi^2	square miles	2.6	square kilometers	km^2
	acres	0.4	hectares	ha
	MASS (weight)			
oz	ounces	28	grams	g
lb	pounds	0.45	kilograms	kg
	short tons (2000 lb)	0.9	tonnes	t
	VOLUME			
tsp	teaspoons	5	milliliters	ml
tbsp	tablespoons	15	milliliters	ml
fl oz	fluid ounces	30	milliliters	ml
c	cups	0.24	liters	l
pt	pints	0.47	liters	l
qt	quarts	0.95	liters	l
gal	gallons	3.8	liters	l
ft^3	cubic feet	0.03	cubic meters	m^3
yd^3	cubic yards	0.76	cubic meters	m^3
	TEMPERATURE (exact)			
°F	Fahrenheit temperature	5/9 (after subtracting 32)	Celsius temperature	°C

*1 in = 2.54 (exactly). For other exact conversions and more detailed tables, see NBS Misc. Publ. 286, Units of Weights and Measures, Price $2.25, SD Catalog No. C13.10:286.

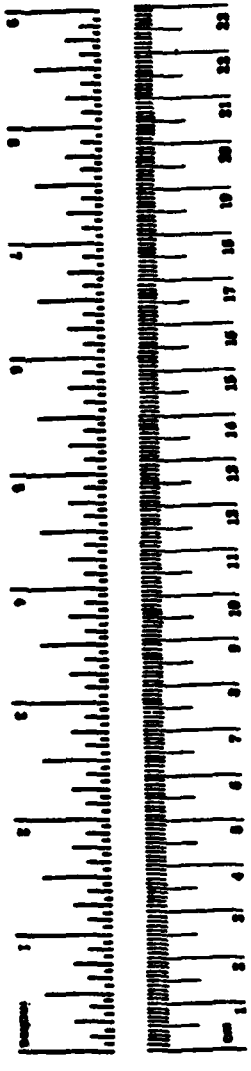

Approximate Conversions from Metric Measures

Symbol	When You Know	Multiply by	To Find	Symbol
	LENGTH			
mm	millimeters	0.04	inches	in
cm	centimeters	0.4	inches	in
m	meters	3.3	feet	ft
m	meters	1.1	yards	yd
km	kilometers	0.6	miles	mi
	AREA			
cm^2	square centimeters	0.16	square inches	in^2
m^2	square meters	1.2	square yards	yd^2
km^2	square kilometers	0.4	square miles	mi^2
ha	hectares (10,000 m^2)	2.5	acres	
	MASS (weight)			
g	grams	0.035	ounces	oz
kg	kilograms	2.2	pounds	lb
t	tonnes (1000 kg)	1.1	short tons	
	VOLUME			
ml	milliliters	0.03	fluid ounces	fl oz
l	liters	2.1	pints	pt
l	liters	1.06	quarts	qt
l	liters	0.26	gallons	gal
m^3	cubic meters	35	cubic feet	ft^3
m^3	cubic meters	1.3	cubic yards	yd^3
	TEMPERATURE (exact)			
°C	Celsius temperature	9/5 (then add 32)	Fahrenheit temperature	°F

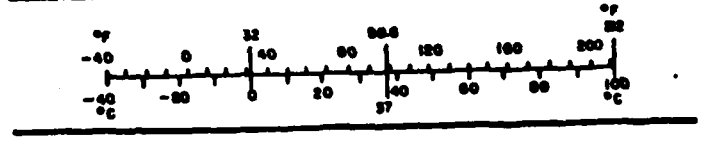

ACKNOWLEDGEMENTS

This work was sponsored by the U.S. Coast Guard Office of Research and Development with major contribution by the Gas Research Institute.

The authors gratefully acknowledge the guidance and assistance of the U.S. Coast Guard Technical Monitors: LCDR Michael Flessner, LT Guy Collona, and LCDR Peter Tebeau. Dr. Kiran Kothari of the Gas Research Institute also reviewed the draft final report and made especially helpful recommendations.

Many persons and organizations have provided data for our analysis; we especially thank

Dr. Donald Ermak and Dr. Ron Koopman--Lawrence Livermore National Laboratory

Drs. Gert Colenbrander, Jonathan Puttock, David Blackmore, and John Rosenfeld--Shell Research Company

Dr. James McQuaid--British Health and Safety Executive

Dr. Rex Britter--Cambridge University

Drs. Robert Boyle and Derek Thomas--National Maritime Institute, UK

Dr. Reed Welker--University of Arkansas

Dr. John Woodward--Exxon Company.

We were assisted in the experimental work on calm-air heavy gas releases by graduate (and former) students in the Department of Chemical Engineering: Dr. Karl Schubert, Mr. Brace Boyden, and Ms. Robin Fites. Mr. Don Bell of the University Research and Special Equipment Shop constructed much of the experimental apparatus, and Research Assistants Don Ward and Marvin Leister constructed a major part of the computer data acquisition system and conducted a number of the experiments.

We especially thank Vicki Asfahl for her professional assistance in preparing this report.

TABLE OF CONTENTS

TABLE OF CONTENTS (continued)

LIST OF FIGURES

LIST OF FIGURES (continued)

LIST OF FIGURES (continued)

LIST OF FIGURES (continued)

LIST OF FIGURES (continued)

LIST OF TABLES

LIST OF SYMBOLS

A_F	frontal area of cloud for air entrainment (m^2)
A_T	top area of cloud for air entrainment (m^2)
a_v	empirical constant (1.0) in Equations II-61 and III-4
B_{EFF}	effective width of gas plume (m)
B_i'	local half width of source seen by observer i (m)
b	half width of horizontally homogeneous central section of gas plume (m)
b_v	empirical constant (1.2) in Equations II-62 and III-6
C_E	constant in density intrusion (spreading) relation
C_p	heat capacity (J/kg K)
C_{p_a}	heat capacity of air (J/kg K)
C_{p_c}	heat capacity of contaminant (J/kg K)
C_{p_w}	heat capacity of water (liquid phase) (J/kg K)
c	concentration (kg/m^3)
c_c	centerline, ground level concentration (kg/m^3)
$c_{c,L}$	vertically averaged layer concentration (kg/m^3)
c_f	friction coefficient
c_1	constant in Equation II-6
c_2	constant in Equation II-7
c_3	constant in Equation II-8
c_4	constant in Equation II-19
c_5	constant in Equation II-19

c_6	constant in Equation II-27
c_c'	centerline, ground level concentration corrected for x-direction dispersion (kg/m^3)
c_1'	constant in Equation II-41
c_2'	constant in Equation II-41
c_*	constant in Equation II-3
D	source diameter (m)
D_h	added enthalpy (J/kg)
$\mathcal{D}$	diffusivity (m^2/s)
d_v	empirical constant (0.64) in Equations II-46 and III-2
E	plume strength (kg/s)
E(t)	source rate (kg/s)
e_v	empirical constant (20) in Equations II-49 and III-3
F	overall mass transfer coefficient (kg/m^2 s)
F_f	mass transfer coefficient due to forced convection (kg/m^2 s)
F_n	mass transfer coefficient due to natural convection (kg/m^2 s)
F_0	buoyancy flux (m^2/s^3)
Fr	Froude number
Gr	Grashoff number
g	acceleration of gravity (m/s^2)
H	height or depth of density intrusion or cloud (m)
$(H/D)_i$	initial height-to-diameter (aspect) ratio
H_a	ambient absolute humidity (kg water/kg bone dry air)

H_{EFF} effective cloud depth (m)

H_h height of head in density-driven flow (m)

H_L total layer depth (m)

H_r hydraulic radius (m)

H_{sat} saturated humidity at the mixture temperature and pressure (kg water/kg bone dry air)

Hum(T) minimum of the ambient air humidity and the saturated air humidity at the mixture temperature (kg water/kg bone dry air)

H_t height of tail in density-driven flow (m)

H^* nondimensional height, $H/V^{1/3}$

H_1 average depth of gravity current head (m)

H_4 depth of inward internal flow in a gravity current head (m)

h enthalpy of source blanket (J/kg)

h_a enthalpy of ambient humid air (J/kg)

h_{AM} enthalpy of a given mixture assuming adiabatic mixing (J/kg)

h_E enthalpy associated with primary source mass rate (J/kg)

h_f heat transfer coefficient due to forced convection (J/m^2 s K)

h_L enthalpy of vertically averaged layer (J/kg)

h_n heat transfer coefficient due to natural convection (J/m^2 s K)

h_0 overall heat transfer coefficient (J/m^2 s K)

h_w	enthalpy associated with mass flux of water from surface (J/kg)
IE	energy converted to internal energy
K_c	vertical turbulent diffusivity, mass (m^2/s)
K_H	vertical turbulent diffusivity, heat (m^2/s)
K_M	vertical turbulent diffusivity, momentum (m^2/s)
K_0	constant in Equations II-72 and III-75 ($m^{1-\gamma_1}$)
K_y	horizontal turbulent diffusivity (m^2/s)
K_z	vertical turbulent diffusivity (m^2/s)
KE	kinetic energy (N m)
k	von Karman's constant, 0.35
k_1	constant in Equation II-47
k_2	constant in Equation II-48
L	source length (m), or turbulence length scale (m)
ℓ	characteristic length $V_i^{1/3}$
M	total cloud mass (kg)
M_a	total mass of air in the cloud (kg)
M_c	total mass of contaminant in the cloud (kg)
M_i	initial cloud mass (kg)
MW	molecular weight
$\dot{M}_a$	mass rate of air entrainment into the cloud (kg/s)
$\dot{M}_{w,s}$	mass rate of water transfer to the cloud from the water surface under the source (kg/s)
N	number of observers

Nu	Nusselt number
PE	potential energy (N m)
Pr	Prandtl number
p	atmospheric pressure (atm)
p_1	empirical constant in Table A.1
p_w^*	vapor pressure of water (atm)
P	cloud momentum (kg m/s)
P_h	momentum of head in density-driven flow (kg m/s)
P_t	momentum of tail in density-driven flow (kg m/s)
P_v	virtual momentum due to acceleration reaction (kg m/s)
Q	volumetric release rate (m^3/s)
Q_E	source mass flux (kg/m^2 s)
Q_e	volumetric entrainment flux (m/s)
Q_1	flux of ambient fluid into front of gravity current head (m/s)
$\dot{Q}_s$	rate of heat transfer from the surface (J/s)
Q_*	atmospheric takeup flux (kg/m^2 s)
Q_{*max}	maximum atmospheric takeup flux of contaminant (kg/m^2 s)
q_s	surface heat flux (J/m^2 s)
q_0	vertical heat flux (J/m^2 s)
q_1	empirical constant in Table A.1
R	gas source cloud radius (m)
R_h	inner radius of head in density-driven flow (m)
R_m	value of R when ($\pi R^2 Q_*$) is a maximum (m)
R_{max}	maximum radius of the cloud (m)

R_p	primary source radius (m)
R^*	nondimensionalized radius (R/ℓ)
Ri_T	Richardson number associated with temperature differences, Equation III-66
Ri_0^c, Ri_0^I	Continuous and instantaneous release Richardson numbers respectively
Ri"	Richardson number associated with density differences corrected for horizontal turbulence velocity
Ri_*'	Richardsnn number associated with density differences corrected for convective scale velocity
Ri_*	Richardson number associated with density differences, Equation III-56
Sc	Schmidt number
Sh	Sherwood number
St_H	Stanton number for heat transfer
St_M	Stanton number for mass transfer
S_y	horizontal concentration scaling parameter (m)
S_z	vertical concentration scaling parameter (m)
S_{z0}	S_z at the downwind edge of the source ($x = L/2$) (m)
S_{z0_m}	value of S_{z0} when ($\pi R^2 Q_*$) is a maximum (m)
T	temperature associated with source blanket enthalpy (K)
$T_{c,L}$	temperature associated with averaged enthalpy (K)
T_s	surface temperature (K)
TE	turbulent kinetic energy (N m)
T_0	contaminant storage temperature (K)
t	time (s)

t_f characteristic time of cloud formation (s)

t_s specified time (s)

t_t cloud travel time to the maximum distance exposed to a given concentration (s)

t_{dn_i} time when observer i encounters downwind edge (s)

t_{up_i} time when observer i encounters upwind edge (s)

t^* nondimensional time t/θ

u_a ambient average velocity (m/s)

u_e horizontal or frontal entrainment velocity (m/s)

u_{EFF} effective cloud advection velocity (m/s)

u_f cloud front velocity (m/s)

u_i velocity of observer i (m/s)

u_j local velocity in j direction (m/s)

u_L average transport velocity associated with H_L (m/s)

u_x wind velocity, along x-direction (m/s)

u_0 wind velocity measured at $z = z_0$ (m/s)

u_1 horizontal r.m.s. turbulence velocity (m/s)

u_3 internal flow out of gravity current head (m/s)

u_4 internal flow into gravity current head (m/s)

u_{10} wind velocity at z = 10 m (m/s)

u_* friction velocity (m/s)

$\bar{u}$ characteristic average velocity (m/s)

V cloud volume (m^3)

V_H heat transfer velocity (0.0125 m/s) in Equation III-16 (m/s)

V_i	initial volume (m^3)
$\overline{V}_a$	specific volume of air (m^3/kg)
$\overline{V}_c$	specific volume of contaminant (m^3/kg)
$\overline{V}_{w,vapor}$	specific volume of water vapor (m^3/kg)
W	gas plume width (m)
W_0	rectangular source width (m)
w_a	mass fraction of air
w_c	mass fraction of contaminant
w_e	vertical entrainment velocity associated with H_L (m/s)
w_t	total entrainment velocity in Equation II-31 (m/s)
w_*	convective scale velocity (m/s)
w_e'	entrainment velocity associated with H_{EFF} (m/s)
$x_i(t)$	x position of observer i at time t (m)
x_{pi}	position of puff center due to observer i (m)
x_t	downwind distance where gravity spreading terminates (m)
x_v	virtual point source distance (m)
x_{dn_i}	x position of downwind edge of source for observer i
x_{up_i}	x position of upwind edge of source for observer i
x,y,z	Cartesian coordinates (m)
x_0	downwind edge of the gas source (m)
$\overline{y}$	average cloud mole fraction
z_R	surface roughness (m)
z_0	reference height in wind velocity profile specification (m)

α	constant in power law wind profile
β	constant in σ_y correlation in Equation III-75
β_1	constant in Equation II-37
β'	coefficient of expansion (K^{-1})
θ	characteristic time scale, $V_i^{1/6} / \sqrt{g \Delta_i'}$
Γ	gamma function
γ	ratio of $(\rho - \rho_a) / c_c$
γ_1	constant in Equation III-75
Δ	ratio of $(\rho - \rho_a)/\rho$
ΔT	temperature driving force (K) $(T_s - T_{c,L})$ or $(T_s - T)$
Δ'	ratio of $(\rho - \rho_a) / \rho_a$
Δ_i'	initial ratio of $(\rho - \rho_a) / \rho_a$
δ	constant in σ_y correlation in Equation III-75
δ_L	empirical constant (2.15) in Equation III-31
δ_v	constant (0.20) in Equation II-59
ε	frontal entrainment coefficient in Equation III-11
ζ	collection of terms defined by Equation III-40 $(m^{-1/(1+\alpha)})$
λ	Monin-Obukhov length (m)
λ_{fus}	latent heat of fusion for water in Equation A-4 (J/kg)
λ_{vap}	latent heat of vaporization for water in Equation A-4 (J/kg)
λ'	modified latent heat for water in Equation A-4 (J/kg)
μ	viscosity (kg/m s)
ρ	density of gas-air mixture (kg/m^3)

ρ_a	ambient density (kg/m^3)
ρ_c	cloud density (kg/m^3)
ρ_i	initial cloud density (kg/m^3)
ρ_L	vertically averaged layer density (kg/m^3)
ρ_0	density of contaminant's saturated vapor at T_o (kg/m^3)
σ_x	x-direction dispersion coefficient (m)
σ_y	Pasquill-Gifford lateral dispersion coefficient (m)
σ_z	z-direction dispersion coefficient (m)
τ_0	surface shear stress (N/m^2)
τ_δ	shear stress at the cloud top (N/m^2)
η	constant of Equation II-5
ϕ	function describing influence of stable density stratification on vertical diffusion, Equation III-54
$\hat{\phi}$	integrated source entrainment function
ψ	logarithmic velocity profile correction function

SUMMARY

The mathematical modeling methods which have been proposed for prediction of dispersion of heavier-than-air gases are reviewed and critiqued. The phenomenology of atmospheric dispersion of heavy gas is described, and a simplified representation of the general heavy gas dispersion scenario is proposed which involves three distinct flow regimes:

--Buoyancy-dominated dispersion (near field)

--Stably stratified shear flow (intermediate field)

--Passive turbulent dispersion (far field)

Modeling concepts based on investigations of laboratory gravity currents are used to describe the flow and dilution processes that characterize the buoyancy-dominated dispersion regime. Measurements of the spreading and dilution of heavy gas volumes released suddenly in calm (laboratory) air are used to demonstrate scaling methods for small releases from 35 to 530 liters, and the laboratory results when scaled to 2000 m^3 volume are consistent with the experimental data from the Thorney Island 2000 m^3 Heavy Gas Trials. A box model is used to describe the laboratory releases, and the gravity spreading and air entrainment velocities are determined from analysis of the laboratory experimental data.

Data from laboratory-stratified shear flow mixing experiments have been used to model the vertical diffusion of heavy gases in the atmospheric constant stress layer. The modeling concepts used in the Shell HEGADAS (HEavy GAs Dispersion from Area Sources) model have been adapted to model the stably stratified shear flow and passive turbulent diffusion regimes. Several important modifications to the HEGADAS model have been made, including provision for heat transfer and convective turbulence, incorporation of additional laboratory-stratified layer mixing data in the vertical entrainment

velocity correlation, and improvements in the method used for modeling the rate of heavy gas entrainment (from the source) by the atmospheric flow. The provision for air entrainment into the gravity spreading gas blanket which may form over some releases, as well as heat exchange between the blanket and the earth surface, extend the applicability of the model to a much wider class of heavy gas release scenarios.

The interactive computer model DEGADIS (DEnse GAs DISpersion), which is proposed for incorporation in the Coast Guard Hazard Assessment Computer System (HACS), has been used to simulate thirty-nine experiments which represent the full range of heavy gas field experiment data presently available. DEGADIS-predicted maximum concentration as a function of distance is compared to the maximum reported concentration for field scale releases of liquefied natural gas (LNG), liquefied petroleum gas (LPG), and Freon-12/air mixtures from the Burro/Coyote, Maplin Sands, and Thorney Island trials. Based upon this comparison, the variability of the distance realized to a concentration level of 5, 2-1/2, or 1% for a given release is quantified based on the predicted distance. The model predicts downwind maximum gas concentration decay with distance, to the hydrocarbon flammable range, consistent with the full range of experimental data. The consistency of the model predictions, which reflect small scale laboratory fluid flow and mixing data, with the results of the wide range of field experimental releases justifies the application of the model to prediction of dispersion from much larger releases.

The DEGADIS model can readily be modified to incorporate better mixing and heat transfer sub-models. It is likely that improvements in these two areas can be expected to provide the most important information for improving the confidence level in heavy gas dispersion prediction. The model has not been demonstrated for application to the prediction of dispersion to the ppm concentration range which characterizes the limits of toxic gas hazard. However,

the model has been developed to be consistent with the existing data base on passive turbulent dispersion in the far field, and it is recommended that the model be evaluated against experimental data which have become available for dispersion of ammonia and nitrogen tetroxide.

I. INTRODUCTION

Risk of accidental release of heavier-than-air gases accompanies many manufacturing, storage, and transportation operations. Although increased awareness of such risks has been fostered by debate on the risks of bulk transport of large quantities of flammable liquid gases (General Accounting Office, 1978; National Research Council, 1980; Office of Technology Assessment, 1980), which in general are considered to be heavier-than-air gases (HTAG), many other chemicals handled and carried in bulk can produce a gas or aerosol "cloud" that is more dense than air when released into the atmosphere (Kaiser and Walker, 1978; Harris, 1978).

Assessment of risk attending such operations involves, in addition to estimation of the probability of release, prediction of the ensuing atmospheric dispersion, since such dispersion eventually results in dilution of the gas with air to concentrations which are nonflammable or within prescribed toxicity limits. Consequently, a prediction of the location of the "boundary" of such clouds (which may be defined as containing gas concentrations above a prescribed lower limit) as a function of time is required for rational risk assessment.

Dispersion of HTAG in the atmosphere differs importantly from the process of dispersion of trace contaminants in the atmosphere. The theory underlying prediction of atmospheric dispersion of trace contaminants (pollutant dispersion) generally assumes that the dispersion is the result of the turbulent motion that characterizes the atmospheric boundary layer. The presence of the pollutant is consequently assumed not to affect the atmospheric flow patterns; then, the problem becomes one of understanding and predicting the atmospheric boundary layer turbulence. Although the characterization of atmospheric flow suffers from the general limits of understanding

turbulent fluid motion, there exists a fairly well developed theoretical basis for prediction of the dispersion of trace contaminants in the atmosphere, along with extensive supporting experimental data derived from atmospheric flow measurements (Pasquill, 1983).

In contrast, the release of large quantities of HTAG into the atmosphere may alter the fluid flow pattern in the atmosphere in the vicinity of the release. For some releases, the gravity-induced flow and the resulting interaction with the atmospheric flow can determine the shape and extent of the area which is exposed to flammable or toxic gas concentrations. The early phases of cloud formation, motion, and dispersion following release of HTAG may involve density-stratified flows which, although studied widely in other contexts, have been studied from the perspective of atmospheric dispersion of HTAG only recently (Turner, 1973).

A number of mathematical modeling techniques for predicting HTAG dispersion have been published. The models, in most cases, were developed for risk assessment studies of liquefied gas fuel importation projects in the U.S. and Europe. When applied to the prediction of the maximum downwind distances which might be reached by flammable gas-air mixtures following catastrophic releases of liquefied natural gas from ship cargo tanks, order of magnitude differences were reported. The large differences in predictions of hazard zones extending from catastrophic scenario LNG releases were in part due to lack of standardization of release and atmospheric conditions simulated, but also reflected different modeling approaches (Havens, 1977). Since 1977, extensive laboratory and field experimental programs have been conducted which provide data for the evaluation of HTAG dispersion models.

This study, sponsored by the U.S. Coast Guard and the Gas Research Institute, attempts to provide an overall assessment of the prediction of atmospheric dispersion of HTAG and to develop a recommended methodology for such predictions for incorporation into the Coast Guard Chemical Hazard Response Information System (CHRIS).

I.1 General Description

The problem is prediction of the dispersion, by mixing with ambient air, of a mass of HTAG released during a finite period of time in the atmospheric boundary layer. The initial gas cloud may result directly from (1) an aboveground release such as a release of pressurized gases, as in a chlorine tank rupture, or (2) indirectly from a ground-level source such as the evaporation of a released liquid as in the case of a spill onto the sea of liquefied petroleum gas (LPG) or natural gas (LNG). The cloud may be initially formed as a mixture of gas or gas-liquid aerosol and humid air. Actual releases will always be of finite time duration and will have a finite, time-dependent boundary (extent).

Appealing to generally accepted concepts of boundary layer flows, the typical development and movement (including dispersion) of a heavy gas cloud is illustrated in Figure I.1. The HTAG source is characterized as time- and position-dependent with the source mass rate E (x,y,t). At time t, a HTAG cloud has formed over the source. Interaction of the vertical flux of gas from the source with the atmospheric flow has resulted in some translation downwind; an upwind movement of the cloud boundary has resulted from gravity-driven lateral flow of the heavy cloud. Characteristic profiles of the cloud boundary at times t_2 and t_3 after completion of gas injection into the atmosphere are depicted. The cloud is described by specification of its height or depth H (x,y,t), local concentration c (x,y,z,t), density ρ (x,y,z,t), enthalpy h (x,y,z,t), and velocity u_j(x,y,z,t). Characteristic vertical profiles of c, H, ρ, and u_j which reflect the assumption of concentration decrease via air entrainment through the top and front boundaries of the cloud (entrainment velocities w_e and u_e respectively) as well as shear stress at the cloud top and bottom surfaces (τ_δ and τ_o respectively), are illustrated.

The local velocity u_j may be the result of density-driving forces which cause a spreading motion, or it may reflect the atmospheric flow into which the gas is injected. In actual releases, some combination of these effects will be important.

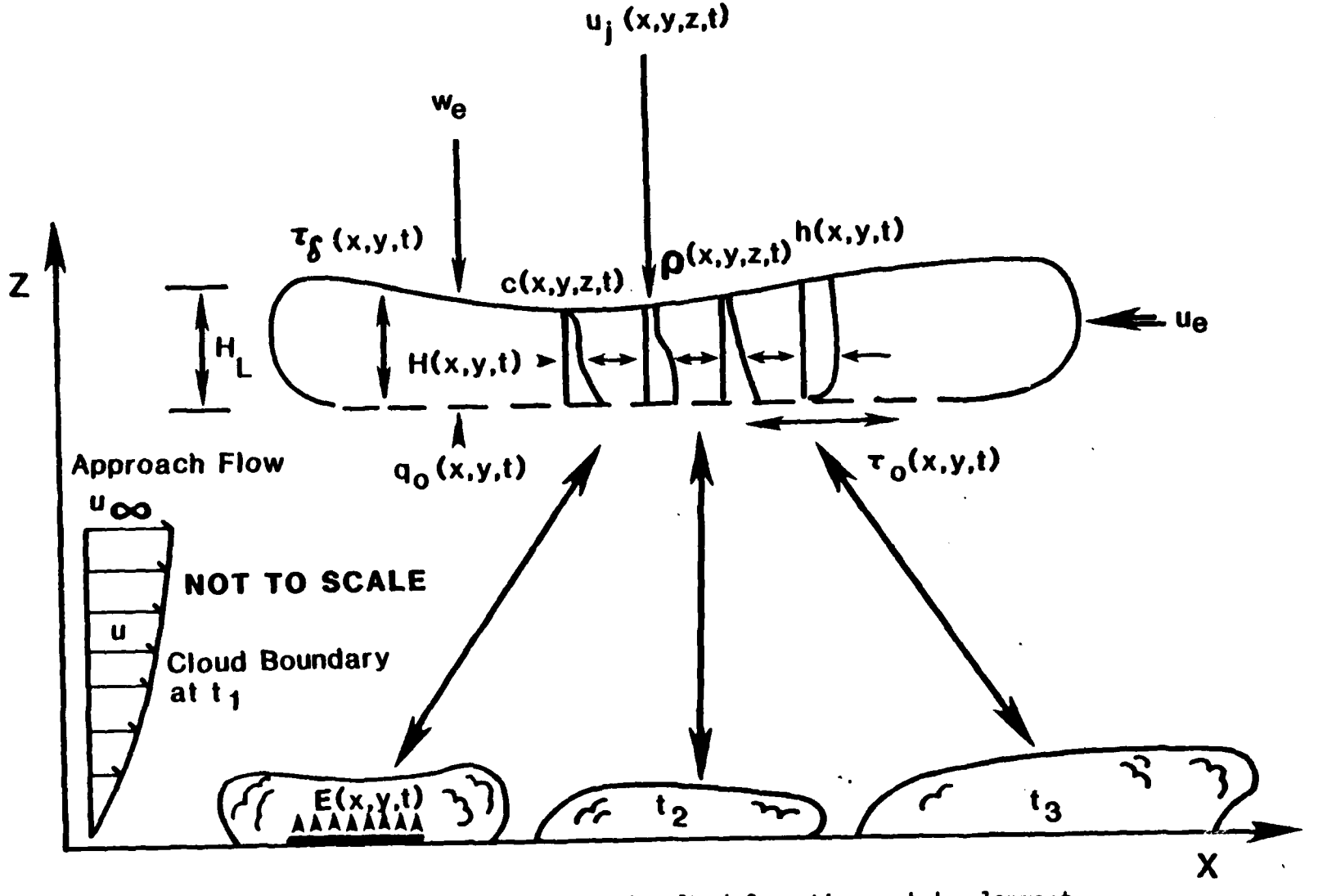

Figure I.1 Heavier-than-air cloud formation and development.

The HTAG cloud formation illustrated in Figure I-1 reflects a cloud formation phase whose duration is small compared to the travel time to the maximum distance exposed to the concentration of interest. This would be the case, for example, if the cloud were formed by rapid evaporation from a rapidly spilled cryogenic liquid. In such cases, the development of the cloud is three-dimensional and highly transient, and a general model of the momentum, mass, and energy transfers is complex and difficult. Several mathematical models, which are applications of different numerical computational procedures for solving the balance equations for momentum, energy, and mass with initial and boundary conditions descriptive of the processes, have been proposed and are being evaluated (Havens, 1979, 1983). Such models are complex and require significant computer solution time (and cost). Furthermore, there remain important questions regarding the validity of many assumptions made in such models (i.e. turbulence closure models) which require further evaluation.

A more often adopted approach to modeling the dispersion of HTAG clouds has been to consider the limiting cases where the cloud formation phase, of characteristic duration t_f, is very small or very large with respect to the time of cloud travel to the maximum distance exposed to the concentration of interest, t_t. When $t_f >> t_t$, a stationary "plume" representation of the HTAG cloud becomes applicable. When $t_f << t_t$, an instantaneous source representation is indicated.

In either case, it is further observed that a typical heavy gas dispersion scenario involves three more or less distinct regimes of fluid flow. Following release, especially for rapid release of a large quantity of heavy gas, a cloud having similar vertical and horizontal dimensions (near the source) may form. The initial behavior of such a cloud is relatively independent of the characteristics of the ambient wind field until the strength of the buoyancy-driven flow (slumping and lateral spreading) decreases sufficiently that the cloud motion begins to be determined by the ambient atmospheric flow. When the cloud motion begins to be determined by the atmospheric flow, the dispersion process can be

described as a stably stratified plume (or cloud) embedded in the mean wind flow. As the dispersion proceeds, the stable stratification due to the heavy gas decreases until the process can be represented as a neutrally buoyant plume (or cloud) in a neutral or stratified mean wind flow. The three regimes,

-- buoyancy-dominated dispersion

-- stably stratified shear flow

-- passive dispersion due to atmospheric turbulence

which may overlap and be present in various degrees in different heavy gas dispersion scenarios, must be accounted for if a model is to be generally applicable. The specific treatment of each of these flow regimes in earlier models, as well as the methodology used to provide transition between the regimes, is quite varied and explains in large part the differences observed when the various models have been applied to the same heavy gas dispersion scenario (Havens, 1977, 1979).

For <u>any</u> atmospheric dispersion problem, the dispersion of the contaminant is passive if the dispersion is entirely the result of the preexisting atmospheric turbulence, and the contaminant does not affect the mean flow field or the turbulence. Consequently, conventional air pollutant passive dispersion techniques (Pasquill, 1983) become applicable to the description of the latter phases of dilution of an originally HTAG cloud. A method for delimiting the zone in which the dispersion process is <u>non-passive</u>, i.e. where the flow and dispersion processes are affected by the presence of the HTAG, is needed for two reasons. First, a determination of whether the release need be described as a HTAG release or, more simply, as a passive pollutant is in order. Second, experimental data must be viewed in relation to the relative importance of the gravity-driven flow vs. atmospheric turbulence-dominated processes which disperse the gas.

I.2 Buoyancy-Dominated Dispersion

Rapid release of a large quantity of HTAG may result in an initial cloud having similar vertical and horizontal dimensions. The immediate behavior of such initially "compact clouds" (Fay, 1984) is controlled by the ensuing buoyancy-driven flow (slumping and lateral spreading). Consequently, the initial cloud behavior is relatively independent of the characteristics of the ambient wind field until the strength of the buoyancy-driven flow decreases to levels at which the cloud motion begins to be controlled by the ambient atmospheric flow.

For HTAG releases with initially similar vertical and horizontal length scales there is now conclusive evidence that the rapid gravity-driven flow which ensues results in large scale turbulent structures which effect considerable dilution of the cloud (Picknett, 1978; Hall et al., 1982; Meroney and Lohmeyer, 1982; Havens and Spicer, 1983; Spicer and Havens, 1984). Since this initial turbulent motion can in some conditions result in dilution of the cloud by a factor of ten to one hundred, it must be accounted for in predictions of HTAG dispersion. Furthermore, an understanding of the dilution processes present during this phase is necessary to accurately predict dispersion of large scale releases in low winds, particularly for gas-air mixture flammability levels, which for hydrocarbons are generally of order one percent.

The spreading motion that follows release of a HTAG volume with similar vertical and horizontal length scales is a classical "gravity current," characterized by the gravity-driven intrusion of one fluid (the HTAG) into a less dense fluid (the atmosphere). Gravity currents are formed in many natural situations (Simpson, 1982), including thunderstorm outflows, sea breeze fronts, and cold front movements in the atmosphere, and a variety of ocean currents driven by temperature, salinity, or suspended solids-induced density differences.

A comprehensive review of laboratory gravity current studies and their relation to gravity currents in the atmosphere and ocean has been recently published by Simpson (1982). Gravity currents formed by instantaneous release of a fixed volume of denser fluid under a layer of less dense fluid pass through three flow regimes. There is first a "slumping phase," during which the current is retarded by the counterflow of the bulk fluid into which the intrusion occurs; this slumping phase prevails until the ratio of the depth of the density current to the bulk fluid is about 0.075 (Huppert and Simpson, 1980). For fixed volume releases in the atmosphere, this phase is extremely short and can be neglected from our consideration. In the immediately ensuing flow phase the dynamics of the current are governed by inertial and buoyancy forces. In this phase, the buoyancy and inertial forces may be roughly considered to be in balance, and the motion of the bulk fluid is unimportant. Finally, there follows a viscous phase, wherein the buoyancy force is roughly balanced by viscous forces. The viscous phase of gravity currents resulting from the fixed volume release of a HTAG is characterized by the virtual absence of further dilution by turbulent mixing; accordingly, we concentrate on the buoyancy-inertial phase of such flows.

During the inertial-buoyancy phase, the motion of the current can be considered quasi-stationary, and the distinguishing features of the flow near the gravity current head are represented in Figure I.2.

Figure I.2. The head of a steady gravity current (Simpson and Britter, 1979, and van Ulden, 1983).

Characteristic features of the flow process illustrated in Figure I.2 are (van Ulden, 1983):

1. At the leading edge a "head" is present with a depth H_1 about twice that of the current behind the head, H_h.
2. An elevated stagnation point is present, below which an insignificant flux Q_1 of ambient fluid is entrained.
3. Behind the head a wake region is present in which significant mixing occurs. An associated significant internal flow in the head is present with a denser fluid layer flowing into the head from behind with a velocity $u_4 \approx 0.2$ times the velocity of the front, and a mixed layer flowing away from the head.
4. The front velocity relative to the flow being intruded into is well described by the relation

$$u_f = C_E(g\Delta' H_h)^{1/2} \qquad \text{(I-1)}$$

with $C_E = 1.15 \pm 0.05$, based on the data from Schmidt (1911), Benjamin (1968), Fannelop et al. (1980), and Huppert and Simpson (1980).

The use of the relation given in Equation I-1 to describe the lateral gravity-driven spreading of a fixed volume release of HTAG, coupled with the representation of the gas cloud as a vertically oriented cylinder whose radius and height change as a result of gravity spreading and air entrainment across the outer surfaces of the cloud has formed the basis for several HTAG dispersion models (van Ulden, 1984; Germeles and Drake, 1975; Fryer and Kaiser, 1979; Cox and Carpenter, 1979; Fay, 1980; Picknett, 1981; Eidsvik, 1980; Fay and Ranck, 1981; and Fay, 1984).

These models have been reviewed by Havens (1982) and Webber (1983). Meroney and Lohmeyer (1982) and van Ulden (1979, 1983) have proposed bulk models for describing gravity currents which account for the acceleration phase of the current which precedes the quasi-steady inertial-buoyancy-controlled phase depicted in Figure I.2. A summary of these modeling techniques drawn upon in

formulating a model for the buoyancy-controlled phase is given in Section II. An extensive laboratory investigation of the gravity spreading and dilution of right circular cylindrical volumes of HTAG released in calm air, from which is derived pertinent data for modeling the gravity spreading and air entrainment during the buoyancy-controlled phase of such releases, is described and discussed in Volume II of this report.

I.3 Stably Stratified Shear Flow

An intermediate phase of the dispersion process is characterized by its similarity to a wide variety of naturally occurring flow processes in which a stably stratified plume is embedded in a mean flow. Such plumes are expected to differ importantly from neutrally buoyant (passive) plumes in three significant ways.

1. A lateral (crosswind) gravity-driven mean flow will persist until the negative buoyancy of the cloud has been reduced (by entrainment) to render the mean flow velocity small compared to an appropriate lateral turbulent velocity characteristic of the atmospheric flow.
2. The density interfaces which define the plume boundaries should act to damp turbulent mixing and consequently reduce vertical mixing (air entrainment) into the HTAG cloud.
3. Because such plumes are characterized by a small vertical to longitudinal ratio, dilution occurs primarily as a result of vertical mixing.

The ground level lateral extent of a negatively buoyant plume embedded in a turbulent boundary layer has been investigated by Britter (1980). Considering the steady release of a gas with density ρ, at a volumetric rate Q m^3/s, from a circular source of diameter D at ground level into a wind field with average velocity u_a, the cross-section of the cloud at the downwind edge of the source is approximated as rectangular with width $W_0 = \frac{\sqrt{\pi}}{2} D$ and height $H = Q / W_0 u_a$. If it is assumed that the lateral gravity-driven

spreading is described by Equation I-1 and the gas-air mixture buoyancy is preserved, the cloud width as a function of downwind distance is then given by

$$W = \left[3\, C_E \left(\frac{g \Delta' Q}{u_a^3} \right)^{1/2} x + W_0^{3/2} \right] \qquad \text{(I-2)}$$

and the rate of lateral spread with respect to downwind distance is

$$\frac{dW}{dx} = \frac{1}{u_a} \frac{dW}{dt} = 2\, C_E \left(\frac{g \Delta' Q}{u_a^3} \right)^{1/2} \left[3\, C_E \left(\frac{g \Delta' Q}{u_a^3} \right)^{1/2} x + W_o^{3/2} \right]^{-1/3} \qquad \text{(I-3)}$$

The lateral gravity-driven spreading rate is indicated to be a function of the length scale $g \Delta' Q / u_a^3$, hence the lateral spreading rate in a given wind field is determined by the buoyancy flux $Q g \Delta'$. The lateral extent of the cloud is then dependent in the near-field on the two length scales D and $g \Delta' Q / u_a^3$.

Britter has experimented with the injection of a dense fluid (saline solution) through the floor (area source) of a water flume. The flume was 0.76 m wide, 10 m long, and the mean flow in the flume was characterized as fully turbulent with Reynolds number, based on bulk velocity and flume depth, greater than 5,000 and a friction velocity equal to the bulk velocity divided by 20. The dense fluid source, which was flush with the flume floor, was a sintered bronze distributor plate with diameter 5 cm, placed in the centerline of the flume. The ranges of variables studied were

$$0 < Q < 60 \text{ cm}^3/\text{s}$$

$$0 < u_a < 40 \text{ cm/s}$$

$$0 < g \Delta' < 200 \text{ cm/s}^2$$

Britter's experiments indicated that the buoyancy-driven lateral velocities were greater than the friction velocity of the mean flow for $xu_a^3 / Q g \Delta' >> 1.3 \times 10^4$. It follows that the transition to passive behavior could be expected to be complete when

$x > 1.3 \times 10^4 \frac{Q g \Delta'}{u_a^3}$ and the plume should be passive from the source

when $\frac{u_a^3 D}{Q g \Delta'} \gtrsim 1000.$

Fluid mixing across the density interface which characterizes a dense plume embedded in a turbulent boundary layer was reviewed by Turner (1973). There is general agreement that entrainment across such plume boundaries is correlated with a bulk Richardson number for the plume defined as $Ri_a = g \Delta' H / u_a^2$ or $Ri_* = g \Delta' H / u_*^2$.

The turbulence which effects mixing in a plume flowing over a solid surface and under a turbulent flow layer may originate in the shear stress at the bottom solid surface or at the density interface. For thin layers "intruding" under a layer, the bottom stress is probably most important, and this case probably best represents the behavior of HTAG plumes in the atmosphere.

McQuaid (1976), Kantha et al. (1977), and Lofquist (1960) have reported experimental studies from which entrainment velocity correlations can be derived for bulk Richardson numbers encompassing the range of interest for HTAG dispersion in the atmosphere. McQuaid reported measurements of the vertical dispersion of carbon dioxide ($\rho / \rho_a = 1.52$) introduced as a floor-level line source in a fully developed rectangular channel flow in a wind tunnel of width 0.3 m, height 0.9 m, and working length 5.5 m. The mean velocity, u_a, in the tunnel ($\simeq 0.8\ u_{max}$) ranged from 0.82 to 3.52 m/s with a friction velocity (in the absence of any HTAG) reported as $u_* = 0.0412\ u_a$. The channel Reynolds' number (based on the mean velocity and the channel hydraulic diameter) ranged correspondingly from 2.5×10^4 to 1.1×10^5. Defining an average plume depth via the

relation $H_{eff} = \frac{Q}{c_{max} u_{EFF}}$, where u_{EFF} is the effective advection velocity, the entrainment velocity of air into the two-dimensional plume becomes $w_e' = u_{EFF} \, d H_{EFF} / dx$. Britter analyzed McQuaid's data and reported the correlation for entrainment velocity with Ri_* shown in Figure I.3.

Kantha et al. measured turbulent entrainment at the interface in a stably stratified two-layer fluid with constant surface stress applied at the free (top) surface. The rate of increase of the mixed layer depth H_L with time was measured photographically using a dye initially distributed in the top (lighter) layer. The Richardson number ($Ri_* = H_L \, g \Delta' / u_*^2$) is constant in such an experiment. One value of the entrainment velocity, defined as

$$w_e = \frac{dH_L}{dt} \qquad \text{(I-4)}$$

was obtained for a given value of u_* and Δ (i.e. for a given Richardson number). Kantha et al. reported measurements of w_e for $30 < Ri_* \leq 1000$. In order to compare the entrainment velocities obtained by Kantha et al., defined by Equation I-4 with the data from McQuaid, H_{EFF} must be related to the mixed layer depth H_L. Assuming that the entrained material is represented as being distributed vertically with a Gaussian concentration profile and that H_{EFF} is defined as the height where the concentration is one-tenth that of the maximum value, $H_L \simeq 2.15 \, H_{EFF}$. The data of Kantha et al. expressed as $w_e' = d H_{EFF} / dt$ is shown in Figure I.3.

Lofquist (1960) also measured turbulent entrainment across a stable density interface formed between a turbulent shear layer of salt water and a quiescent pure water layer above and presented the entrainment velocity as a function of a Froude number

$$Fr^2 = \frac{u_a^2}{g \Delta' H_r} \qquad \text{(I-5)}$$

where H_r is the hydraulic radius of the rectangular channel in which the experiments were conducted. The data presented by Lofquist have been re-expressed in the form

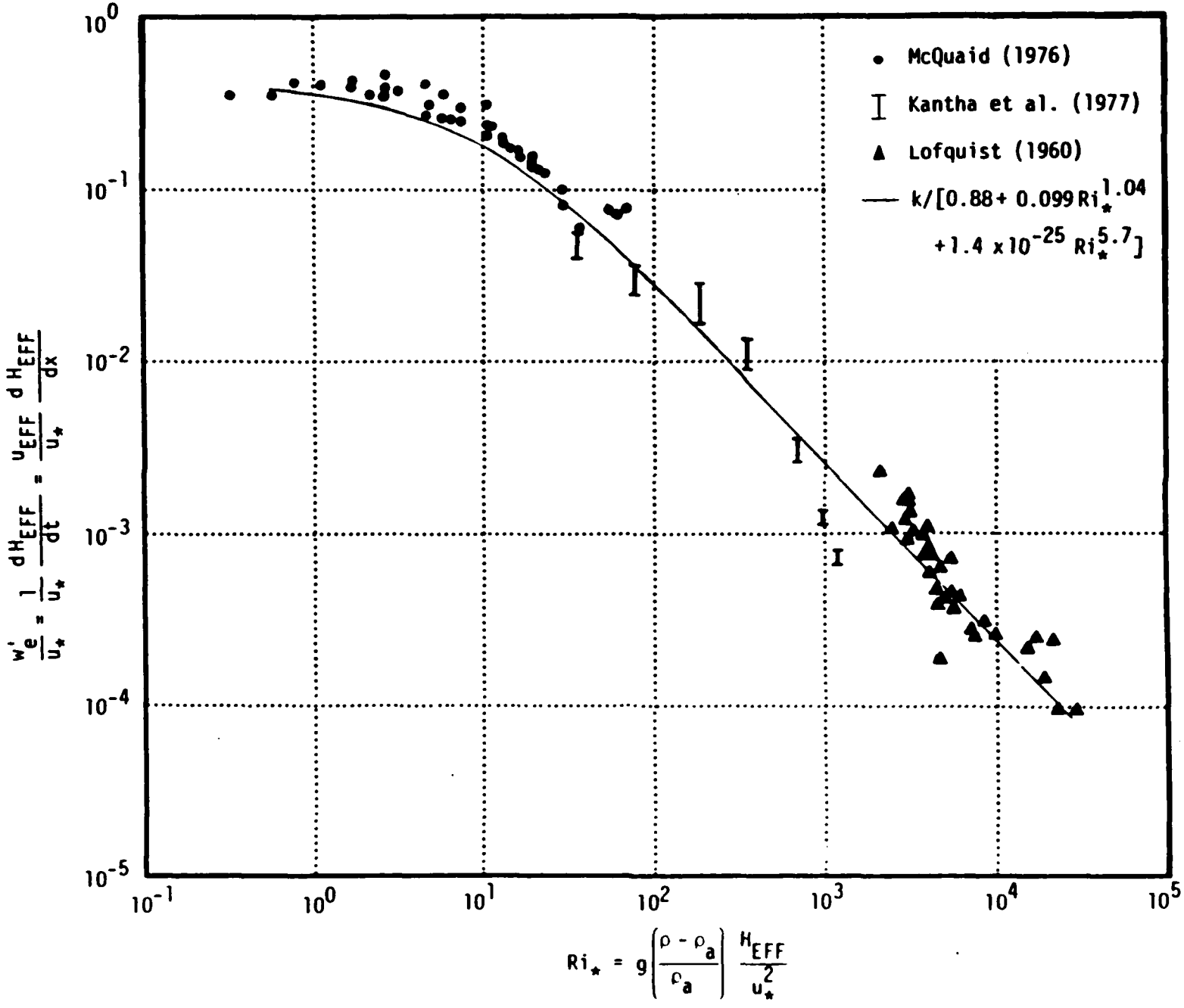

Figure I.3. Correlation of entrainment velocity with bulk Richardson number.

$$w_e' = \frac{d H_{EFF}}{dt} = f(Ri_*) \qquad \text{(I-6)}$$

and included in Figure I.3.

The combined data of McQuaid, Kantha et al., and Lofquist shown in Figure I.3 were curve-fitted to give

$$w_e' / u_* = k(1 + \alpha)/[0.88 + 0.099\ Ri_*^{1.04} + 1.4 \times 10^{-25}\ Ri_*^{5.7}] \qquad \text{(I-7)}$$

where α is the power for a power law wind velocity profile (Equation III-50). This functionality is obtained if the vertical turbulent diffusivity is given by

$$K_z = k\, u_* z / \phi\ (Ri_*)$$

and the vertical concentration distribution is of the form

$$c(x,z) = c_c(x)\ \exp\left[-\left(\frac{z}{s_z(x)}\right)^{1+\alpha}\right]$$

as developed in Section III. For curve-fitting, a value of 0.2 was used for α. The limiting value ($Ri_* = 0$) of $w_e' / u_* = k / 0.88$ incorporates the ratio of eddy diffusivities for heat (thermal energy) and momentum, K_m / K_H, and $k = 0.35$, as determined by Businger et al. (1971) from measurements in the neutral atmospheric surface stress layer. The eddy diffusivity for mass K_c is assumed equal to that for heat (energy) transfer under the conditions reported by Businger et al.

The effect of vertical density stratification on vertical mixing shown by the data is consistent with a passive limit for w_e' / u_* of 0.4 suggested by the solution of the diffusion equation (Equation I-19) with a constant wind velocity and mass diffusivity given by

$$K_c = k u_* z \tag{I-8}$$

Furthermore, the dependence of w_e' on Ri_* for large Ri_* approaches

$$w_e' \propto Ri_*^{-1} \tag{I-9}$$

as suggested from dimensional reasoning by Turner (1973).

I.4 Passive Dispersion due to Atmospheric Turbulence

At some distance from the source, gas will be sufficiently dilute to justify its consideration as a trace material, and the dispersion can be modeled using approaches developed for atmospheric pollutant dispersion (Hanna et al., 1982; Pasquill, 1983).

Considering quasi-steady releases at ground level in the atmospheric flow field from a Lagrangian point of view, the crosswind (lateral) and vertical spread of a contaminant occurs as a result of small scale-distorting processes. However, the trajectories of successive sections of the plume may be irregularly displaced by larger scale fluctuations in the flow (plume meander). Thus the time average concentration experienced downwind of a point source not only diminishes with distance from the source but also varies with time. This property of the time-mean concentration results from dispersive motions with length scales larger than the plume cross-section. It follows that the time-mean crosswind distribution from a source may not be described adequately as a diffusion process with the gradient transfer hypothesis because of the displacement of the plume by such larger scale fluctuations in the flow. However, it is assumed that vertical spread from a ground level source is controlled by dispersive motions whose scale is restricted by the presence of the boundary (and therefore are small with respect to the vertical spread), and vertical dispersion from ground level sources has been widely modeled using the gradient transfer hypothesis in the diffusion equation. Vertical dispersion in the surface layer from ground level sources is conventionally modeled using the gradient transfer hypothesis combined with application of similarity principles developed by Monin (1959) and Batchelor (1964) and extended for stratified flow by Gifford (1962).

The vertical velocity gradient responsible for maintaining the stress in the surface layer is assumed to be a function of the surface stress τ_0, the density ρ, and the height z. From dimensional principles

$$\frac{du_x}{dz} = \left(\frac{\tau_0}{\rho}\right)^{1/2} \Big/ kz \equiv u_* / kz \qquad \text{(I-10)}$$

Equation I-10 defines the friction velocity u_*, and the experimentally determined value of k (von Karman constant) is variously reported as 0.35 to 0.40. Integration of Equation I-10 gives the logarithmic velocity profile

$$u_x = \frac{u_*}{k} \ln \frac{z}{z_0} \qquad \text{(I-11)}$$

where z_0 is an integration constant which represents the height at which the velocity is taken to be zero.

Equation I-11 is valid for neutrally stable flow. If there is an upward or downward flux of heat (q_0) through the surface layer, vertical density variation will result, and the density stratification results in modification of the flow field. The vertical momentum flux is then the result of buoyancy flux as well as mechanical shear; the flux of buoyancy is

$$F_0 = \frac{g \beta'}{\rho C_p} q_0 \qquad \text{(I-12)}$$

where β' is the expansion coefficient of the fluid in the flow field. A length scale which quantifies the relative importance of shear-related and buoyancy-related vertical momentum transfer is defined by combining the buoyancy and momentum fluxes:

$$\lambda = u_*^3 / F_0 \qquad \text{(I-13)}$$

where λ is the Monin-Obukhov length. For q_0 negative (heat and momentum transfer in the same direction), λ is positive, and the associated stable stratification of the fluid layer tends to suppress turbulence. If q_0 is positive, an unstable density stratification results ($\lambda < 0$), tending to increase vertical turbulent transfer. A neutrally stable fluid layer corresponds to infinite λ.

From dimensional arguments, a modified form of Equation I-10 is derived to describe the vertical velocity profile in a stratified shear layer

$$\frac{du_x}{dz} = \frac{u_*}{kz}\,\phi_M\left(\frac{z}{\lambda}\right) \qquad \text{(I-14)}$$

with ϕ_M determined from experimental measurements of vertical momentum transfer. A widely used analytic representation of ϕ_M based on field wind profile measurements and proposed by Businger et al. (1971) is:

$$\phi_M = \left(1 - 15\,\frac{z}{\lambda}\right)^{-1/4} \qquad \lambda < 0 \text{ (unstable)} \qquad \text{(I-15)}$$

$$\phi_M = 1 + 4.7\,\frac{z}{\lambda} \qquad \lambda > 0 \text{ (stable)} \qquad \text{(I-16)}$$

The vertical eddy diffusivity, defined as the ratio of momentum flux to the mean velocity gradient,

$$K_M = \tau_0 / \rho\,\frac{du_x}{dz} \qquad \text{(I-17)}$$

becomes, using Equation I-14 and noting that $\tau_0 = \rho\, u_*^2$,

$$K_M = \frac{k\, u_*\, z}{\phi_M} \qquad \text{(I-18)}$$

For two-dimensional, steady state, vertical diffusion in the surface stress layer, the diffusion equation is

$$u_x \frac{\partial c}{\partial x} = \frac{\partial}{\partial z}\left(K_c \frac{\partial c}{\partial z}\right) \qquad \text{(I-19)}$$

where K_c is the mass eddy diffusivity. It is common practice to invoke Reynolds' analogy between mass and momentum transfer processes to assume $K_c = K_M$, although there is experimental evidence that the eddy diffusivities for mass and heat or thermal

energy (K_H) are greater than K_M. Businger et al. (1971) showed that the ratio K_H / K_M was about 1.3 in neutrally stable flow ($\lambda = \infty$), decreases to near 1.0 with increasing stability ($z/\lambda \rightarrow 2.0$) and increases to about 2.5 for decreasing stability ($z/\lambda \rightarrow -2.5$).

The application of Equation I-19, with suitable descriptions of $u_x(z)$ and $K_c(z)$, for modeling vertical dispersion in the surface layer of the atmosphere has been demonstrated (Hanna et al., 1982; Pasquill, 1983).

II. REVIEW OF AVAILABLE MODELS

A number of mathematical techniques for predicting HTAG dispersion have been published. These models can be (somewhat arbitrarily) classified in three categories.

1. Box models which represent the initial development of a cloud (in the case of an instantaneous release) or a cross-sectional slice of a cloud (in the case of a steady continuous release) as a uniformly mixed volume. The shape, thermodynamic properties, and position of the cloud are modeled using correlations derived for the velocity of density intrusions and fluid entrainment across density interfaces. This model type often incorporates a transition, usually to a Gaussian model, to describe passive dispersion (controlled by atmospheric turbulence) of the gas in the far field.
2. K-theory models which assume constitutive relations between turbulent fluxes and the gradients in mean variables velocity, temperature, and concentration, coupled with the time-averaged incompressible flow balance equations for mass, momentum, and energy to predict the temporal and spatial variation of cloud properties.
3. There are several models which involve greater simplification of the equations of motion, energy, and mass than is found in the K-theory models. Some still require solution of partial differential equations to predict cloud state variables such as the models proposed by Zeman (1980), Rosenzweig (1980), and Fannelop (1980) and refinements thereof, such as the SLAB model published by Lawrence Livermore National Laboratories (Morgan et al., 1983a) which are one-dimensional time-dependent models

designed to describe diffusion and gravity-driven flow of a HTAG release in the atmosphere. Several models (te Riele, 1977; Flothmann and Nikodem, 1980; Colenbrander, 1980) assume power law concentration profiles of the form

$$c(x,y,z) = c_c(x) \exp \left[- \left(\frac{y}{y_s} \right)^a - \left(\frac{z}{z_s} \right)^b \right] \qquad \text{(II-1)}$$

and some couple this assumption with a K-theory representation of turbulent mass transfer within the cloud (Colenbrander, 1980).

The K-theory and SLAB models were not considered suitable for incorporation in an interactive computer system such as HACS and will not be described here. It is appropriate to note that the SLAB model and FEM3, a K-theory model published by Lawrence Livermore National Laboratories (Chan et al., 1982), utilize concepts to describe the effect of stable density stratification on vertical dispersion which are similar to those used in other models such as Colenbrander (1980), Eidsvik (1980), and the model recommended herein.

Vertical entrainment of air into a gas layer is expected to be a function of the stabilizing effect of the density gradient relative to the shear flow characterized by vertical turbulence. If the HTAG flow is viewed as being superimposed on the local atmospheric flow and convection-induced turbulence is neglected, a characteristic vertical turbulence velocity can be represented as a friction velocity of the flow, where

$$u_* = \left(\frac{1}{2} c_F \right)^{1/2} u \qquad \text{(II-2)}$$

c_F is a surface-friction drag coefficient and u is a characteristic wind velocity u_a, or, as represented in some models, the weighted vector sum of the gravity spreading velocity and the characteristic wind velocity

$$u^2 = (c_* u_f)^2 + u_a^2 \qquad \text{(II-3)}$$

The vertical density stratification of the flow is measured by a form of the overall Richardson Number

$$Ri_* = \frac{g\Delta H}{u_*^2} \text{ or } \frac{g\Delta' H}{u_*^2}, \quad Ri'_* = \frac{g\Delta H}{w^2} \text{ or } \frac{g\Delta' H}{w^2} \qquad \text{(II-4)}$$

where w is given by

$$w^2 = u_*^2 + \eta w_*^2 \qquad \text{(II-5)}$$

w_* represents the convection scale velocity, and η is an empirical constant (Zeman and Tennekes, 1977).

Classical boundary layer analysis (Pasquill, 1983; Turner, 1973) suggests that in the constant stress layer of the atmosphere, the vertical entrainment velocity should be proportional to the friction velocity in the absence of stratification and inversely proportional to the Richardson number for stratified flow.

$$w_e = c_1 u_* \qquad \text{for } Ri \to 0 \qquad \text{(II-6)}$$

$$w_e = c_2 u_*/Ri \qquad \text{for } Ri \gg 1 \qquad \text{(II-7)}$$

These equations have been demonstrated for boundary layers adjacent to the earth's surface.

Velocity shear is also produced at the interface between a spreading HTAG layer and the overlying atmospheric flow. Turbulent mixing across such a surface can result from breaking waves associated with instabilities generated at the interface (Turner, 1973). Some HTAG cloud models have provided for air entrainment via this mechanism; the entrainment is assumed proportional to the difference in velocity across the cloud top. For a spreading "top hat profile" gas layer, such entrainment is represented by

$$w_e = c_3(\bar{u} - u_a) \qquad \text{(II-8)}$$

where $\bar{u}$ is the average cloud top velocity. In the following, some approaches to air entrainment modeling are summarized.

II.1 Box Models

A number of models have been proposed in this category; however it is possible to consider general forms which have been used to model gravity spreading and air entrainment into the homogeneous volume or cloud. This model type is further categorized based on the methodology used to describe the gravity-driven HTAG flow. In earlier models, the dynamics of the HTAG flow was simply described as a quasi-steady density intrusion, reflecting the assumption of exchange of cloud potential energy for lateral kinetic energy of the flow; this category is referred to as a hydrostatic approximation box model. Refinement to include a momentum balance on the cloud spreading process which describes more realistically the acceleration from rest as well as the ensuing slumping and lateral spreading process have appeared in some models.

Since these models assume uniform thermodynamic properties, their use is restricted to the representation of two types of HTAG clouds, illustrated in Figure II.1.

1. An instantaneously released quantity of gas with a known initial volume, usually represented as a vertically oriented cylinder whose radius and height change as a result of gravity spreading and air entrainment across the outer surfaces of the cloud. The cylindrical cloud is usually assumed to be translated with wind.
2. A steady plume with rectangular cross-section (axis along the wind direction) whose thermodynamic properties vary with downwind position and whose width and height change as a result of gravity spreading (assumed lateral only) and air entrainment across the outer surfaces.

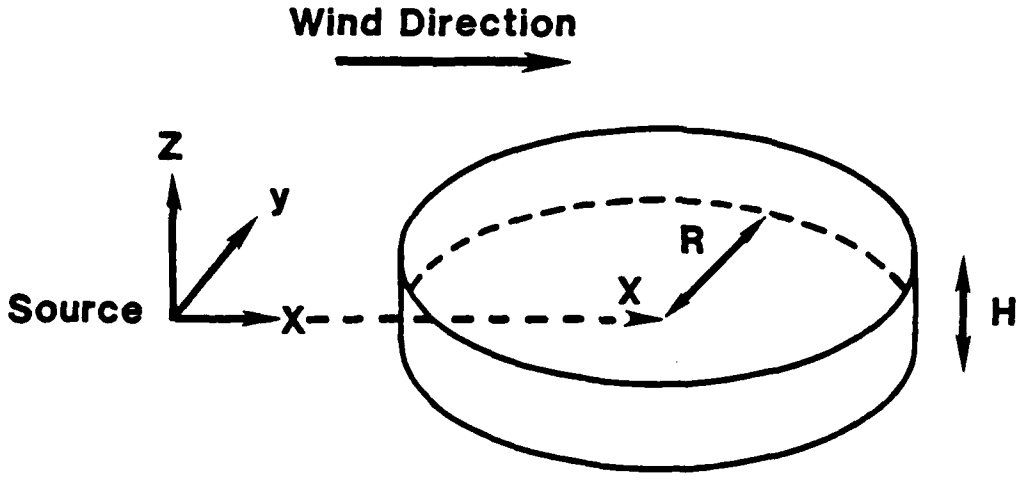

Cloud shape for Instantaneous Release

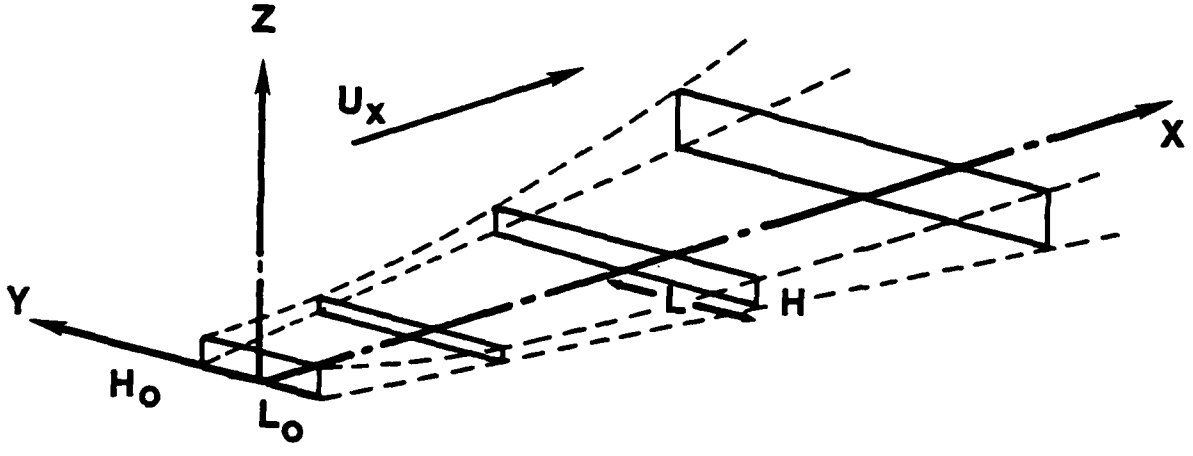

Cloud shape for Continuous Releases

Figure II.1 Box model cloud representation

In either case, the models require analytical expressions for the spreading velocity (i.e. the velocity of the cloud edge) and the entrainment of air at the cloud boundaries.

II.1.1 Hydrostatic Approximation Box Models

All proponents of this approach have modeled the velocity of the cloud edge using a density intrusion relation

$$u_f = C_E \left[g \left(\frac{\rho - \rho_a}{\rho} \right) H \right]^{1/2} = C_E [g \Delta H]^{1/2} \qquad \text{(II-9)}$$

or

$$u_f = C_E \left[g \left(\frac{\rho}{\rho_a} - 1 \right) H \right]^{1/2} = C_E [g \Delta' H]^{1/2} \qquad \text{(II-10)}$$

Equation II-10 follows from Equation II-9 when $\rho \simeq \rho_a$. The density of the cloud is affected by energy transfer from the cloud surroundings as well as the entrainment of air into the cloud. No consideration of the different approaches to modeling the surface-to-cloud heat transfer has been included here. It is probable, however, that such heat transfer may importantly affect the dispersion of cryogenic gases such as LNG; some investigators have indicated that air entrainment may be significantly enhanced due to convection-generated turbulence (Eidsvik, 1980; Fay and Ranck, 1981). Both of these effects are discussed in Section IV.

Although box model treatments of air entrainment have given widely disparate results, most of the differences are attributable to differences in interpretation of the sparse data base used to determine empirical entrainment coefficients. Box models can be represented as requiring entrainment velocities which are applied in the general form

$$\dot{M}_a / \rho_a = w_e A_T + u_e A_F \qquad \text{(II-11)}$$

where $w_e A_T$ and $u_e A_F$ are vertical and horizontal entrainment rates represented as the product of a characteristic area and velocity. Because the HTAG clouds are generally shallow and grow laterally due to gravity forces, the second term in Equation II-11 is normally assumed to be important only in the gravity spreading-dominated stages of the cloud development. The horizontal entrainment velocity has most often been modeled by

$$u_e = \varepsilon u_f \qquad \text{(II-12)}$$

or

$$u_e = \frac{\varepsilon u_f^2}{u_f(t=0)} \qquad \text{(II-13)}$$

Equation II-13, proposed by Eidsvik (1980), reduces to Equation II-12 in the limit $t \to 0$, and gives an effective horizontal entrainment velocity which decreases to zero for $A_T / A_F \gg 1$. Details of specific models are summarized chronologically in the following.

van Ulden (1974) characterized the HTAG flow with the Richardson number $Ri_* = g\Delta H / u_*^2$. He suggested that cloud frontal entrainment is very small and that cloud top entrainment during the gravity-dominated spread, which he defined as $Ri_* \gg 4 / C_E^2$, is negligible. Thus van Ulden's model of the gravity spread phase indicates minimal cloud volume growth (and dilution) given by

$$\dot{M}_a / \rho_a = \frac{dV}{dt} = u_e A_F \cong 0.05\, u_f A_F$$

van Ulden suggested that atmospheric turbulence-induced mixing will begin to control when the spreading velocity has been reduced to 2 u_* ($Ri_* = 4 / C_E^2$) and thereafter models the cloud dilution using a classical Gaussian passive dispersion model. It appears that van Ulden's (1974) model entrainment parameters were based primarily on analysis of the growth of a heavy Freon-air cloud following essentially instantaneous vaporization of 1000 kg liquid Freon

dumped into water. It is important to note that measurements of the initially formed visible cloud indicated a rapid, initial, approximately ten-fold dilution of the Freon, and van Ulden modeled the subsequent dispersion only.

Germeles and Drake (1975) neglected cloud frontal entrainment and modeled top entrainment using Equation II-8. Germeles and Drake suggested $c_3 = 0.1$ based on their Froude number extrapolation of Lofquist's (1960) data for entrainment across a density/shear interface between a salt water flow and overlying quiescent pure water. The flow in Lofquist's experiments was three-dimensional (the flow was in a channel with comparable width and depth), and although Lofquist's correlation of the data utilized a Froude number which incorporated the hydraulic radius of the heavy layer, this appears not to have been accounted for in Germeles' and Drake's extrapolation. Analysis indicates an order of magnitude uncertainty in the value of the entrainment coefficient of 0.1 inferred from the Germeles-Drake extrapolation if the geometry of the flow is taken into account. Also, the top entrainment coefficient of 0.1 inferred by Germeles and Drake is sensitive to the value of C_E in the front spreading velocity equation (Equation II-10). If $C_E = 1.0$ is assumed, in contrast to $C_E = 2^{1/2}$ as suggested by Germeles-Drake, their extrapolation gives $c_3 = 0.01$ at the front velocity. Finally, the extrapolated value of $c_3 = 0.1$ would appear, in any case, to be applicable only to the top area near the cloud front (since it reflects the Froude number at the front) and should be smaller for those areas of the cloud top which are spreading at lower velocity.

Cox and Carpenter (1980) recommended modeling frontal entrainment using Equation II-12 with $\epsilon = 0.6$ and top entrainment using the following expressions

$$w_e = 0.15\, u_1 \qquad \text{for } Ri'' \to 0$$
$$w_e = 0.1\, u_1 / Ri'' \qquad \text{for } Ri'' \gg 1 \qquad \text{(II-15)}$$

where u_1 is the horizontal r.m.s. turbulence velocity of the wind flow and Ri" is defined as

$$Ri'' = \frac{g\Delta' L}{u_1^2} \qquad \text{(II-16)}$$

u_1 is assumed to be proportional to u_*, so that

$$u_1 = \left(\frac{u_1}{u_*}\right) u_* \qquad \text{(II-17)}$$

Values of u_1 / u_*, attributed to Pasquill (1974), of 3.0, 2.4, and 1.6 for very unstable, neutral, and very stable atmospheric flows respectively, were used. The turbulence scale length L is correlated with height above ground (cloud depth) and atmospheric stability using data from Taylor et al. (1970). Using the suggested values for u_1 / u_* along with estimates of L / h from Taylor et al., Equation II-15 can be rewritten in the form of Equations II-6 and II-7, along with a stability-dependent proportionality constant, as follows:

	w_e Vertical Entrainment Velocity	
Pasquill Stability Class	Ri" → 0	Ri" >> 1
B	0.45 u_*	3.0 u_*/Ri"
D	0.36 u_*	2.0 u_*/Ri"
F	0.24 u_*	0.7 u_*/Ri"

The Cox and Carpenter model changes to a Gaussian profile model when the cloud spreading velocity decreases to $u_f = u_a \frac{d\sigma_y}{dx}$ where $\sigma_y(x)$ is the crosswind dispersion coefficient for point source, passive plumes proposed by Pasquill and Gifford (Pasquill, 1974).

Fryer and Kaiser (1979) used the same top and frontal entrainment velocity models as Cox and Carpenter but suggested transition to a Gaussian dispersion model when either of the following two conditions apply:

$$u_f < 2.14\ u_a \left(\frac{h}{2}\right) \frac{d\sigma_y}{dx} \quad \text{and} \quad Ri < 0.1$$

or (II-18)

$$\Delta' < 8.16 \times 10^{-4}$$

Fay (1980) suggested considering both w_e and u_e proportional to u_f during the gravity flow-dominated regime ($u_f >> u_*$), so that

$$\dot{M}_a / \rho_a = c_4 u_f A_T + c_5 u_f A_F \qquad \text{(II-19)}$$

Based on his analysis of Ellison and Turner's (1959) laboratory experiments with steady stratified fluid layers flowing above or below a quiescent fluid, Fay suggested an upper limit of 0.01 for c_4, and based on his analysis of Simpson and Britter's (1979) gravity intrusion experiments, he suggested a value for c_5 of 0.05.

Picknett (1981) correlated the concentration and visible cloud dimension data from a series of instantaneous releases on land of approximately 40 m^3 of Freon-air mixtures ranging in initial relative density (ρ / ρ_a) from about 2.0 to 5.0. Picknett fitted the large initial entrainment inferred from the data using the frontal entrainment relation (Equation II-12) with $\varepsilon = 0.82$. He modeled top entrainment using Equation II-7 with $c_2 = 0.15$. Picknett terminated the gravity spreading phase, and transitioned to a Gaussian passive dispersion model when the Richardson number of the spreading layer decreased to $Ri_* = 7$.

Eidsvik's (1980) top hat model does not transition to a Gaussian passive dispersion model. Instead, the model uses air top entrainment relations incorporating Equation II-7 (dominant during the early gravity spread phase when $Ri_* >> 1$) and Equation II-6 (dominant during the later phase of the cloud dilution when density-driven flows have subsided, as indicated by $Ri_* \rightarrow 0$). Incorporating Eidsvik's suggested model parameter values and using a different Ri_*', his equation for vertical (top) entrainment is

$$w_e = \frac{0.39\ w}{1 + Ri_*' / 19.7} \qquad \text{(II-20)}$$

which in the absence of thermal convection effects (Eidsvik included recommended measures of convective turbulence velocities which are not considered at this point) is given by Equation II-5 with $n = 0.29$.

The friction velocity u_* is determined using Equation II-2 and a surface drag coefficient along with a characteristic velocity u calculated using Equation II-3; the constant c_* is dependent on the geometry of flow ($c_* = 2/3$ for axisymmetric and 1/2 for one-dimensional spreading). The Richardson number Ri_*' is then defined as

$$Ri_*' = \frac{g\Delta H}{w^2} \qquad \text{(II-21)}$$

Using Equations II-2, 3, and 9, the Richardson number Ri_*' can be expressed as

$$Ri_*' = \frac{u_f^2}{\frac{2}{E}\ (1/2\ c_f)((c_*\ u_f)^2 + u_a^2)} \qquad \text{(II-22)}$$

In the limit as $u_f / u_a << 1$,

$$w_e\Big|_{u_f << u_a} = 0.39\ w \qquad \text{(II-23)}$$

which is consistent with the assumed dependence of w_e on u_* given by Equation II-6.

For $u_f >> u_a$, however, w_e approaches (for $c_f << 1.0$, $C_E = 1.3$, and $c_* = 2/3$)

$$w_e\Big|_{u_f >> u_a} \cong 1.35\ c_f^{3/2}\ u_f \qquad \text{(II-24)}$$

Eidsvik cites recommended values for c_f of 2×10^{-3} for flow over water and 1.4×10^{-2} for flow over land. For this range, and with $C_E = 1.3$, $c_* = 2/3$, w_e given by Equation II-24 varies between $0.0001\ u_f$ and $0.002\ u_f$. It should be noted that Eidsvik's limiting (as $u_f >> u_a$) entrainment expression of Equation II-24, with a coefficient of order 10^{-4} to 10^{-3}, infers a different entrainment mechanism from that of Germeles' and Drake's suggested entrainment relation (Equation II-8). Eidsvik's model neglects entrainment due to shear at the interface (he indicates that Kelvin-Helmholtz instability might provide a mechanism for such entrainment, but assumes it to be effectively damped out because of the strong density stratification across the interface) whereas Germeles' and Drake's suggested entrainment is associated with the shear at the interface.

In a subsequent review of the box model formulation for HTAG dispersion, Fay and Ranck (1981) correlated the experimental data from HTAG wind tunnel releases by Hall (1979) and Meroney (1982) and field experiments by Feldbauer et al. (1972), van Ulden (1974), Picknett (1978), and Koopman et al. (1979, 1981) with a zero frontal entrainment ($c_f = 0$) and top entrainment velocity given by

$$w_e = \frac{c_1 c_2 u_*}{\sqrt{c_1^2 Ri_*^2 + c_2^2}} \qquad \text{(II-25)}$$

Fay and Ranck reported correlation of their model with the isothermal HTAG release data they analyzed which indicated $c_1 = 2.5$ and $c_2 = 0.5$. They stated that the model correlation with data for nonisothermal gases, which was primarily LNG experimental release data, indicated $c_1 = 2.5$ and $c_2 = 5.0$.

Finally, Fay (1984) has suggested that for initially compact clouds, i.e. where vertical and longitudinal initial dimensions are similar, there is rapid mixing during the period following release during which the buoyancy-dominated flow is controlling. Based primarily on his analysis of the no-wind HTAG release data of Hall (1982), Meroney and Lohmeyer (1982), and Havens and Spicer (1983),

Fay proposed modeling the entrainment during the buoyancy-dominated flow period with the relation

$$\dot{M}_a / \rho_a = 0.5\ V^{5/6}\ g \left[\frac{\rho - \rho_a}{\rho_a}\right]^{1/2} \qquad \text{(II-26)}$$

which reflects the assumption of a constant, global entrainment rate with a constant cloud height. For releases in wind, Fay proposes

$$\dot{M}_a / \rho_a = 0.6\ V^{5/6}\ (g\Delta')^{1/2} + c_6(\pi R^2)\ u_* / Ri_* \qquad \text{(II-27)}$$

with $c_6 = 0.6$, as representative of the dispersion in the previously mentioned no-wind releases as well as near instantaneous wind tunnel releases reported by Hall (1979, 1982) and Meroney and Lohmeyer (1982).

II.1.2 Non-Hydrostatic Approximation Box Models

van Ulden (1979), Meroney and Lohmeyer (1982), and van Ulden (1983) have proposed methods for modeling the gravity slumping/spreading phase of instantaneously released HTAG clouds. These methods incorporate a momentum balance to describe the acceleration from rest and subsequent motion of a HTAG flow.

van Ulden (1979) analyzed a nonstationary gravity current resulting from an instantaneous release of a mass M of HTAG. Described here is van Ulden's analysis, applied to the axisymmetric lateral spreading of an instantaneously released "cloud."

An energy balance on a control volume sufficiently large to contain all influences of the spreading cloud requires that the total energy remain unchanged during the spreading process:

$$\frac{d\,PE}{dt} + \frac{d\,KE}{dt} + \frac{d\,TE}{dt} + \frac{d\,IE}{dt} = 0 \qquad \text{(II-28)}$$

In Equation II-28, PE and KE represent the potential and kinetic energy of the cloud, respectively. TE represents the turbulent kinetic energy, and IE represents the irreversible conversion of kinetic (and turbulent) energy to internal thermal energy.

If the volume, mass, and density of the cloud are initially V_i, M_i, and ρ_i, respectively, and the density of surrounding air is ρ_a, the buoyancy of the gas is $g\left(\frac{\rho_i - \rho_a}{\rho_a}\right)V_i$, and the potential energy is

$$PE = (M_i - \rho_a V_i)\, g\, H/2 = g\,\Delta M\, H/2 \qquad \text{(II-29)}$$

Since ΔM, the amount by which the initial gas mass exceeds that of an equivalent volume of air, is constant, it follows that

$$\frac{d\,PE}{dt} = \frac{1}{2}\, g\,\Delta M \frac{dH}{dt} \qquad \text{(II-30)}$$

If it is assumed that the spreading gas cloud assumes the shape of a right cylinder,

$$\frac{dH}{dt} = -\frac{2H}{R}\frac{dR}{dt} + \frac{dV/dt}{\pi R^2}$$

$$= -2\,H/R\frac{dR}{dt} + w_t \qquad \text{(II-31)}$$

The first term on the R.H.S. of Equation II-31 represents the downward velocity of the cylinder top surface which would occur if the volume of the cylinder remained constant, and the second term represents the upward velocity of the top surface due to an increase in volume by entrainment of air.

The kinetic energy of the cylindrically shaped gas-air mixture volume is given by

$$KE = \frac{\rho(t)}{2}\int_0^R 2\pi r H\,(u(r))^2 dr \qquad \text{(II-32)}$$

Continuity requirements dictate that $u(r) = \frac{r}{R}u_f$, so that Equation II-32 gives

$$KE(t) = \frac{1}{4}M u_f^2 \ , \qquad \text{(II-33)}$$

and it follows that

$$\frac{dKE}{dt} = \frac{1}{2}M u_f \frac{du_f}{dt} + \frac{1}{4}u_f^2\frac{dM}{dt} \qquad \text{(II-34)}$$

Since $dM/dt = \rho_a \frac{dV}{dt} = \pi R^2 \rho_a w_t$, Equation II-34 can be written as

$$\frac{dKE}{dt} = \frac{1}{2}M u_f \frac{du_f}{dt} + \frac{1}{4}u_f^2 M \frac{\rho_a w_t}{\rho H} \qquad \text{(II-35)}$$

A balance equation for energy associated with turbulence in the flow is proposed:

$$\frac{dTE}{dt} = \text{turbulent energy produced by shear, SP} \qquad \text{(II-36)}$$

- turbulent energy transformation into potential energy due to entrainment, "buoyant destruction," BD
- turbulent energy dissipation into thermal energy, $\frac{d\,IE}{dt}$

It is assumed that the production of fluid turbulence by shear occurs mainly at the leading edge, and contributions from friction at the cloud lower surface and upper surface behind the leading edge are neglected. Since the advancing cloud front encounters undisturbed air at a rate proportional to $2\pi RHu_f$, and the undisturbed air must be accelerated to a velocity of the order of u_f, van Ulden suggests that the rate of turbulent energy production by shear be represented as

$$SP = \beta_1(2\pi RHu_f)(\tfrac{1}{2}\rho_a u_f^2) = \beta_1 \frac{\rho_a}{\rho}\frac{M}{R} u_f^3 \qquad \text{(II-37)}$$

Assuming that the buoyant destruction term in Equation II-36 is just equal to the potential energy gain by entrainment of air and substituting Equations II-35, 36, 37 into Equation II-28, the energy balance equation for the "cloud" is written to obtain an equation for the front velocity

$$\frac{du_f}{dt} + \frac{1}{2}u_f \frac{\rho_a w_t}{\rho H} - \frac{2g\Delta\rho H}{\rho R} + \frac{2\beta_1}{R}\frac{\rho_a}{\rho} u_f^2 = 0 \qquad \text{(II-38)}$$

If air entrainment is neglected and the motion is assumed stationary ($\frac{du_f}{dt} = 0$), Equation II-38 reduces to

$$u_f = \left[\frac{g}{\beta_1}\frac{\Delta\rho}{\rho_a} H\right]^{1/2} \qquad \text{(II-39)}$$

and the hydrostatic spreading velocity model is retrieved.

Meroney and Lohmeyer (1982) used Equation II-38 as developed by van Ulden, modified to reflect the assumption that the turbulent energy production rate at the cloud edge scales with the cloud density rather than air density:

$$\text{i.e.} \quad SP = \beta_1 M \frac{u_f^3}{R} \quad \text{instead of} \quad \beta_1 \frac{\rho_a}{\rho} M \frac{u_f^3}{R} \qquad \text{(II-40)}$$

Meroney and Lohmeyer assumed that during the gravity spreading phase of the HTAG motion, entrainment would occur at the top and front surfaces of the cloud as in Equation II-11 and further represented w_e and u_e as proportional to the front velocity u_f

$$\begin{aligned} u_e &= c_1' u_f \\ w_e &= c_2' u_f \end{aligned} \qquad \text{(II-41)}$$

Then

$$\frac{dV}{dt} = 2 c_1' \pi R H u_f + c_2' \pi R^2 u_f \qquad \text{(II-42)}$$

Replacing the total entrainment rate (Equation II-31), Equation II-38 was expressed by Meroney and Lohmeyer as

$$\frac{du_f}{dt} + \frac{\rho_a u_f^2}{\rho}\left[\frac{c_2'}{2H} + \frac{c_1'}{R}\right] - \frac{2 g \Delta\rho H}{\rho R} + \frac{2\beta_1}{R} u_f^2 = 0 \qquad \text{(II-43)}$$

Meroney and Lohmeyer conducted a series of instantaneous releases of hemicylindrical volumes of Freon-air mixtures in calm air and, based on the analyses thereof, suggested the following values for the constants in Equation II-43: $\beta_1 = 0.9$, $c_1' = 0.1$, $c_2' = 0.1$.

van Ulden (1983) proposed a new bulk model which also incorporates a balance equation for momentum to describe the development of an entraining gravity current in rectangular coordinates. The current is divided into a "head" and "tail" with characteristic lengths and velocities as illustrated in Figure II.2. Considering a radial axisymmetrical current, the front moves with velocity $u_f(t)$ at position $R(t)$. The tail region, which extends to $r = R_h$, advances with the layer-averaged velocity $u_h(t)$. The height (or depth) of the tail and head regions are H_t and H_h respectively. In the following van Ulden's development is adapted for a cylindrical coordinate system.

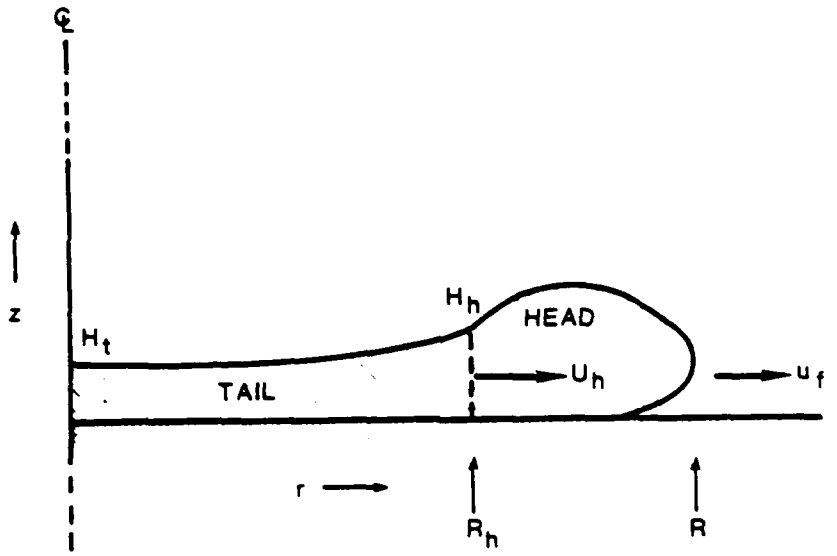

Figure II.2 The unsteady gravity current (van Ulden, 1983)

The radial component momentum balance on the gravity spreading cloud is represented as

$$\frac{dP}{dt} = F_p \left\{\begin{array}{l}\text{static pressure force, due to negative} \\ \text{buoyancy of the gravity current}\end{array}\right\}$$

$$+ F_D \left\{\begin{array}{l}\text{dynamic force, equal to the sum of the} \\ \text{drag force on the head of the current and} \\ \text{the lift force arising from asymmetry of} \\ \text{the ambient flow around the current head}\end{array}\right\}$$

$$+ F_a \left\{\begin{array}{l}\text{force due to acceleration/deceleration} \\ \text{reaction by the ambient fluid}\end{array}\right\} \qquad \text{(II-44)}$$

The static pressure force, obtained by integrating the static pressure over the boundary of the current, is

$$F_p = (\tfrac{1}{2} g \Delta\rho H_t)(2\pi R H_t) = \pi g \Delta\rho R H_t^2 \qquad \text{(II-45)}$$

Neglecting the shear stress at the bottom, the dynamic force on the current is the sum of the drag force on the head of the current and the lift force that arises due to asymmetry in the ambient flow around the head. The drag force is represented as

$$F_D = -\frac{d_v}{2} \rho_a u_f^2 (2\pi R_h a_v H_h) = -a_v d_v \pi R H_h \rho_a u_f^2 \qquad \text{(II-46)}$$

where d_v is an effective drag coefficient and the constant a_v is an empirical ratio of the average head depth H_1 to H_h ($a_v = H_1 / H_h$).

The horizontal acceleration reaction F_a is approximated by the reaction to an accelerating elliptical cylinder with an aspect ratio H/R (Batchelor, 1967):

$$F_{a_R} = -\frac{d}{dt} (k_1 \rho_a \pi R H^2 u_f) \qquad \text{(II-47)}$$

and the vertical acceleration reaction is represented as

$$F_{a_z} = - \frac{d}{dt} (k_2 \rho_a \pi R H^2 u_f) \qquad \text{(II-48)}$$

where k_1 and k_2 are coefficients of order one. Using a single constant, Equations II-47 and II-48 give

$$F_a = e_v \pi \rho_a \frac{d(R H^2 u_f)}{dt} \qquad \text{(II-49)}$$

Using Equations II-45, 46, and 49, the momentum balance (Equation II-44) becomes

$$\frac{dP}{dt} = \pi g \Delta\rho R H_t^2 - a_v d_v \pi \rho_a R H_h u_f^2 - e_v \pi \rho_a \frac{d(R^2 H u_f)}{dt} \qquad \text{(II-50)}$$

As before (1979), van Ulden assumed that the potential energy decrease due to slumping of the cloud is offset by the production of kinetic energy, which through the action of shear, is partly transformed to turbulent kinetic energy. Part of the turbulent kinetic energy is transformed back into potential energy due to entrainment of air by the cloud. van Ulden assumes that this "buoyant destruction" of kinetic energy is proportional to the rate of production of turbulent kinetic energy, and appealed to the analysis of Simpson and Britter (1979) to argue that the turbulent kinetic energy production rate should scale as $\pi \rho_a H R u_f^3$. Then,

$$\frac{1}{2} g \Delta\rho H \frac{dV}{dt} = \epsilon \pi \rho_a H R u_f^3 \qquad \text{(II-51)}$$

which can be written

$$\frac{dV}{dt} = \frac{\varepsilon(2\pi RH)u_f}{\left[\frac{g\Delta\rho H}{\rho_a u_f^2}\right]} = \frac{\varepsilon(2\pi RH)u_f}{Ri_*} \qquad \text{(II-52)}$$

where ε is an empirically determined coefficient.

The volume integral

$$V = 2\pi \int_0^R h(r,t) r dr \qquad \text{(II-53)}$$

where $h(r,t)$ is to be expressed in terms of H_h and H_t, and the momentum integral

$$P = 2\pi \int_0^R \rho\, u(r,t)\, h(r,t)\, r\, dr = P_t + P_h \qquad \text{(II-54)}$$

are then approximated with separate analyses of the head and tail of the current.

In the tail of the current, the shallow water equations are assumed applicable. It is assumed that the shape of the current is quasi-stationary in time, and the layer-averaged density difference is assumed horizontally uniform. It follows that the volume and momentum of the tail are given by

$$V_t = \pi R_h^2 (H_t + H_h) / 2. \qquad \text{(II-55)}$$

$$P_t = \frac{2}{5}\rho (\frac{2}{3} H_t + H_h) \pi R_h^3 \frac{u_f}{R} \qquad \text{(II-56)}$$

A momentum balance for the head region, assuming quasi-steady state, indicates that the static and dynamic pressure forces on the head should be balanced by the net flux of momentum due to flow into and out of the head. The static pressure and drag are, respectively

$$F_p = (1/2\, g \Delta\rho H_h)(2\pi R_h H_h) = \pi g \Delta\rho R_h H_h^2 \qquad \text{(II-57)}$$

$$F_D = - d_v (1/2\, \rho_a u_f^2)[2\pi R_h (a_v H_h)]$$

$$= - a_v d_v \rho_a u_f^2 \pi R_h H_h \qquad \text{(II-58)}$$

Near the surface, the inward flow (u_4 in Figure I.2) carries momentum into the head, while the return flow (u_3 in Figure I.2) carries momentum out of the head. Assuming $u_3 \simeq u_4$, $H_4 \simeq \frac{1}{2} H_h$, and $u_4 \simeq \delta_v u_f$, the momentum flux into the head is approximately

$$Q_h \simeq \delta_v^2 \rho_a u_f^2 [2\pi R_h H_h] \qquad \text{(II-59)}$$

Upon rearranging, the momentum balance on the head gives

$$\frac{\rho_a u_f^2}{g \Delta\rho H_h} = 1. / (d_v a_v - 2\delta_v^2)$$

$$= C_E^2 \qquad \text{(II-60)}$$

with $\delta_v = 0.2$, $d_v = 0.64$; Equation II-60 then specifies the head velocity boundary condition. The volume of the head is determined by assuming that the head length scales with H_1, and it follows that

$$R - R_h = b_v H_1 \tag{II-61}$$

where b_v is an empirical constant. The volume of the head becomes

$$V_h = \pi a_v b_v (R + R_h) H_h^2 \tag{II-62}$$

If the layer-averaged velocity is assumed to increase linearly with r, it follows that

$$u_h = u_f \left[\frac{R_h}{R}\right] \tag{II-63}$$

and

$$P_h = \frac{2\pi}{3} \rho a_v \frac{u_f H_h}{R} \left[R^3 - R_h^3\right] \tag{II-64}$$

Along with the definition of u_f,

$$\frac{dR}{dt} = u_f \tag{II-65}$$

Equations II-50, 52, 60, 61, 63, and 65 can be solved to determine ρ, H_t, H_h, V, P_h, and P_t.

II.1.3 Comparison of Box Model Predictions for No-Wind Releases

Figure II.3 illustrates the substantial differences in dilution of a 1 m^3 cylinder (H/D = 1) of Freon-12 gas (sp. gr. = 4.19) instantaneously released in calm air, as predicted by the models proposed by van Ulden (1974), Germeles-Drake (1975), Cox-Carpenter (1979), Fryer and Kaiser (1979), Eidsvik (1980), Fay (1980), Meroney and Lohmeyer (1982), van Ulden (1983), and Fay (1983) are described in the previous two sections.

Figure II.3 also summarizes the cloud average concentration vs. cloud radial extent obtained by spatial integration of the radial and vertical cloud concentrations determined from the laboratory calm-air heavy gas releases conducted under this contract (Volume II, this report). Finally, the average cloud concentration decay with distance predicted with a model adapted from van Ulden (1983), which incorporates empirical constant values to fit the experimentally determined cloud average concentration decay with distance (or time), is also shown in Figure II.3. This model, which has been incorporated in the DEGADIS model recommended herein, will be described in detail in Section III.

II.2 Advanced Similarity Models

Experimental concentration data from passive ground level source plume dispersion experiments are generally well described as Gaussian (Hanna, 1982; Pasquill, 1983). The spatial distribution of concentration from a point source is represented as

$$c(x,y,z) = c_c(x) \exp\left[-\frac{1}{2}\left(\frac{y}{\sigma_y}\right)^2 - \frac{1}{2}\left(\frac{z}{\sigma_z}\right)^2\right] \qquad \text{(II-66)}$$

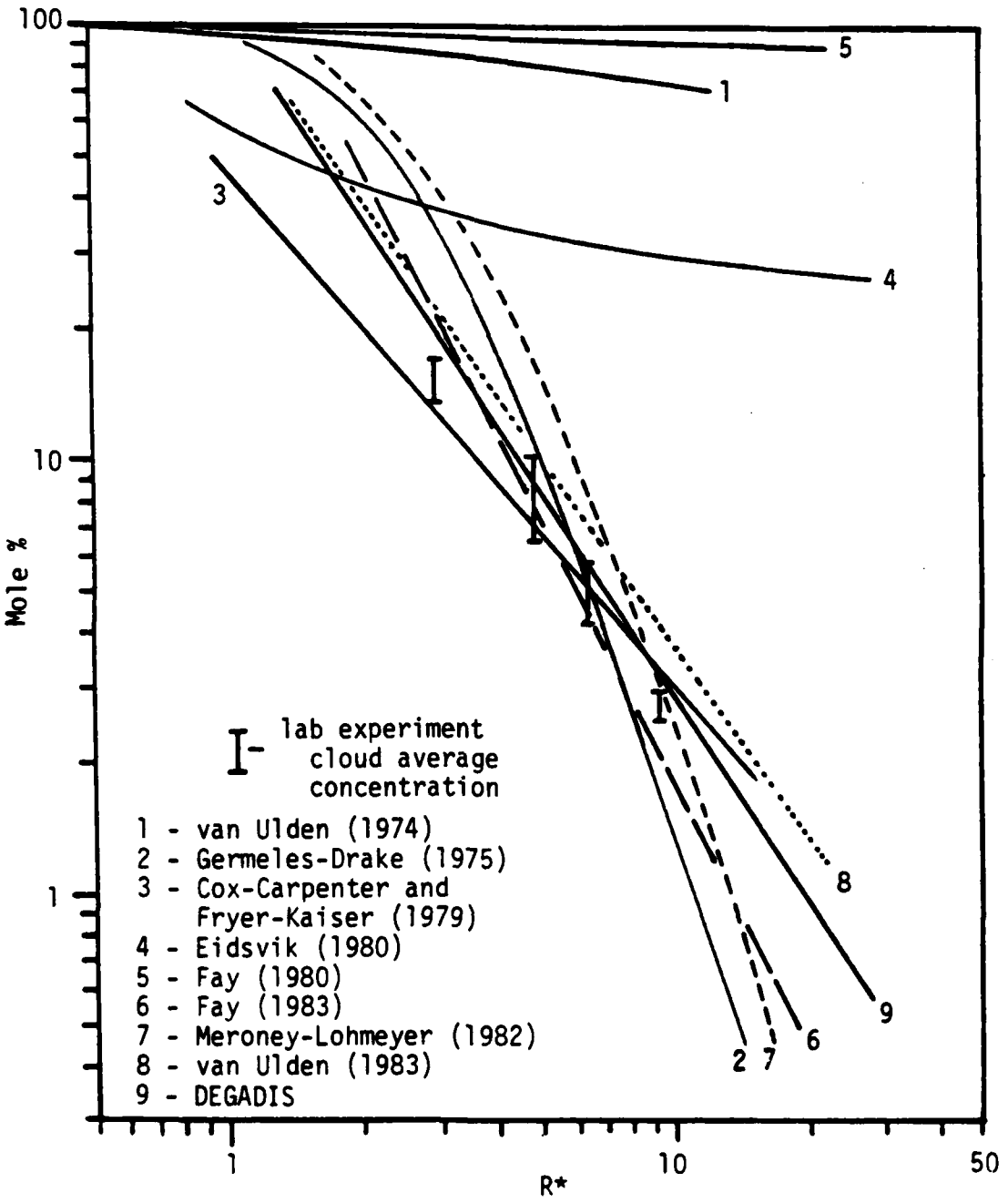

Figure II.3. Box model predictions for instantaneous 1 m^3 Freon-12 release in calm air.

where $c_c(x)$ is the centerline concentration at ground level ($z = 0$) and σ_y, σ_z are the standard deviations of the concentration distribution in the y and z directions. Correlations of σ_y and σ_z as functions of distance downwind of the plume source and atmospheric stability have been developed based on a combination of theoretical and field experimental data. The most frequently used correlations of dispersion data in terms of σ_y and σ_z are based on field atmospheric tracer dispersion experiments conducted during the 1950s and 1960s. The Project Prairie Grass experiments (Haugen, 1959) involved concentration measurements at distances to about 1 km downwind of near ground level, point source, steady releases of a tracer material; they are the basis for the σ_y and σ_z correlations developed by Pasquill (1961) and adapted by Gifford (1961, 1968, 1976) into the form given in Figure II.4. Analytical formulas for σ_y and σ_z, based on the data from the Prairie Grass experiments as well as experimental data from passive, elevated ($z = 108$ m) tracer release experiments conducted at Brookhaven National Laboratory, have been proposed by Smith (1968), Briggs (1973), and Pasquill (1975). Laboratory data from stably stratified shear flow experiments also support a Gaussian description of vertical concentration profiles (McQuaid (1976)).

The assumption of a Gaussian similarity form for vertical and horizontal concentration profiles in a HTAG plume was proposed by te Reile (1977) and further developed by Colenbrander (1980, 1983). Both considered a model for atmospheric dispersion of HTAG emitted from an idealized rectangular source of width 2B and length L as illustrated in Figure II.5. The gas source center is at $x = y = z = 0$ with x representing downwind direction, and y and z horizontal (crosswind) and vertical directions respectively. Power law profiles for the velocity and gas concentration are assumed:

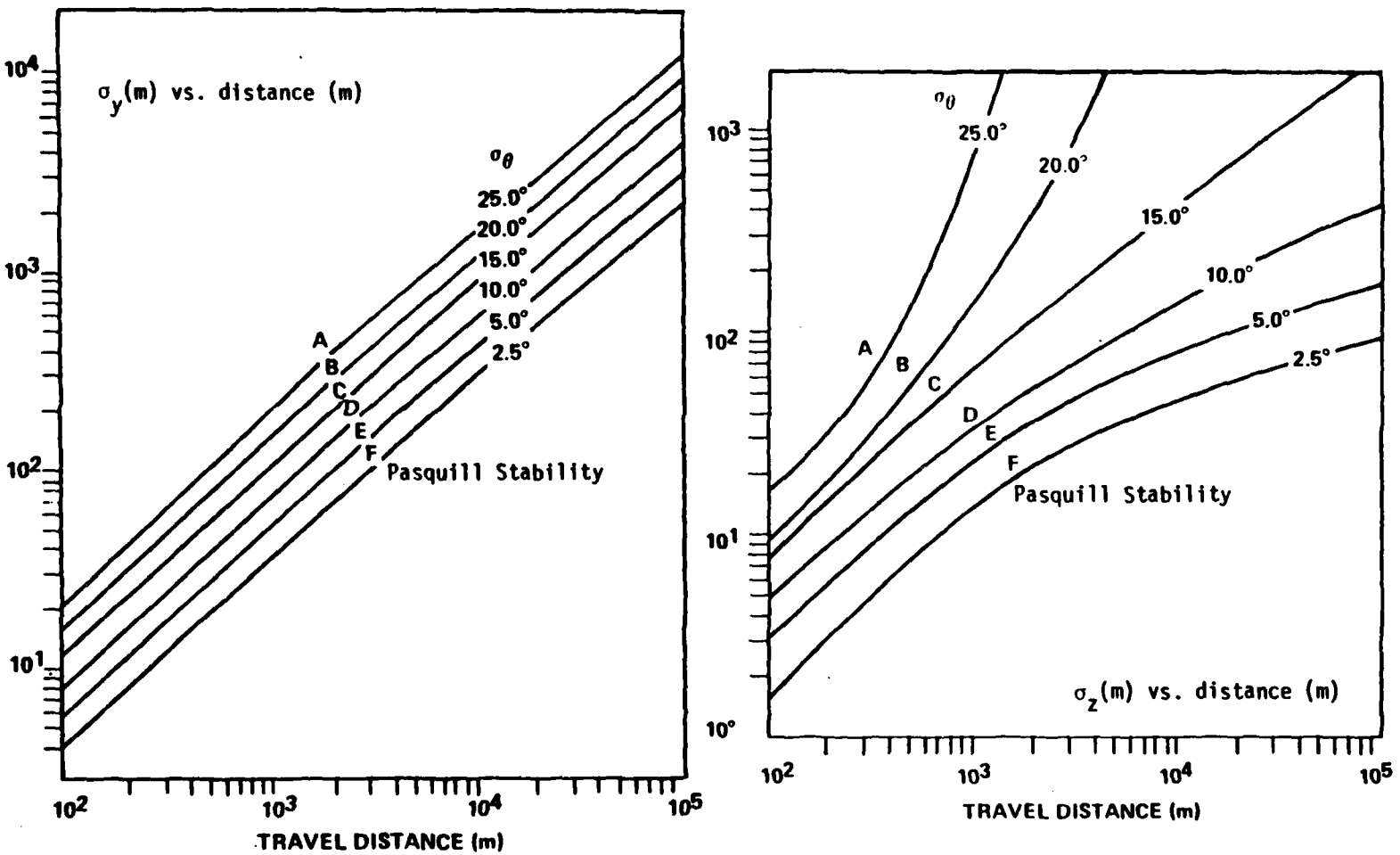

Figure II.4. Field data correlations for σ_y and σ_z for passive dispersion.

$$u_x = u_0 (z / z_0)^{\alpha} \qquad \text{(II-67)}$$

$$c(x,y,z) = c_c(x) \exp \left[-\left(\frac{|y| - b(x)}{S_y(x)} \right)^2 - \left(\frac{z}{S_z(x)} \right)^{1+\alpha} \right]$$

$$\text{for } |y| > b \qquad \text{(II-68)}$$

$$c(x,y,z) = c_c(x) \exp \left[-\left(\frac{z}{S_z(x)} \right)^{1+\alpha} \right]$$

$$\text{for } |y| < b$$

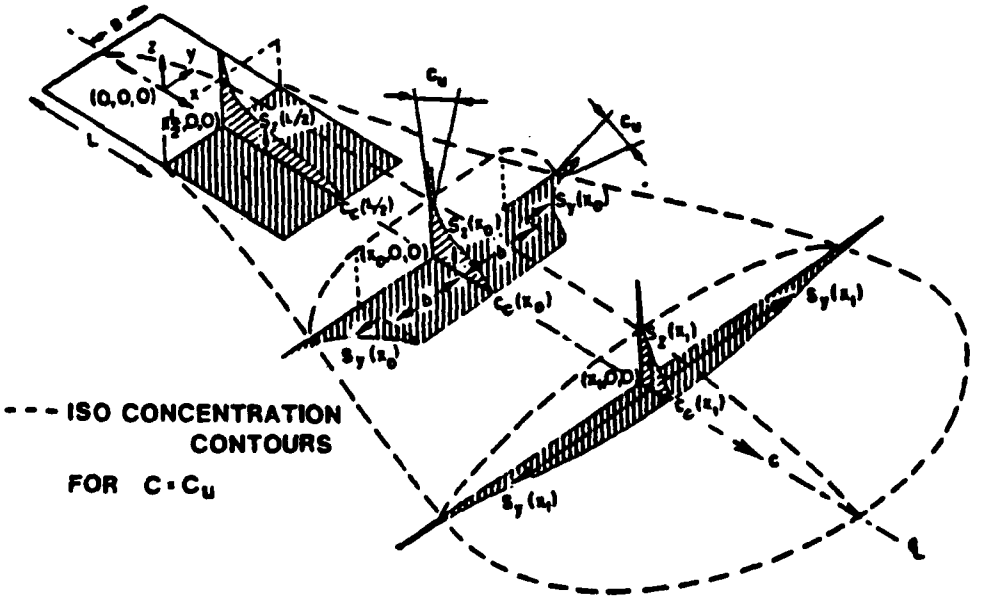

Figure II.5. Form of assumed concentration profiles--
te Reile (1977) and Colenbrander (1980).

The concentration profile has a center section of width 2b which is represented as dispersing only in the vertical direction to account for the relatively uniform concentration field which develops over a uniform area source. Horizontal diffusion processes are associated with gas concentration gradients at the "edge" of the uniform center section. As a result of the similarity assumptions in Equations II-67 and II-68, the variables c_c, b, S_y, and S_z are functions of downwind distance (x) only and are therefore constrained by ordinary differential equations.

Both te Reile and Colenbrander suggested modeling the vertical and horizontal dispersion scales S_z and S_y by requiring that the concentration profiles satisfy the corresponding two-dimensional diffusion equations

$$u_x \frac{\partial c}{\partial x} = \frac{\partial}{\partial z}\left[K_z \frac{\partial c}{\partial z}\right] \qquad \text{(II-69)}$$

and

$$u_x \frac{\partial c}{\partial x} = \frac{\partial}{\partial y}\left[K_y \frac{\partial c}{\partial y}\right] \qquad \text{(II-70)}$$

with turbulent diffusivities described by

$$K_z = \frac{k\, u_* \, z}{\phi\,(Ri_*)} \qquad \text{(II-71)}$$

and

$$K_y = K_0\, u_x\, W^{\gamma_1} \qquad \text{(II-72)}$$

Colenbrander proposed the function ϕ

$$\phi(Ri_*) = 0.74 + 0.25\, Ri_*^{0.7} + 1.2 \times 10^{-7}\, Ri_*^{3} \qquad \text{(II-73)}$$

based on his analysis of HTAG entrainment velocities measured by McQuaid (1976) and Kantha et al (1977) (see Section I).

Equation II-70 models the horizontal turbulent diffusion as a gradient transfer process. As previously stated, such a representation is questionable because the horizontal scales of turbulence may not be small compared to the time average plume width. Consequently, the determination of S_y in Equation II-70 as a function of x is forced to reflect results of experimental data on horizontal dispersion of passive plumes from point sources, such as the $\sigma_y(x)$ correlations developed by Pasquill and Gifford. te Reile and Colenbrander assumed that a horizontal turbulent diffusivity is proportional to the mean wind velocity and to the "width" of the cloud raised to a power γ_1 where the width is defined (see Figure II.5) to be

$$W = b + \frac{\sqrt{\pi}}{2} S_y \qquad \text{(II-74)}$$

Noting that $S_y = \sqrt{2}\ \sigma_y$ and representing the σ_y vs. x correlation of Figure II.4 by $\sigma_y = \delta x^{\beta}$ where δ and β are constants dependent on the Pasquill-Gifford stability class, Equations II-70, II-72, and II-74 determine an equation for S_y. Colenbrander modeled the lateral growth of the plume due to gravity spreading using the gravity intrusion velocity specification of Equation II-9:

$$\frac{dW}{dt} = \sqrt{\frac{g(\rho(c_c) - \rho_a(z \approx 0))}{\rho(c_c)} H_{EFF}} \qquad \text{(II-75)}$$

with the effective depth H_{EFF} defined by

$$H_{EFF} = \frac{1}{c_c} \int_0^{\infty} c\, dz = \frac{\Gamma(1/1+\alpha)}{1+\alpha} S_z \qquad \text{(II-76)}$$

Defining a mean downwind advection rate u_{EFF}

$$u_{EFF} = \frac{\int_0^\infty c\, u_x\, dz}{\int_0^\infty c\, dz} = u_0 \left(\frac{z}{z_0}\right)^\alpha \frac{1}{\Gamma(1/1+\alpha)} \qquad \text{(II-77)}$$

it follows that the downwind lateral growth of the cloud can be modeled by

$$\frac{dW}{dx} = \frac{1}{u_{EFF}} \frac{dW}{dt} \qquad \text{(II-78)}$$

Equations which determine S_y, S_z, and b as a function of x are integrated until b = 0 (denoted by $x = x_t$). At that time, lateral gravitational spreading of the cloud is terminated, and S_y at greater distances is specified by the relation:

$$S_y = \sqrt{2}\, \sigma_y = \sqrt{2}\, \delta(x + x_v)^\beta \qquad \text{(II-79)}$$

where x_v is the virtual point source location determined from the value of S_y at $x = x_t$.

Finally, the total mass flux of gas for a steady release is independent of x and given by

$$E = \int_0^\infty \int_{-\infty}^\infty c\, u_x\, dx\, dy = \frac{2\, c_c(x)\, u_0\, S_z^{1+\alpha}\, W}{(1+\alpha)\, z_0^\alpha} \qquad \text{(II-80)}$$

For a given gas source rate E, $c_c(x)$ is determined once values of S_y, S_z, and b are known.

III. FORMULATION OF THE DENSE GAS DISPERSION (DEGADIS) MODEL FOR THE U.S. COAST GUARD HAZARD ASSESSMENT COMPUTER SYSTEM (HACS)

The DEGADIS (DEnse GAs DISpersion) model is an adaptation of the Shell HEGADAS model described by Colenbrander (1980) and Colenbrander and Puttock (1983). DEGADIS also incorporates some techniques used by van Ulden (1983). If the primary source release rate exceeds the maximum atmospheric takeup rate, a HTAG blanket is formed over the primary source. This near-field, buoyancy-dominated regime is modeled using a lumped parameter model of a HTAG "secondary source" cloud which incorporates air entrainment at the gravity-spreading front using a frontal entrainment velocity. If the primary source release rate does not exceed the maximum atmospheric takeup rate, the released gas is taken up directly by the atmosphere and dispersed downwind. For either source condition, the downwind dispersion phase of the calculation assumes a power law concentration distribution in the vertical direction and a modified Gaussian profile in the horizontal direction with a power law specification for the wind profile (Figure III.1). The source model represents a spatially averaged concentration of gas present over the primary source, while the downwind dispersion phase of the calculation models an ensemble average of the concentration downwind of the source.

III.1 HTAG Source Cloud Formation

A lumped parameter model of the formation of the HTAG source cloud or blanket, which may be formed from a primary source such as an evaporating liquid pool or otherwise specified ground level emission source, or by an initially specified gas volume of prescribed dimensions for an instantaneous release, is illustrated in Figure III.1. The gas blanket is represented as a cylindrical gas volume

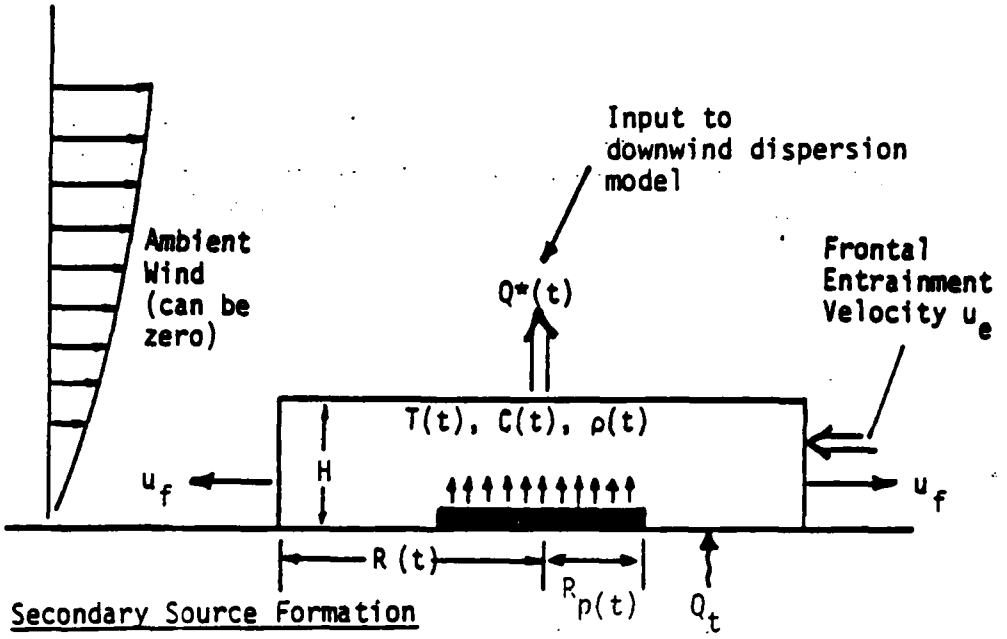

$$c(x,y,z) = c_c(x)\exp\left[-\left(\frac{|y|-b(x)}{S_y(x)}\right)^2 - \left(\frac{z}{S_z(x)}\right)^{1+a}\right], |y| > b$$

$$c(x,y,z) = c_c(x)\exp\left[-\left(\frac{z}{S_z(x)}\right)^{1+a}\right], |y| \le b$$

$$u_x = u_0\left(\frac{z}{z_0}\right)^a$$

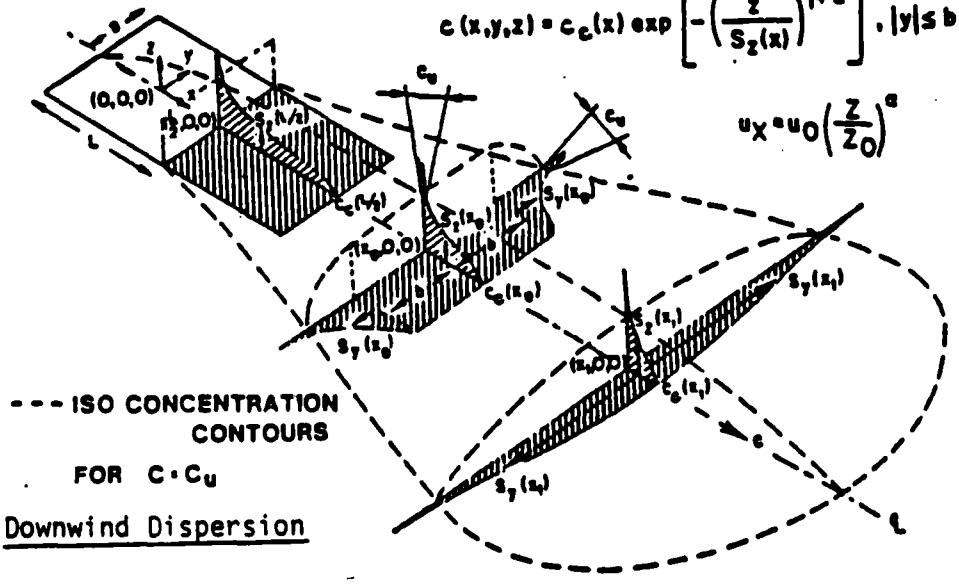

Figure III.1. Schematic diagram of HACS-DEGADIS HTAG dispersion model.

which spreads laterally as a density-driven flow with entrainment from the top of the source blanket by wind shear and air entrainment into the advancing front edge. The source blanket will continue to grow over the primary source until the atmospheric takeup rate from the top is matched by the air entrainment rate from the side and, if applicable, by the rate of gas addition from under the blanket. Of course, the blanket is not formed if the atmospheric takeup rate is greater than the evolution rate of the primary source. For application of the downwind calculation procedure, the blanket is modeled as being stationary over the center of the source ($x = 0$).

III.1.1 Extent

If a HTAG blanket is present, the emission rate from the blanket is the maximum atmospheric takeup rate. That is, for $E(t) / \pi R_p^2(t) > Q_{*max}$, a *source blanket* is formed over the liquid source. The blanket frontal (spreading) velocity is modeled as

$$u_f = C_E \sqrt{g\left(\frac{\rho - \rho_a}{\rho_a}\right) H} \qquad \text{(III-1)}$$

where ρ is the average density of the source blanket and is applicable only for $\rho > \rho_a$; the value of C_E used is 1.15, based on measurements of cloud spreading velocity (Volume II). This gravity intrusion relationship will overpredict velocities for instantaneous, aboveground releases since no initial acceleration phase is included. In this case, the following procedure adapted from van Ulden (1983) is recommended.

For instantaneous gas releases, the radially symmetric cloud is considered to be composed of a tail section with height H_t and radius R_h and a head section with height H_h. A momentum balance is used to account for the acceleration of the cloud from rest

exhibited for experiments such as this work (Volume II) and the British Health and Safety Executive's Thorney Island Trials (Section IV.6) described by McQuaid (1983). Since this area of the model is meant to describe the near-field buoyancy-dominated flow regime, the effect of any ambient momentum will be ignored. There are three main forces acting on the cloud including: a static pressure force (F_p), a dynamic drag force (F_d), and a force which accounts for the acceleration reaction of the ambient fluid represented as a rate of virtual momentum change with respect to time $\left(-\frac{dP_v}{dt}\right)$. Denoting the momentum of the head and tail as P_h and P_t respectively, the momentum balance becomes

$$\frac{dP}{dt} = \frac{d}{dt}(P_h + P_t) = F_p + F_d - \frac{dP_v}{dt}$$

or

$$\frac{d}{dt}(P_h + P_t + P_v) = F_p + F_d$$

The terms in the momentum balance are evaluated differently for early times before a gravity current head has developed and for times after the head has developed (Figure II.2) as described in Section II.1.2, Equations II-44 - 65.

For early times, some earlier simplifying assumptions do not apply. In order to model the initial cloud shape, the tail and head height are considered constant with respect to radius. The momentum balance on the cloud is given by

$$\frac{d}{dt}[P_h + P_t] = \pi g(\rho - \rho_a)\,[R_h\, H_t^2 + a_v b_v\, H_h^3] - \pi\, a_v d_v\, \rho_a R H_h\, u_f^2 - \frac{dP_v}{dt} \qquad \text{(III-2)}$$

where the first term on the right-hand side represents the static pressure force on the head and the second term represents the drag force on the bottom surface of the cloud. A third force is an acceleration reaction by the ambient fluid which is represented by

$$\frac{dP_v}{dt} = e_v \pi \rho_a \frac{d(RH^2 u_f)}{dt} \qquad \text{(III-3)}$$

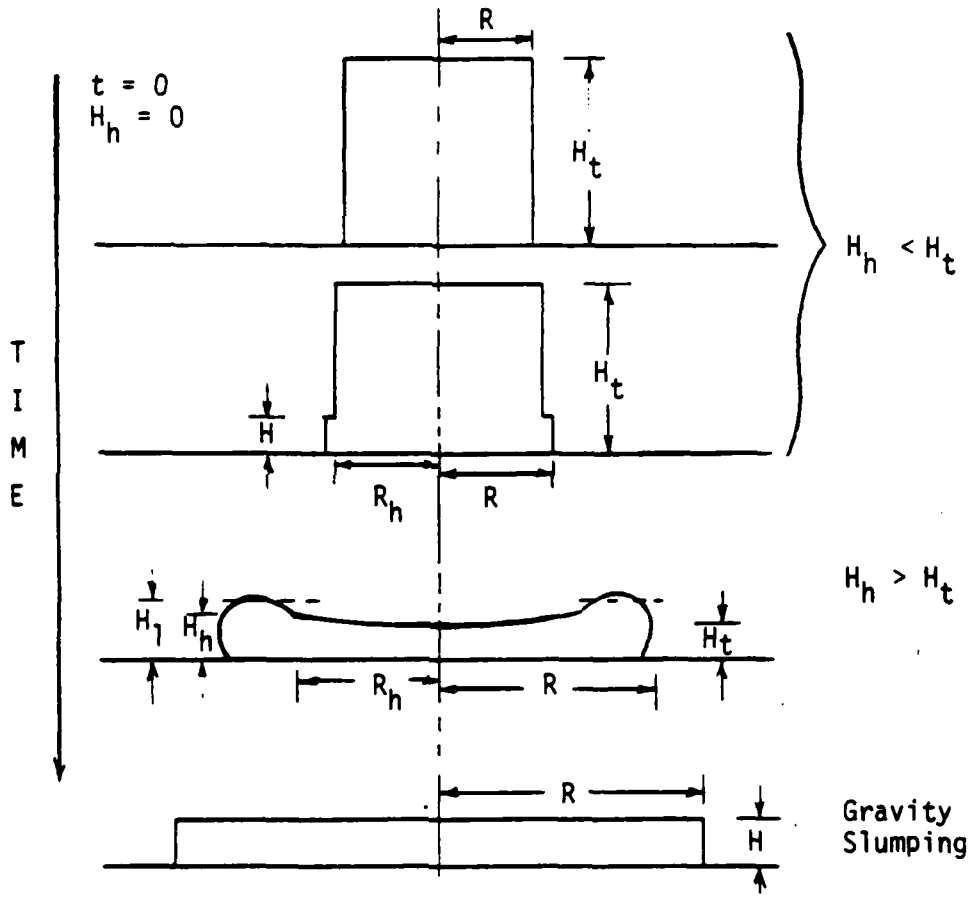

Figure III.2. Schematic diagram of a radially spreading cloud.

The dimensions of the head are determined by

$$R_h = R - a_v b_v H_h \qquad \text{(III-4)}$$

and

$$H_h = \left(\frac{u_f}{C_E}\right)^2 \Big/ [g(\rho - \rho_a)/\rho_a] \qquad \text{(III-5)}$$

The constants a_v, b_v, d_v, and e_v are assigned values 1.3, 1.2, 0.64, and 20., respectively, based on analysis of the still-air HTAG release experiments described in Section VI. When the height of the tail H_t is assumed uniform with respect to radius, it follows that

$$H_t = \left[\frac{M}{\rho} - \pi a_v^2 b_v (R + R_h) H_h^2\right] \Big/ (\pi R_h^2) \qquad \text{(III-6)}$$

where M is the total mass of the cloud. The momentum of the head P_h and tail P_t are determined by

$$P_h = \frac{2}{3}\pi a_v \frac{\rho H_h (R^3 - R_h^3)}{R} u_f \qquad \text{(III-7)}$$

and

$$P_t = \frac{2}{3}\pi \frac{\rho H_t R_h^3}{R} u_f \qquad \text{(III-8)}$$

Equations III-2 through III-8 determine the momentum of the blanket as a function of time, and thus the frontal velocity u_f. The cloud accelerates from rest because $H_h = 0$ initially; when the cloud accelerates to the point that $H_h \geq H_t$, the frontal velocity is determined from Equations II-44 through II-65 using the values of the constants a_v, b_v, d_v, and e_v given above. When the frontal velocity from the momentum balance is the same as Equation III-1, the momentum balance is no longer applied and the frontal velocity is given by Equation III-1.

The blanket radius R as a function of time is determined by

$$\frac{dR}{dt} = u_f \qquad \text{(III-9)}$$

For ground level sources, the blanket spreading is stopped $\left(\frac{dR}{dt} = 0\right)$ when the total mass of the cloud is decreasing with time. The radius of the blanket is restricted to be greater than or equal to the radius of the primary (liquid) source R_p if it is present.

III.1.2 Material and Energy Balances

The balance on the total mass of gas in the source blanket ($M = \pi R^2 H \rho$) is

$$\frac{dM}{dt} = \frac{d}{dt}\left[\pi R^2 H \rho\right] = E(t) + \dot{M}_a + \dot{M}_{w,s} - \left[\frac{Q_{*max}}{w_c}\right]\left[\pi R^2\right] \qquad \text{(III-10)}$$

where $E(t)$ is the gas evolution rate from the primary (liquid) source. For spills over water, the water entrainment term ($\dot{M}_{w,s}$) is included in the source blanket description and is calculated from Equation III-24, and the air entrainment rate is

$$\dot{M}_a = 2\pi R H_h (\varepsilon u_f) \rho_a \Big/ \left[g \Delta' H / u_f^2\right] \qquad \text{(III-11)}$$

the value of ε is estimated to be 0.6, based on the still-air HTAG release experimental data of Volume II.

The balance on the mass of contaminant in the source blanket ($M_c = w_c \pi R^2 H \rho$) is

$$\frac{dM_c}{dt} = \frac{d}{dt}\left[w_c \pi R^2 H \rho\right] = E(t) - Q_{*max}(\pi R^2) \qquad \text{(III-12)}$$

and the mass balance on the air in the source blanket ($M_a = w_a \pi R^2 H \rho$) is

$$\frac{dM_a}{dt} = \frac{d}{dt}\left[w_a \pi R^2 H \rho\right] = \frac{\dot{M}_a}{1 + H_a} - \left[\frac{Q_{*max}}{w_c}\right] w_a (\pi R^2) \qquad \text{(III-13)}$$

where the ambient humidity is H_a and the mass fraction of contaminant and air are $w_c = M_c / M$ and $w_a = M_a / M$, respectively.

The energy balance on the source blanket ($h \pi R^2 H \rho$) gives

$$\frac{d}{dt}\left[h\pi R^2 H\rho\right] = h_E E(t) + h_a \dot{M}_a + h_w \dot{M}_{w,s} - h\left[\frac{Q_{*max}}{w_c}\right](\pi R^2) + \dot{Q}_s \qquad \text{(III-14)}$$

where h_E is the enthalpy of the emitted gas, h_a is the enthalpy of the ambient humid air, and h_w is the enthalpy of any water vapor entrained by the blanket if over water. There are three alternate submodels included for the heat transfer ($\dot{Q}_s$) from the surface to the cloud.

The simplest method for calculating the heat transfer between the substrate and the gas cloud is to specify a constant heat transfer coefficient for the heat transfer relation

$$\dot{Q}_s = q_s\left[\pi(R^2 - R_p^2)\right] = h_0 \Delta T\left[\pi(R^2 - R_p^2)\right] \qquad \text{(III-15)}$$

where $\dot{Q}_s$ is the rate of heat transfer to the cloud, q_s is the heat flux, and ΔT is the temperature difference. For the calculation of heat transfer over the source, the temperature difference is based on the average temperature of the blanket.

In the evaluation of the Burro and Coyote series of experiments, Koopman et al. (1981) proposed the following empirical heat transfer coefficient relationship for heat transfer between a cold LNG cloud and the ground

$$h_0 = V_H \rho C_p \qquad \text{(III-16)}$$

where the value of V_H was estimated to be 0.0125 m/s. This constant can be varied in the model.

From the heat transfer coefficient descriptions for heat transfer from a flat plate, the following relationships can be applied. For

natural convection, the heat transfer coefficient is estimated using the Nusselt Nu, Grashoff Gr, and Schmidt Sc numbers, McAdams (1954), from

$$Nu = 0.14\ (Gr\,Sc)^{1/3} \tag{III-17}$$

Or

$$h_n = 0.14 \left[\frac{g\,\rho^2\,C_p^3\,\mu}{T\,Pr^2}\,\Delta T\right]^{1/3} \tag{III-18}$$

where h_n is the heat transfer coefficient due to natural convection and Pr is the Prandtl number. In order to simplify the calculations, the parameter group

$$\left[Pr^{-2}\ (C_p\,MW)^3 \left(\frac{\mu}{MW\,T}\right)\right]^{1/3} \tag{III-19}$$

is estimated to be 60 in mks units. The actual value of the group is 47.25, 58.5, and 73.4 for air, methane, and propane, respectively. Equation III-18 then becomes

$$h_n = 18\left[\left(\frac{\rho}{MW}\right)^2 \Delta T\right]^{1/3} \tag{III-20}$$

where the density ρ, molecular weight MW, and temperature difference ΔT are based on the average composition of the gas blanket.

For forced convection after Treybal (1980), the Colburn analogy is applied to a flat plate using the Stanton number for heat transfer St_H and the Prandtl number as

$$St_H\,Pr^{2/3} = \frac{C_f}{2} = \left(\frac{u_*}{\bar{u}}\right)^2 \tag{III-21}$$

Or,

$$h_f = (\bar{\rho} C_p) \, Pr^{-2/3} \left(\frac{u_*}{\bar{u}}\right)^2 \qquad \text{(III-22)}$$

where h_f is the heat transfer coefficient due to forced convection. If the velocity is evaluated at the top of the gas blanket and the Pr is estimated to be 0.741,

$$h_f = \left[1.22 \frac{u_*^2}{u_0} \left(\frac{z_0}{H}\right)^{\alpha}\right] \rho C_p \qquad \text{(III-23)}$$

The overall heat transfer coefficient is then the maximum of the forced and natural coefficients, i.e. $h_0 = \max(h_f, h_n)$. The heat flux and transfer rate are then estimated by Equation III-15.

If the gas blanket is formed over water, water will be transferred from the surface to the cloud by a partial pressure driving force associated with the temperature difference between the surface and the gas blanket. The rate of mass transfer of water is

$$M_{w,s} = \frac{F_0}{p} \left(p^*_{w,s} - p^*_{w,c}\right) \left[\pi(R^2 - R_p^2)\right] \qquad \text{(III-24)}$$

where F_0 is the overall mass transfer coefficient. The driving force is the difference of the vapor pressure of water at the surface temperature $p^*_{w,s}$ and the vapor pressure of water at the cloud temperature $p^*_{w,c}$. The natural convection coefficient is based on the heat transfer coefficient and the analogy between the Sherwood number Sh and the Nusselt number Nu suggested by Bird et al. (1960); or

$$Sh = Nu = 0.14 \, (Gr \, Sc)^{1/3} = \frac{F_n L}{\mathcal{D}} \left(\frac{MW}{\rho}\right) \qquad \text{(III-25)}$$

where Sc is the Schmidt number. If the Schmidt number is taken as 0.6, and $\left(\frac{\mu}{T\,MW}\right)$ is estimated to be 2.2×10^{-9} in mks units,

$$F_n = 9.9 \times 10^{-3} \left[\left(\frac{\rho}{MW}\right)^2 \Delta T\right]^{1/3} \qquad \text{(III-26)}$$

For forced convection, Treybal (1980) suggests that the Stanton number for mass transfer St_M and the Stanton number for heat transfer St_H are related by

$$St_M = St_H \left(\frac{Pr}{Sc}\right)^{2/3} = 1.15\ St_H \qquad \text{(III-27)}$$

Or,

$$F_f = \frac{20.7\ h_0}{\sqrt{MW}\ C_p} \qquad \text{(III-28)}$$

The overall mass transfer coefficient F_0 is calculated as the larger of the natural and forced convection coefficients.

For the case when the primary (liquid) source emission rate E(t) is larger than the atmospheric takeup rate $Q_{*max}\,\pi R_p^2$, Equations III-10, III-12 III-13, and III-14 are integrated for the mass, concentration, and enthalpy of the gas blanket along with an appropriate equation of state (i.e. relationship between enthalpy and temperature and between temperature and density) from Appendix A.

For the case when the emission rate is insufficient to form a gas blanket, the flux of contaminant is no longer determined by the maximum atmospheric takeup rate. Consider the boundary layer formed by the emission of gas into the atmosphere above the primary source. If the source is modeled to have a uniform width 2b and entrain no air along the sides of the layer, the balance on the total material ($\rho_L\ u_L\ H_L$) in a differential slice of the layer is

$$\frac{d}{dx}\left[\rho_L\, u_L\, H_L\right] = \rho_a\, w_e + \left(\frac{Q_*}{w_c}\right) \qquad \text{(III-29)}$$

where w_e is the vertical rate of air entrainment into the layer given by Equation III-61, ρ_L is the average density of the slice, and Q_* / w_c is the total flux of gas from the primary (liquid) source. The balance on the mass flow rate of contaminant ($w_c\, \rho_L\, u_L\, H_L$) at any ($x - x_{up}$) is

$$c_{c,L}\, u_L\, H_L = Q_*\, L \qquad \text{(III-30)}$$

With an equation of state to relate $c_{c,L}$ and ρ_L, Equation III-29 is integrated from the upwind edge of the source ($x = x_{up}$) to the downwind edge ($x = L + x_{up}$).

In order to generate the initial conditions for the downwind dispersion calculations, the maximum concentration c_c and the vertical dispersion parameter S_z are needed. Since Equations III-29 and III-30 are written for a vertically averaged layer, consider the vertical average of the power law distribution. The height of the layer H_L is the height to some concentration level, say 10% of the maximum. Although strictly a function of α, this value is modeled by

$$H_L = \delta_L\, H_{EFF} \qquad \text{(III-31)}$$

where H_{EFF} is the effective height defined by Equation III-57 and δ_L is 2.15. The vertically averaged concentration $c_{c,L}$ can be defined by

$$c_{c,L}\, H_L = \int_0^\infty c\, dz \qquad \text{(III-32)}$$

And similarly, the effective transport velocity u_L is defined by

$$c_{c,L}\, u_L\, H_L = \int_0^\infty c\, u_x\, dz \qquad \text{(III-33)}$$

With Equation III-31 and defining relations for H_{EFF} and u_{EFF} (Equations III-57 and III-71, respectively), it follows that

$$c_c = \delta_L c_{c,L} \qquad \text{(III-34)}$$

$$u_L H_L = \delta_L \left[\frac{u_0 z_0}{1+\alpha}\right] \left[\frac{s_z}{z_0}\right]^{1+\alpha} \qquad \text{(III-35)}$$

and

$$\delta_L\, w_e' = w_e \qquad \text{(III-36)}$$

where w_e' is given by Equation III-61.

III.1.3 Maximum Atmospheric Takeup Rate

The maximum atmospheric takeup rate will be the largest takeup rate which satisfies Equations III-29 and III-30. As well, the maximum concentration of contaminant in the power law profile at the downwind edge of the source will be the source contaminant concentration $(c_c)_s$. If Equations III-29 and III-30 are combined along with the assumption of adiabatic mixing of ideal gases with the same molal heat capacity (i.e. $\left[\frac{\rho - \rho_a}{c_c}\right] = \gamma = \text{constant}$), the maximum takeup flux is modeled by

$$Q_{*max} = (c_c)_s \frac{k\, u_* (1+\alpha)}{\hat{\phi}} \left[\frac{\delta_L}{\delta_L - 1}\right] \qquad \text{(III-37)}$$

where

$$\frac{1}{\hat{\phi}} = \frac{1}{L} \int_0^L \frac{dx}{\phi} \qquad \text{(III-38)}$$

An upper bound of the atmospheric takeup flux can be characterized by the condition where the source begins to spread as a gravity intrusion against the approach flow. In water flume experiments, Britter (1980) measured the upstream and lateral extent of a steady state plume from a circular source as a function of Ri_*. A significant upstream spread was obtained for $Ri_* > 32$, and lateral spreading at the center of the source was insignificant for $Ri_* < 8$. The presence of any significant lateral spreading represents a lower bound on the conditions of the maximum takeup flux.

The integral of Equation III-38 is calculated using a local Richardson number of

$$Ri_*(x) = \zeta (x - x_{up})^{\frac{1}{1+\alpha}} \qquad \text{(III-39)}$$

where

$$\zeta = g \left[\frac{\rho - \rho_a}{\rho_a}\right] \frac{z_0}{u_*^2} \frac{\Gamma\left[\frac{1}{1+\alpha}\right]}{1+\alpha} \left[\frac{k u_* (1+\alpha)}{\phi_c} \left(\frac{1+\alpha}{u_0 z_0}\right) \left(\frac{\delta_L}{\delta_L - 1}\right)\right]^{\frac{1}{1+\alpha}} \qquad \text{(III-40)}$$

and where the value of ϕ_c is 3.1 (corresponding to $Ri_* = 20$ ($8 < Ri_* < 32$)). Using this $Ri_*(x)$ and the first two terms of $\phi(Ri_*)$, Equation III-38 is approximated as

$$\frac{1}{\hat{\phi}} = \frac{1}{0.099\, L\, \zeta^{1.04}} \ln\left[\frac{0.88 + 0.099 \zeta^{1.04} L^{\frac{1.04}{1+\alpha}}}{0.88}\right] \qquad \text{(III-41)}$$

which then specifies the maximum atmospheric takeup flux.

III.1.4 Transient HTAG Release Simulation

If a steady state spill is being simulated, the transient source calculation is carried out until the source characteristics are no longer varying significantly with time. The maximum centerline concentration c_c, the horizontal and vertical dispersion parameters S_y and S_z, the half width b, and if necessary, the enthalpy h are used as initial conditions for the downwind calculation specified in a transient spill.

If a transient spill is being simulated, the spill is modeled as a series of pseudo-steady state releases. Consider a series of observers traveling with the wind over the transient gas source described above; each observer originates from the point which corresponds with the maximum upwind extent of the gas blanket ($x = -R_{max}$). The desired observer velocity is the average transport velocity of the gas u_{EFF} from Equation III-71; however, the value of u_{EFF} will differ from observer to observer with the consequence that some observers may be overtaken by others. For a neutrally buoyant cloud, u_{EFF} becomes a function of downwind distance alone which circumvents this problem. With this functionality, Colenbrander (1980) models the observer velocity as

$$u_i(x) = \frac{u_0}{\Gamma\left[\frac{1}{1+\alpha}\right]} \left(\frac{S_{z_{0m}}}{z_0}\right)^{\alpha} \left[\frac{x + R_{max}}{\frac{\sqrt{\pi}}{2} R_m + R_{max}}\right]^{\alpha/(1+\alpha)} \qquad \text{(III-42)}$$

where $S_{z_{0m}}$ is the value of S_{z_0} when the averaged source rate ($\pi R^2 Q_*$) is a maximum, and the subscript i denotes observer i. Noting that $u_i(x) = \frac{dx_i}{dt}$, observer position and velocity as functions of time are determined.

AD-A171 522 DEVELOPMENT OF AN ATMOSPHERIC DISPERSION MODEL FOR HEAVIER-THAN-AIR GAS M... (U) ARKANSAS UNIV FAYETTEVILLE DEPT OF CHEMICAL ENGINEERING J A HAVENS ET AL. MAY 85 2/2

UNCLASSIFIED USCG-D-22-85 DTCG23-80-C-20029 F/G 20/4 NL

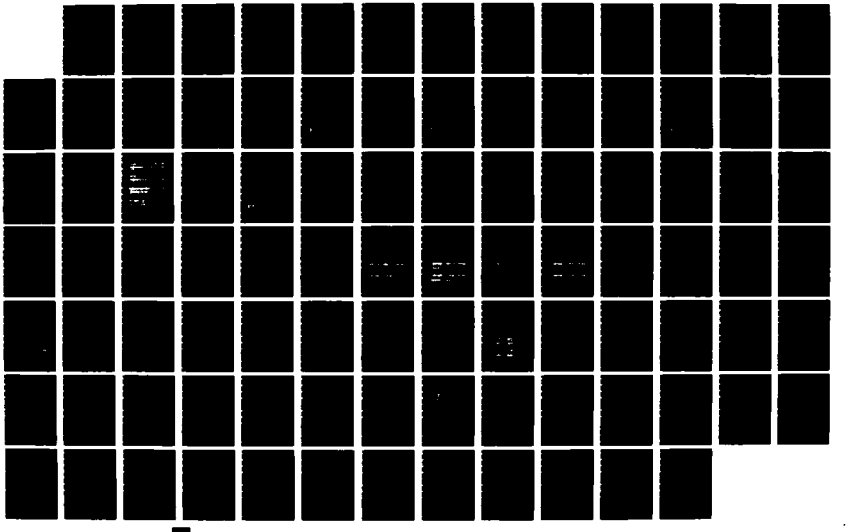

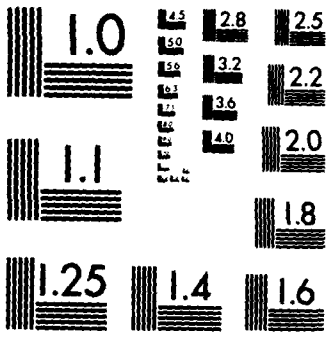

MICROCOPY RESOLUTION TEST CHART
NATIONAL BUREAU OF STANDARDS-1963-A

A pseudo-steady state approximation of the transient source is obtained as each observer passes over the source. If t_{up_i} and t_{dn_i} denote the times when observer i encounters the upwind and downwind edges of the source respectively, then the source fetch seen by observer i is:

$$L_i = x_{up_i} - x_{dn_i} \tag{III-43}$$

The width of the source $2B_i'(t)$ is defined by

$$B_i'^2(t) = R^2(t) - x_i^2(t) \tag{III-44}$$

Then, the gas source area seen by observer i is

$$2L_i b_i = 2 \int_{t_{up_i}}^{t_{dn_i}} B_i' u_i \, dt \tag{III-45}$$

where $2b_i$ is the average width.

The takeup rate of contaminant $(Q_* Lb)_i$ is calculated by

$$2(Q_* Lb)_i = 2 \int_{t_{up_i}}^{t_{dn_i}} Q_* B_i' u_i \, dt \tag{III-46}$$

The total mass flux rate from the source is

$$2(\rho_L u_L H_L b)_i = 2 \int_{t_{up_i}}^{t_{dn_i}} \left[\rho_a w_e' + \left(\frac{Q_*}{w_c} \right) \right] B_i' u_i \, dt \tag{III-47}$$

With these equations, the average composition of the layer can be determined at each $x = x_{up}$ over the source. With the enthalpy of the layer given by

$$(h_L \rho_L u_L H_L b)_i = \int_{t_{up_i}}^{t_{dn_i}} h \left(\frac{Q_*}{w_c}\right) B_i' u_i \, dt \qquad \text{(III-48)}$$

due to the choice of the reference temperature as the ambient temperature along with a suitable equation of state relating enthalpy, temperature, and density, the source can be averaged for each observer. After the average composition of the layer is determined at the downwind edge, an adiabatic mixing calculation is performed between this gas and the ambient air when applicable. This calculation represents the function between density and concentration for the remainder of the calculation if the calculation is adiabatic; it represents the adiabatic mixing condition if heat transfer is included in the downwind calculation.

For each of several observers released successively from $x = -R_{max}$, the observed dimensions L and b, the downwind edge of the source x_{dn}, the average vertical dispersion coefficient S_z, the average takeup flux Q_*, the centerline concentration c_c, and if applicable, the average enthalpy h_L can be determined for each observer. With these input values, a steady state calculation is made for each observer. The distribution parameters for any specified time t_s are determined by locating the position of the series of observers at time t_s, i.e. $x_i(t_s)$. The corresponding concentration distribution is then computed from the assumed profiles.

III.2 Steady State Downwind Dispersion

The model treats dispersion of gas entrained into the wind field from an idealized rectangularly shaped source of width 2b and length L. The circular source cloud is represented as an equivalent area square ($L^2 = \pi R^2 = 2bL$). Similarity forms for the concentration profiles are assumed which represent the plume as being composed of a horizontally homogeneous section in which only vertical dispersion is considered, with Gaussian concentration profile edges as follows:

$$c(x,y,z) = c_c(x) \exp\left[-\left(\frac{|y| - b(x)}{S_y(x)}\right)^2 - \left(\frac{z}{S_z(x)}\right)^{1+\alpha}\right] \quad \text{for } |y| > b$$

$$= c_c(x) \exp\left[-\left(\frac{z}{S_z(x)}\right)^{1+\alpha}\right] \quad \text{for } |y| \leq b \qquad \text{(III-49)}$$

A power law wind velocity profile is assumed

$$u_x = u_0\left(\frac{z}{z_0}\right)^{\alpha} \qquad \text{(III-50)}$$

where the value of α is determined by a weighted least squares fit of the logarithmic profile

$$u_x = \frac{u_*}{k}\left[\ln\left(\frac{z + z_R}{z_R}\right) - \psi\left(\frac{z}{\lambda}\right)\right] \qquad \text{(III-51)}$$

Functional forms for ψ and typical values of α are given in Table III-1 for different Pasquill stability categories. With these profiles, the parameters of Equation III-49 are constrained by ordinary differential equations.

III.2.1 Vertical Dispersion

The vertical dispersion parameter S_z is determined by requiring that it satisfy the diffusion equation

$$u_x \frac{\partial c}{\partial x} = \frac{\partial}{\partial z} K_z \frac{\partial c}{\partial z} \qquad \text{(III-52)}$$

with the vertical turbulent diffusivity given by

$$K_z = \frac{k\, u_* z}{\phi(Ri_*)} \qquad \text{(III-53)}$$

The function $\phi(Ri_*)$ is a curve fit of laboratory scale data for vertical mixing in stably density-stratified fluids reported by McQuaid (1976), Kantha et al. (1977), and Lofquist (1960) for $Ri_* > 0$. For $Ri_* < 0$, the function $\phi(Ri_*)$ is taken from Colenbrander (1983) and has been modified so the passive limit of the two functions agree as follows:

$$\phi(Ri_*) = 0.88 + 0.099\, Ri_*^{1.04} + 1.4 \times 10^{-25}\, Ri_*^{5.7} \qquad Ri_* \geq 0$$

$$= 0.88 / (1 + 0.65\, |Ri_*|^{0.6}) \qquad Ri_* < 0$$

(III-54)

The friction velocity is calculated using Equation III-51 from a known velocity u_0 at a specific height z_0. Combining the assumed similarity forms for concentration and velocity, Equations III-49, III-50, III-52, and III-53 give

TABLE III-1

TYPICAL ATMOSPHERIC BOUNDARY LAYER STABILITY AND WIND PROFILE CORRELATIONS

Pasquill Stability Category	Monin-Obukhov Length (λ) as a Function of Surface Roughness z_R(m)[1]	Typical Power Law Exponents α in Eqn. (III-50)	Corrections to Logarithmic Profiles as Given by Businger et al. (1971) ψ in Eqn. (III-51)
A	$-11.4\ z_R^{0.10}$	0.108	$\psi = 2\ln\left[\frac{1+a}{2}\right] + \ln\left[\frac{1+a^2}{2}\right] - 2\tan^{-1}(a) + \frac{\pi}{a}$, with $a = (1 - 15(z/\lambda))^{1/4}$
B	$-26.0\ z_R^{0.17}$	0.112	
C	$-123\ z_R^{0.30}$	0.120	
D	∞	0.142	$\psi = 0$
E	$123\ z_R^{0.30}$	0.203	$\psi = -4.7\,(z/\lambda)$
F	$26.0\ z_R^{0.17}$	0.253	

[1] Curve fit of data from Pasquill (1974).

$$\frac{d}{dx}\left[\left(\frac{u_0 z_0}{1+\alpha}\right)\left(\frac{S_z}{z_0}\right)^{1+\alpha}\right] = \frac{k u_* (1+\alpha)}{\phi(Ri_*)} \qquad \text{(III-55)}$$

where the Richardson number Ri_* is computed as

$$Ri_* = g\left(\frac{\rho - \rho_a}{\rho_a}\right)\frac{H_{EFF}}{u_*^2} \qquad \text{(III-56)}$$

and the effective cloud depth is defined as

$$H_{EFF} = \frac{1}{c_c}\int_0^\infty c\,dz = \Gamma\left(\frac{1}{1+\alpha}\right)\frac{S_z}{1+\alpha} \qquad \text{(III-57)}$$

Equation III-55 can be viewed as a volumetric balance on a differential slice of material downwind of the source. For a mass balance over the same slice, one obtains

$$\frac{d}{dx}\left[\rho_L u_L H_L\right] = \rho_a w_e \qquad \text{(III-58)}$$

which is the same result as Equation III-29 without the source term. With Equations III-35 and III-36, this is

$$\frac{d}{dx}\left[\rho_L u_{EFF} H_{EFF}\right] = \rho_a w_e' \qquad \text{(III-59)}$$

Using the assumption of adiabatic mixing of ideal gases with the same constant molal heat capacity (i.e. $\frac{\rho - \rho_a}{c_c}$ = constant) along with the contaminant material balance, the mass balance becomes

$$\frac{d}{dx}\left[u_{EFF}\, H_{EFF}\right] = w_e' \qquad \text{(III-60)}$$

which leads to

$$w_e' = \frac{w_e}{\delta_L} = \frac{k\, u_* (1 + \alpha)}{\phi(Ri_*)} \qquad \text{(III-61)}$$

Equations III-59 and III-61 are combined to give

$$\frac{d}{dx}\left[\rho_L\, u_{EFF}\, H_{EFF}\right] = \frac{\rho_a\, k\, u_* (1 + \alpha)}{\phi(Ri_*)} \qquad \text{(III-62)}$$

for situations even when $\frac{\rho - \rho_a}{c_c}$ is not constant.

When heat transfer from the surface is present, vertical mixing will be enhanced by the convective turbulence due to heat transfer. Zeman and Tennekes (1977) model the resultant vertical turbulence velocity (Equation II-5) as

$$\frac{w}{u_*} = \left[1 + \frac{1}{4}\left(\frac{w_*}{u_*}\right)^2\right]^{1/2} \qquad \text{(III-63)}$$

where w_* is the convective scale velocity described by

$$\left(\frac{w_*}{u_*}\right) = \left[\frac{g\, h}{u_* \bar{u}}\, \frac{(T_s - T_{c,L})}{T_{c,L}}\right]^{2/3} \qquad \text{(III-64)}$$

If $\bar{u}$ is evaluated at H_{EFF},

$$\frac{w}{u_*} = \left[1 + Ri_T^{2/3}\right]^{1/2} \qquad \text{(III-65)}$$

where

$$Ri_T = g \left[\frac{T_s - T_{c,L}}{T_{c,L}}\right] \frac{H_{EFF}}{u_* u_0} \left[\frac{z_0}{H_{EFF}}\right]^{\alpha} \qquad \text{(III-66)}$$

and $T_{c,L}$ is the temperature obtained from the energy balance of Equations III-80 and III-81. Equation III-62 is modified to account for this enhanced mixing by

$$\frac{d}{dx}\left[\rho_L u_{EFF} H_{EFF}\right] = \frac{\rho_a k w(1 + \alpha)}{\phi(Ri'_*)} \qquad \text{(III-67)}$$

where $Ri'_* = Ri_* \left(\frac{u_*}{w}\right)^2$.

Although derived for two-dimensional dispersion, this is extended for application to a HTAG plume which spreads laterally as a density intrusion:

$$\frac{d}{dx}\left[\rho_L u_{EFF} H_{EFF} B_{EFF}\right] = \frac{\rho_a k w(1 + \alpha)}{\phi(Ri'_*)} B_{EFF} \qquad \text{(III-68)}$$

where the plume effective half width is defined by

$$B_{EFF} = b + \frac{\sqrt{\pi}}{2} S_y \qquad \text{(III-69)}$$

and determined using the gravity intrusion relation

$$\frac{d B_{EFF}}{dt} = C_E \left[g\left(\frac{\rho - \rho_a}{\rho}\right) H_{EFF}\right]^{1/2} \qquad \text{(III-70)}$$

The average transport velocity in the plume is defined by

$$u_{EFF} = \frac{\int_0^\infty c\, u_x\, dz}{\int_0^\infty c\, dz} = u_0 \left(\frac{S_z}{z_0}\right)^\alpha \Bigg/ \Gamma\left(\frac{1}{1+\alpha}\right) \qquad \text{(III-71)}$$

and the lateral spread of the cloud is modeled by

$$\frac{dB_{EFF}}{dx} = \frac{1}{u_{EFF}} \frac{dB_{EFF}}{dt} = C_E \left[\frac{g\, z_0\, \Gamma^3\left[\frac{1}{1+\alpha}\right]}{u_0^2 (1+\alpha)}\right]^{1/2} \left[\frac{\rho - \rho_a}{\rho_a}\right]^{1/2} \left(\frac{S_z}{z_0}\right)^{(\frac{1}{2}-\alpha)} \qquad \text{(III-72)}$$

III.2.2 Horizontal Dispersion

The crosswind similarity parameter $S_y(x)$ is also determined by requiring that it satisfy the diffusion equation

$$u_x \frac{\partial c}{\partial x} = \frac{\partial}{\partial y}\left[K_y \frac{\partial c}{\partial y}\right] \qquad \text{(III-73)}$$

with the horizontal turbulent diffusivity given by

$$K_y = K_0\, u_x\, B_{EFF}^{\gamma_1} \qquad \text{(III-74)}$$

When $b = 0$, $S_y = \sqrt{2}\,\sigma_y$, where σ_y is the similarity parameter correlated by Pasquill (1974) in the form $\sigma_y = \delta x^\beta$. Furthermore, Equations III-73 and III-74 require that

$$\sigma_y \frac{d\sigma_y}{dx} = K_0\, B_{EFF}^{\gamma_1} \qquad \text{(III-75)}$$

where $\gamma_1 = 2 - 1/\beta$ and $K_0 = \frac{2\beta}{\pi} (\delta\sqrt{\pi/2})^{1/\beta}$. Then

$$S_y \frac{dS_y}{dx} = \frac{4\beta}{\pi} B_{EFF}^2 \left[\frac{\delta\sqrt{\pi/2}}{B_{EFF}}\right]^{1/\beta} \qquad \text{(III-76)}$$

where Equation III-76 is also assumed applicable for determining S_y when b is not zero.

At the downwind distance x_t where b = 0, the crosswind concentration profile is assumed Gaussian with S_y given by

$$S_y = \sqrt{2}\,\delta(x + x_v)^{\beta} \qquad \text{(III-77)}$$

where x_v is a virtual source distance determined by

$$S_y(x_t) = \sqrt{2}\,\delta(x_t + x_v)^{\beta} \qquad \text{(III-78)}$$

The gravity spreading calculation is terminated for $x > x_t$.

For a steady plume, the centerline concentration c_c is determined from the material balance

$$E = \int_0^{\infty}\int_{-\infty}^{\infty} c\,u_x\,dy\,dz = 2c_c \left(\frac{u_0 z_0}{1+\alpha}\right)\left(\frac{S_z}{z_0}\right)^{1+\alpha} B_{EFF} \qquad \text{(III-79)}$$

where E is the plume source strength.

III.2.3 Energy Balance

For some simulations of cryogenic gas releases, heat transfer to the plume in the downwind dispersion calculation may be important, particularly in low wind conditions. The source calculation determines a gas/air mixture initial condition for the downwind dispersion problem. Air entrained into the plume is assumed to mix adiabatically. Heat transfer to the plume downwind of the source adds additional heat. This added heat per unit mass D_h is determined by an energy balance on a uniform cross-section as

$$\frac{d}{dx}\left[D_h \rho_L u_{EFF} H_{EFF}\right] = q_s / \delta_L \qquad \text{(III-80)}$$

where q_s is determined by Equation III-15 along with the desired method of calculating h_0. Equation III-80 is applied when b = 0 and is extended to

$$\frac{d}{dx}\left[D_h \rho_L u_{EFF} H_{EFF} B_{EFF}\right] = q_s B_{EFF} \Big/ \delta_L \qquad \text{(III-81)}$$

when b > 0. Since the average density of the layer ρ_L cannot be determined until the temperature (i.e. D_h) is known, a trial and error procedure is required.

Equations III-55, 56, 57, 65-69, 72, and 76-81 are combined with an equation of state relating cloud density to gas concentration and temperature and are solved simultaneously to predict S_z, S_y, c_c, and b as functions of downwind distance beginning at the downwind edge of the gas source.

III.3 Correction for Along-Wind Dispersion

In a similar fashion to Colenbrander (1980), an adjustment to the values of c_c is applied to account for dispersion parallel to the wind direction. The calculated centerline concentration $c_c(x)$ is considered to have resulted from the release of successive planar puffs of gas ($c_c(x)\Delta x$) without any dispersion in the x-direction. If it is assumed that each puff diffuses in the x-direction as the puff moves downwind independently of any other puff and that the dispersion is one-dimensional and Gaussian, the x-direction concentration dependence is given by

$$c_c'(x, x_{p_i}) = \frac{c_c(x_{p_i})\,\Delta x_i}{\sqrt{2\pi}\,\sigma_x} \exp\left[-\frac{1}{2}\left[\frac{x - x_{p_i}}{\sigma_x}\right]^2\right] \qquad \text{(III-82)}$$

where x_{p_i} denotes the position of the puff center due to observer i.

After Beals (1971), the x-direction dispersion coefficient σ_x is assumed to be a function of distance from the downwind edge of the gas source ($X = x - x_0$) and atmospheric stability given by

$$\begin{aligned} \sigma_x(X) &= 0.02\,X^{1.22} \quad \text{unstable}, \quad x \geq 130 \text{ m} \\ &= 0.04\,X^{1.14} \quad \text{neutral}, \quad x \geq 100 \text{ m} \\ &= 0.17\,X^{0.97} \quad \text{stable}, \quad x \geq 50 \text{ m} \end{aligned} \qquad \text{(III-83)}$$

where ($X = x - x_0$) and σ_x are in meters. The concentration at x is then determined by superposition, i.e., the contribution to c_c at a given x from neighboring puffs is added to give an x-direction corrected value of c_c'. For N observers,

$$c_c'(x) = \sum_{i=1}^{N} \frac{c_c(x_{p_i})}{\sqrt{2\pi}\,\sigma_x} \exp\left[-\frac{1}{2}\left[\frac{x - x_{p_i}}{\sigma_x}\right]^2\right] \Delta x_i \qquad \text{(III-84)}$$

and for large N,

$$c_c'(x) = \frac{1}{\sqrt{2\pi}} \int_0^{\infty} \frac{c_c(\xi)}{\sigma_x(\xi - \xi_0)} \exp\left[-\frac{1}{2}\left[\frac{x - \xi}{\sigma_x(\xi - \xi_0)}\right]^2\right] d\xi \quad \text{(III-85)}$$

The corrected centerline concentration c_c' is used in the assumed profiles in place of c_c, along with the distribution parameters S_y, S_z, and b.

III.4 The DEGADIS Computer Model

The model described in the previous section has been programmed in Digital Equipment Company (DEC) VAX FORTRAN and resides on a DEC VAX 11-730 under VMS.

Volume III of this report contains a flow chart of the DEGADIS computer model, a complete FORTRAN code listing, and an example DEGADIS interactive computer session.

IV. COMPARISON OF SIMULATIONS WITH SELECTED FIELD EXPERIMENT DATA

The DEGADIS model has been used to simulate a collection of thirty-nine field experimental HTAG releases. The tests simulated include small, continuous LPG releases (order 0.1 - 1.0 kg/s) on land from diked sources, continuous LPG and LNG releases onto water with release rates of the order 10 - 100 kg/s, near-instantaneous releases of LNG of approximately 5000 kg onto water, and instantaneous releases of Freon-12/air mixtures of approximately 5000 kg on land. The meteorological conditions encompassed wind speeds of approximately 1 - 10 m/s, relative humidity from essentially zero to about 85%, and estimated atmospheric stabilities ranging from Pasquill B to F.

In the following sections, the individual HTAG dispersion test series simulated are briefly described, and the simulation results are compared with field experimental measurements. For those tests which can be reasonably represented as either instantaneous or steady continuous releases, a "release Richardson number," Ri_0, is presented. This Richardson number may be useful for demarcating HTAG releases which exhibit significant departures from passive dispersion behavior (Puttock, 1982). The final section summarizes observations of the agreement between reported field experimental gas concentration measurements and DEGADIS model predictions.

IV.1 LPG Releases on Land from Diked Area Sources

Welker (1982) reported vapor dispersion measurements for propane releases into concrete-lined pits nominally 1.5, 3, and 6 meters square in a variety of wind and atmospheric stability conditions. Measurements of gas concentration at ground level at positions estimated to be in the centerline of the plume path were reported.

Table IV.1 gives the estimated source strength and meteorological data for ten of these tests which have been simulated with DEGADIS. The reported measured gas concentrations (taken at a height above ground of 0.15 m) were obtained with a catalytic type hydrocarbon sensor having a response time estimated to be between 1 and 5 s. Figures IV.1 through IV.10 show the DEGADIS model-predicted ground level centerline gas concentration compared with the reported maximum and time-averaged gas concentrations for Welker's tests 275-1, 281-2, 296-1, 297-1, 297-3, 298-1, 298-2, 302-1, 334-1, and 334-2 respectively.

TABLE IV-1

SUMMARY OF SOURCE AND METEOROLOGICAL DATA
FOR SELECTED PROPANE RELEASES FROM WELKER

Run No.	Width (m)	Propane Evap. Rate (kg/s)	Wind Speed m/s[1]	Stability[2]	Air Temperature[3] (K)	Relative Humidity %
275-1	1.52	0.0189	4.52	B	301.5	28
281-2	3.04	0.057	3.09	B	302.6	21
296-1	3.04	0.071	4.29	D	294	40
297-1	3.04	0.058	4.34	C	296	23
297-3	3.04	0.051	3.67	D	298	38
298-1	3.04	0.055	2.01	C	294	23
298-2	3.04	0.044	2.15	B	296	30
302-1	3.04	0.073	7.47	D	295	69
334-1	6.10	0.249	2.37	C	~279	~10
334-2	6.10	0.551	2.77	C	~279	~10

[1] at ~8.0 ft. (2.44 m) height

[2] Pasquill Category, estimated by Welker

[3] Surface temperature estimated $T_s = T_{air} + 1 - 3°K$
Surface roughness estimated = 0.01 m

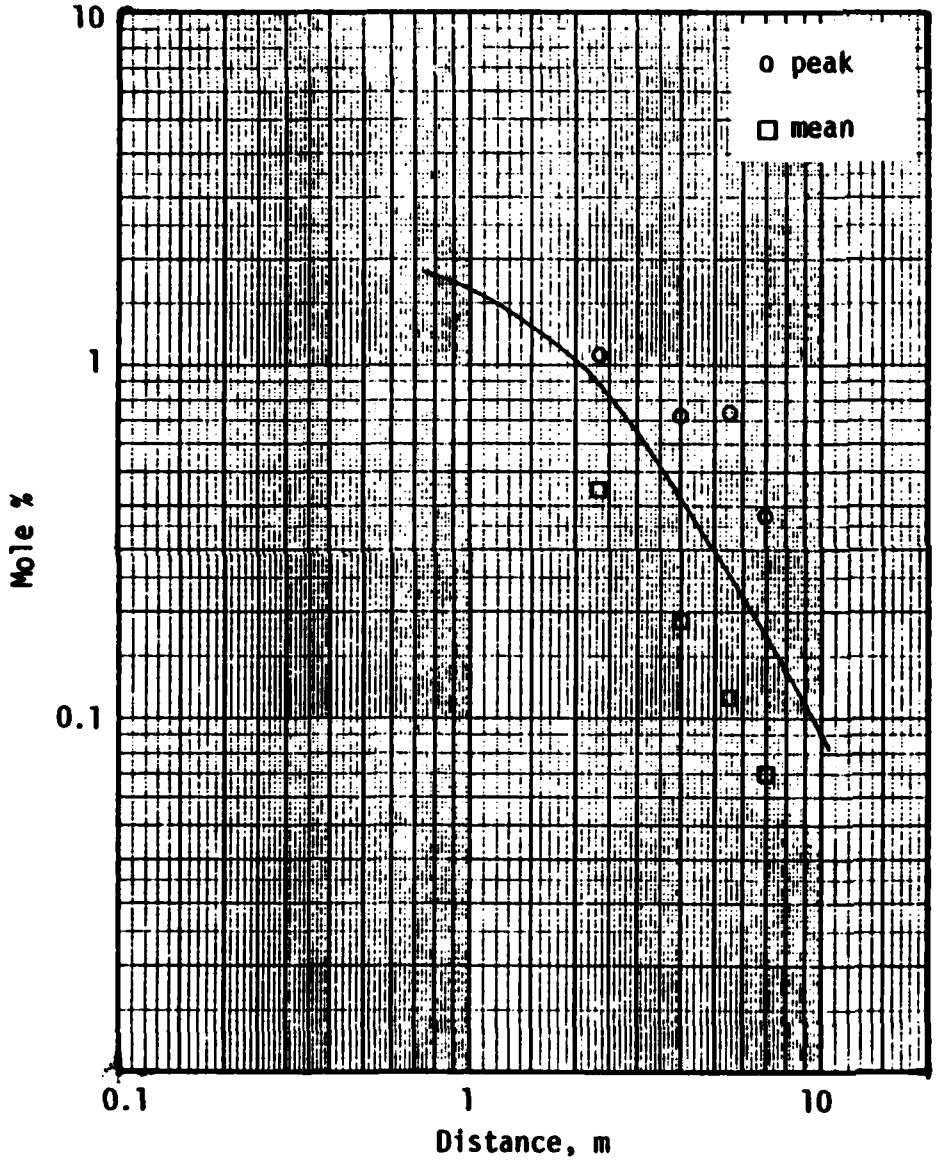

TEST WELKER 275-1

Source Description

Type: Continuous propane

Primary Source Width (m)	:	1.52
Secondary Source Width (m)	:	1.52
Primary Source Flux (kg/m^2 s)	:	8.13 E-3
Rate (kg/s)	:	0.0188
Temperature (K)	:	231.0

Meteorological Conditions

Wind Velocity (m/s)	:	4.52
@ Height (m)	:	2.44
Surface Roughness (m)	:	0.01
Pasquill Stability	:	B
Monin-Obukhov Length (m)	:	-11.8
Air Temperature (K)	:	301.5
Relative Humidity (%)	:	28
Surface Temperature (K)	:	305

Release Richardson Number

Volumetric Release Rate (m^3/s)	:	7.88 E-3
Characteristic Width (m)	:	1.52
Estimated Friction Velocity (m/s)	:	0.31

$$Ri_0^C = g\left[\frac{\rho_j - \rho_a}{\rho_a}\right]\frac{Q}{u\,u_*^2\,D} = 0.12$$

Figure IV.1. DEGADIS-predicted centerline maximum concentration vs. maximum measured concentration--Welker 275-1.

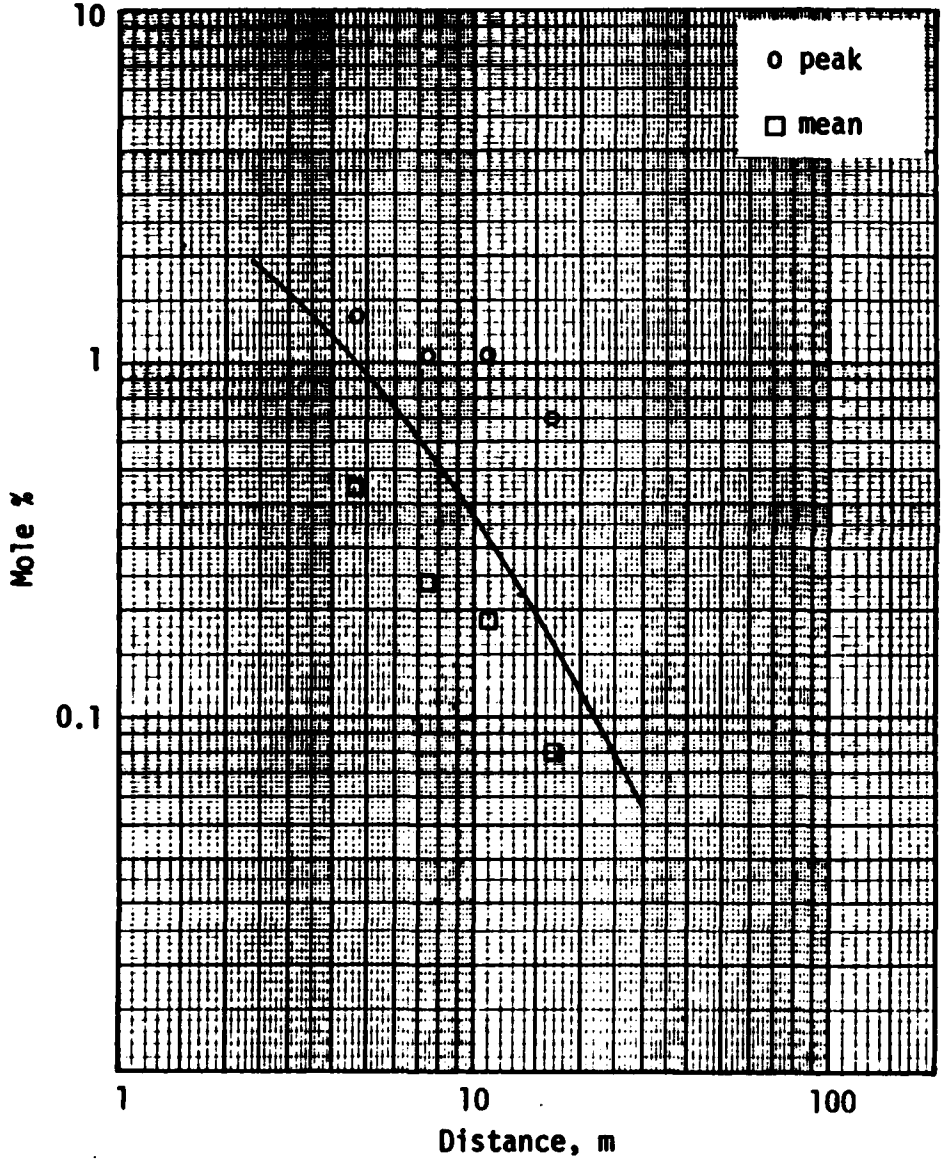

TEST WELKER 281-2

Source Description

Type: Continuous propane

Primary Source Width (m)	:	3.05
Secondary Source Width (m)	:	3.05
Primary Source Flux (kg/m^2 s)	:	6.13 E-3
Rate (kg/s)	:	0.057
Temperature (K)	:	231.0

Meteorological Conditions

Wind Velocity (m/s)	:	3.09
@ Height (m)	:	2.44
Surface Roughness (m)	:	0.01
Pasquill Stability	:	B
Monin-Obukhov Length (m)	:	-11.8
Air Temperature (K)	:	302.6
Relative Humidity (%)	:	21
Surface Temperature (K)	:	305

Release Richardson Number

Volumetric Release Rate (m^3/s)	:	.02
Characteristic Width (m)	:	3.05
Estimated Friction Velocity (m/s)	:	0.21

$$Ri_0^C = g\left[\frac{\rho_i - \rho_a}{\rho_a}\right]\frac{Q}{u\,u_*^2 D} = 0.6$$

Figure IV.2. DEGADIS-predicted centerline maximum concentration vs. maximum measured concentration--Welker 281-2.

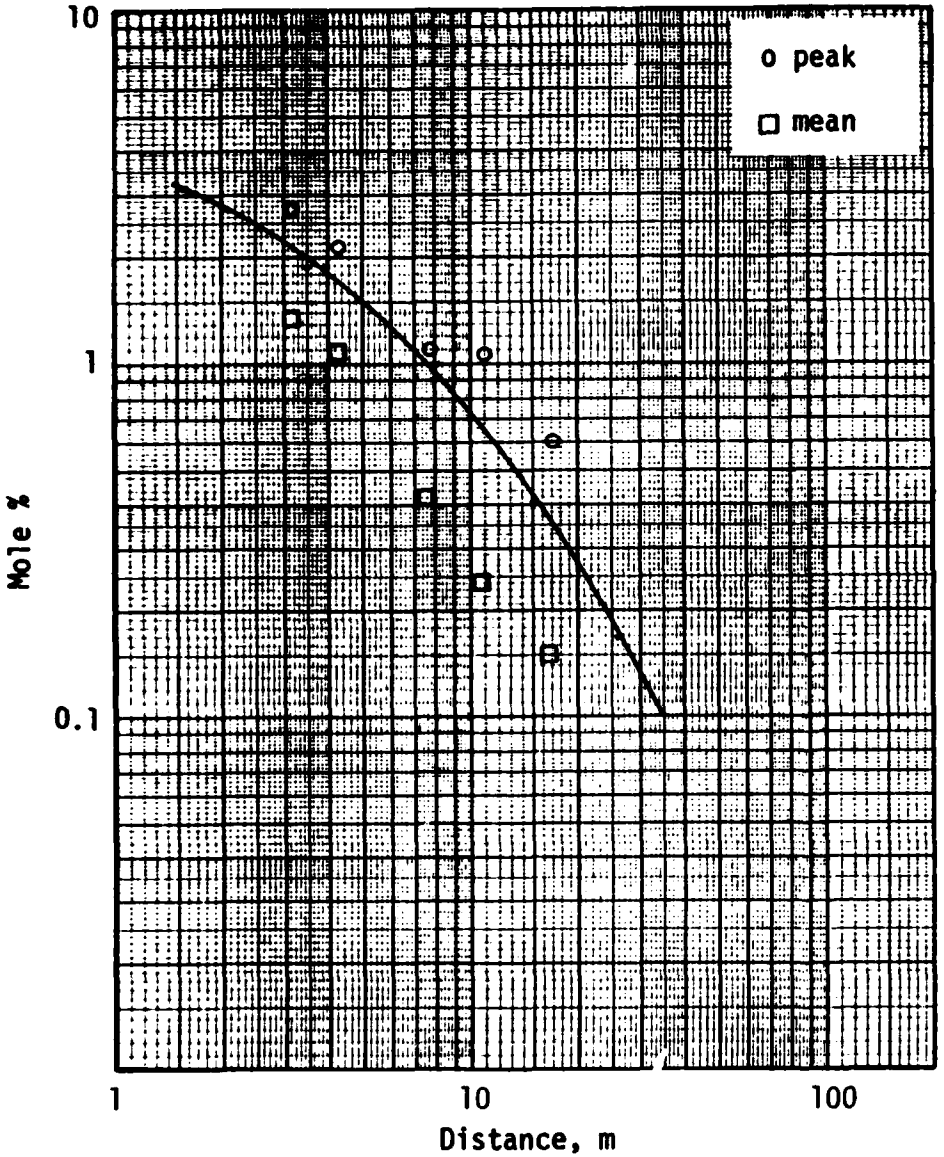

TEST WELKER 291-6

Source Description

Type: Continuous propane

Primary Source Width (m)	:	3.05
Secondary Source Width (m)	:	3.05
Primary Source Flux (kg/m^2 s)	:	7.64 E-3
Rate (kg/s)	:	0.071
Temperature (K)	:	231.0

Meteorological Conditions

Wind Velocity (m/s)	:	4.29
@ Height (m)	:	2.44
Surface Roughness (m)	:	0.01
Pasquill Stability	:	D
Monin-Obukhov Length (m)	:	∞
Air Temperature (K)	:	294
Relative Humidity (%)	:	40
Surface Temperature (K)	:	295

Release Richardson Number

Volumetric Release Rate (m^3/s)	:	.03
Characteristic Width (m)	:	3.05
Estimated Friction Velocity (m/s)	:	0.27

$$Ri_0^C = g\left[\frac{\rho_i - \rho_a}{\rho_a}\right]\frac{Q}{u\,u_*^2\,D} = 0.3$$

Figure IV.3. DEGADIS-predicted centerline maximum concentration vs. maximum measured concentration--Welker 296-1.

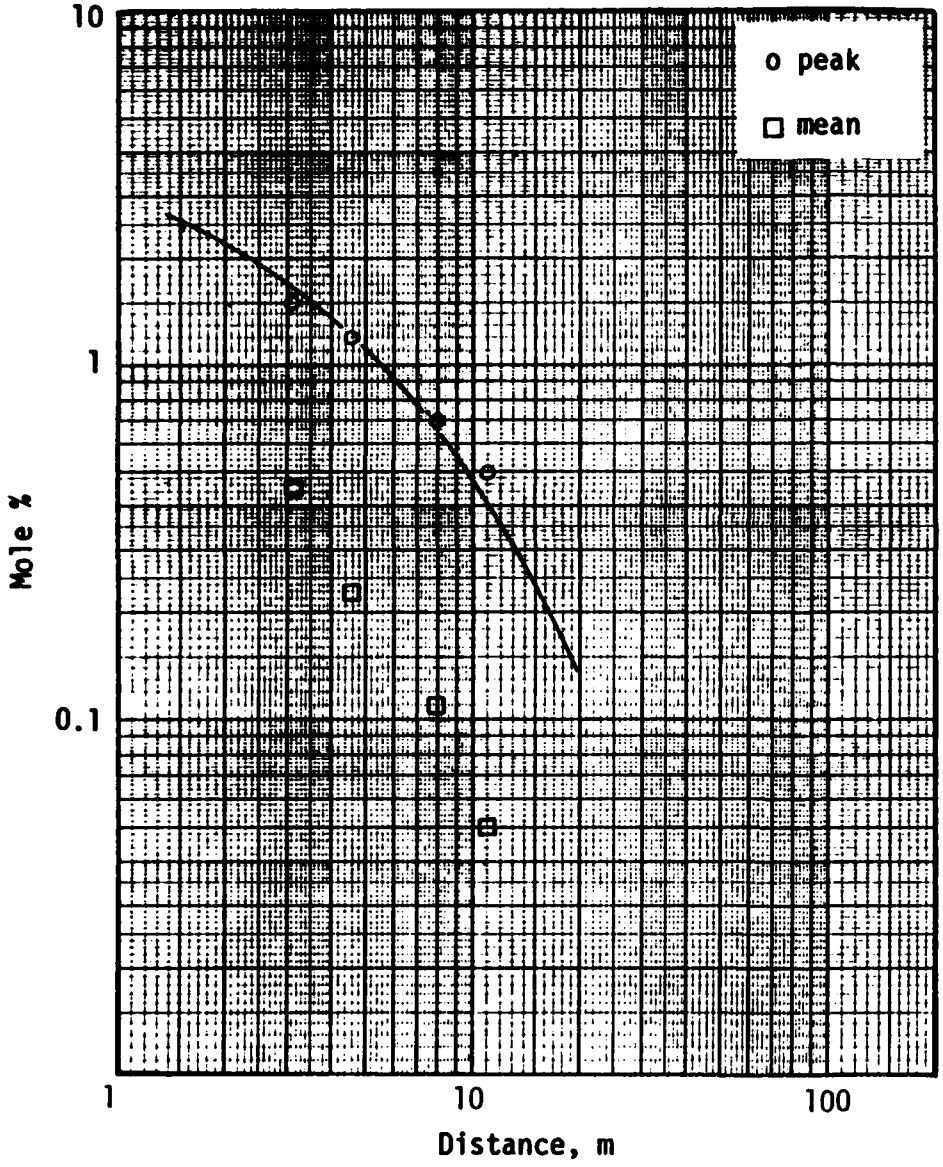

TEST WELKER 297-1

Source Description

Type: Continuous propane

Primary Source Width (m)	:	3.05
Secondary Source Width (m)	:	3.05
Primary Source Flux (kg/m^2 s)	:	6.24 E-3
Rate (kg/s)	:	0.058
Temperature (K)	:	231.0

Meteorological Conditions

Wind Velocity (m/s)	:	4.34
@ Height (m)	:	2.44
Surface Roughness (m)	:	0.01
Pasquill Stability	:	C
Monin-Obukhov Length (m)	:	-30.4
Air Temperature (K)	:	296
Relative Humidity (%)	:	23
Surface Temperature (K)	:	296

Release Richardson Number

Volumetric Release Rate (m^3/s)	:	.02
Characteristic Width (m)	:	3.05
Estimated Friction Velocity (m/s)	:	0.29

$$Ri_0^C = g\left[\frac{\rho_i - \rho_a}{\rho_a}\right]\frac{Q}{u\,u_*^2\,D} = 0.2$$

Figure IV.4. DEGADIS-predicted centerline maximum concentration vs. maximum measured concentration--Welker 297-1.

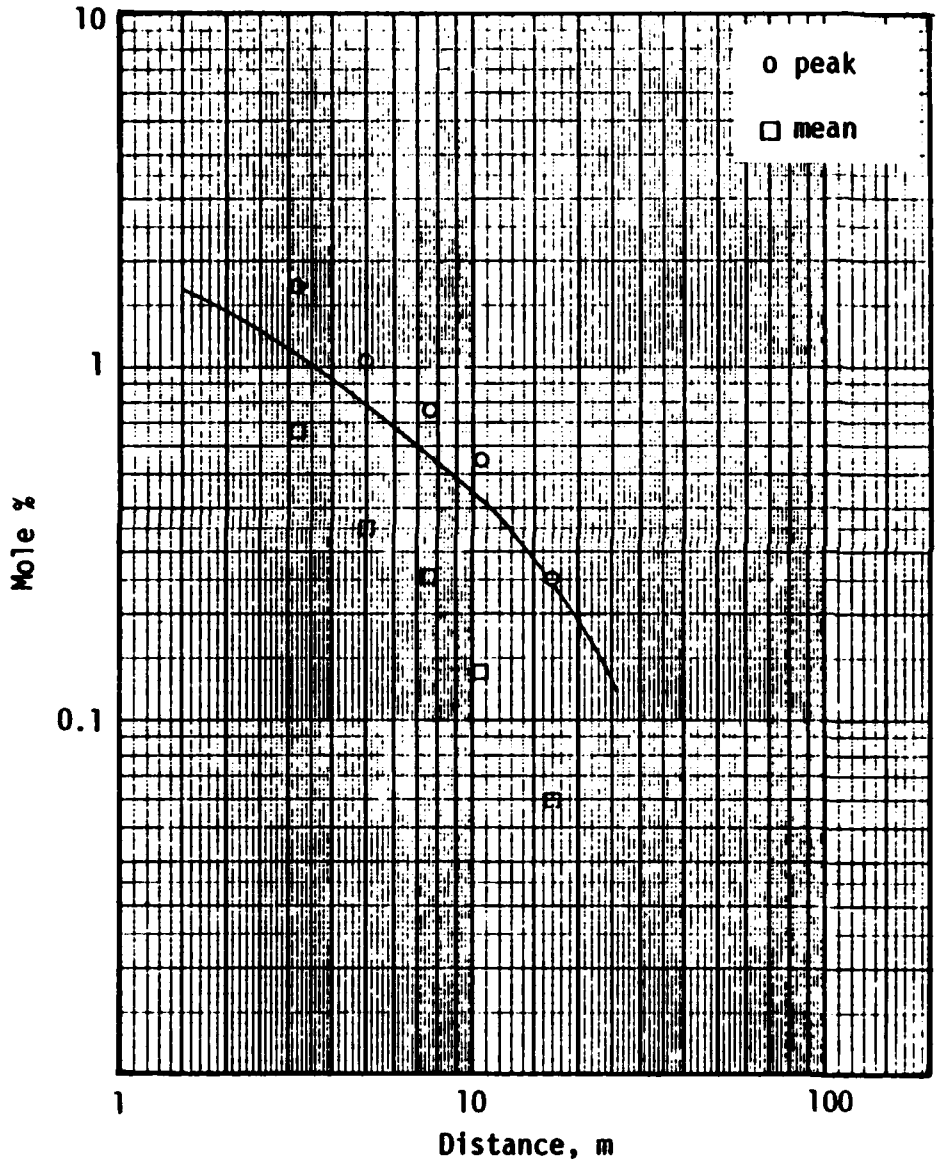

TEST WELKER 297-3

Source Description

Type: Continuous propane

Primary Source Width (m)	:	3.05
Secondary Source Width (m)	:	3.05
Primary Source Flux (kg/m^2 s)	:	5.49 E-3
Rate (kg/s)	:	0.051
Temperature (K)	:	231.0

Meteorological Conditions

Wind Velocity (m/s)	:	3.67
@ Height (m)	:	2.44
Surface Roughness (m)	:	0.01
Pasquill Stability	:	D
Monin-Obukhov Length (m)	:	∞
Air Temperature (K)	:	298
Relative Humidity (%)	:	38
Surface Temperature (K)	:	300

Release Richardson Number

Volumetric Release Rate (m^3/s)	:	2.13 E-2
Characteristic Width (m)	:	3.05
Estimated Friction Velocity (m/s)	:	0.23

$$Ri_0^C = g\left[\frac{\rho_i - \rho_a}{\rho_a}\right]\frac{Q}{u\,u_*^2\,D} = 0.35$$

Figure IV.5. DEGADIS-predicted centerline maximum concentration vs. maximum measured concentration--Welker 297-3.

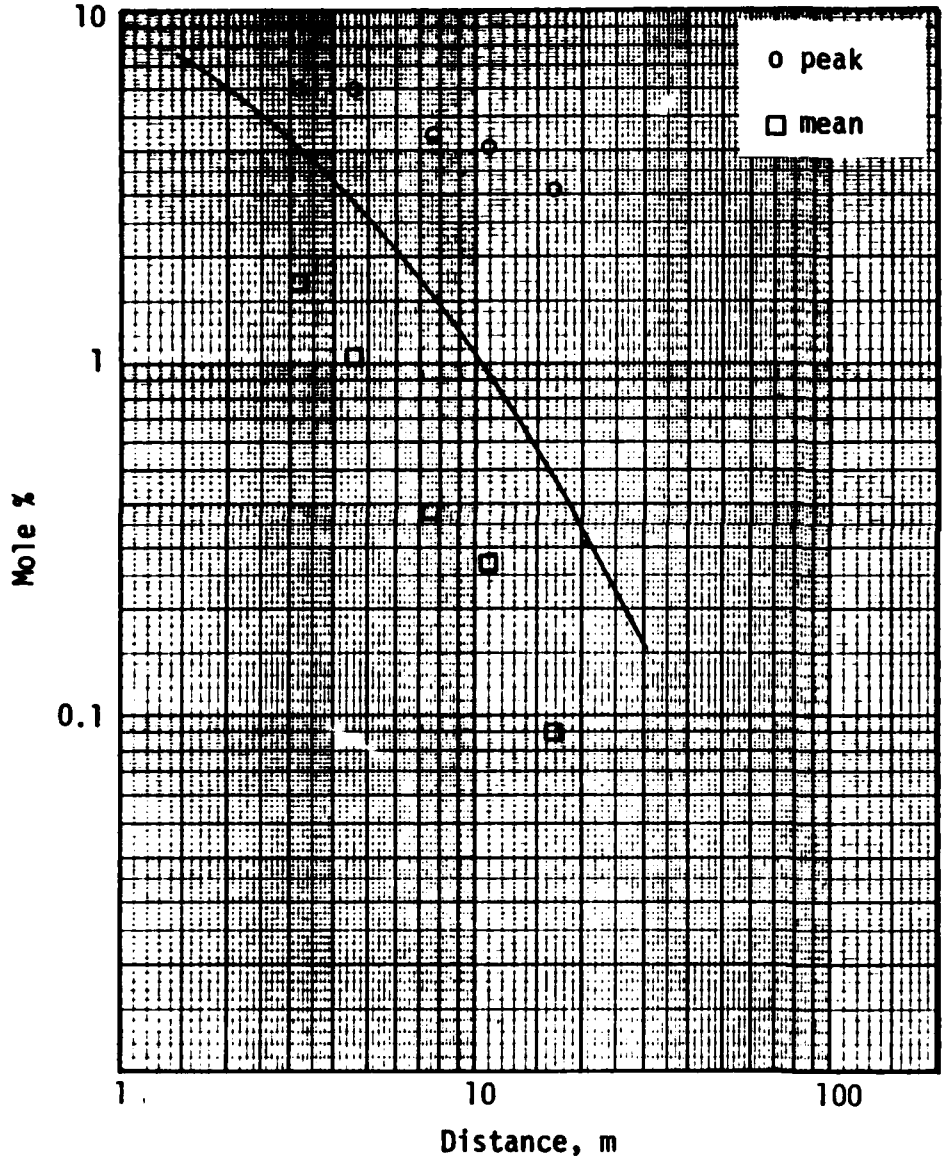

TEST WELKER 298-1

Source Description

Type:	Continuous propane	
Primary Source Width (m)	:	3.05
Secondary Source Width (m)	:	3.05
Primary Source Flux (kg/m^2 s)	:	5.92 E-3
Rate (kg/s)	:	0.055
Temperature (K)	:	231.0

Meteorological Conditions

Wind Velocity (m/s)	:	2.01
@ Height (m)	:	2.44
Surface Roughness (m)	:	0.01
Pasquill Stability	:	C
Monin-Obukhov Length (m)	:	-30.4
Air Temperature (K)	:	294
Relative Humidity (%)	:	23
Surface Temperature (K)	:	295

Release Richardson Number

Volumetric Release Rate (m^3/s)	:	.02
Characteristic Width (m)	:	3.05
Estimated Friction Velocity (m/s)	:	0.13

$$Ri_0^C = g\left[\frac{\rho_i - \rho_a}{\rho_a}\right]\frac{Q}{u\,u_*^2\,D} = 2.1$$

Figure IV.6. DEGADIS-predicted centerline maximum concentration vs. maximum measured concentration--Welker 298-1.

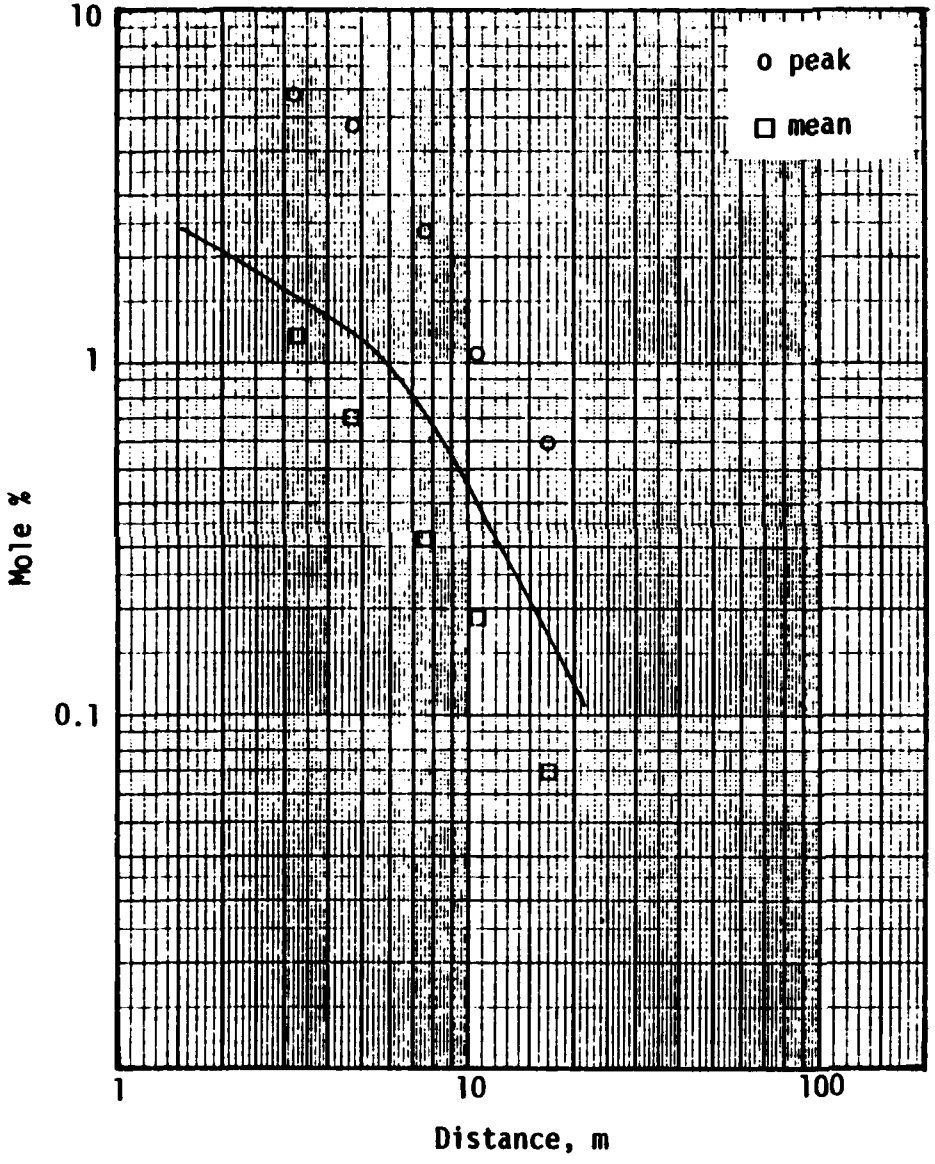

TEST WELKER 298-2

Source Description

Type: Continuous propane		
Primary Source Width (m)	:	3.05
Secondary Source Width (m)	:	3.05
Primary Source Flux (kg/m^2 s)	:	4.73 E-3
Rate (kg/s)	:	0.044
Temperature (K)	:	231.0

Meteorological Conditions

Wind Velocity (m/s)	:	2.15
@ Height (m)	:	2.44
Surface Roughness (m)	:	0.01
Pasquill Stability	:	B
Monin-Obukhov Length (m)	:	-11.8
Air Temperature (K)	:	296
Relative Humidity (%)	:	30
Surface Temperature (K)	:	298

Release Richardson Number

Volumetric Release Rate (m^3/s)	:	1.8 E-2
Characteristic Width (m)	:	3.05
Estimated Friction Velocity (m/s)	:	0.15

$$Ri_0^C = g\left[\frac{\rho_1 - \rho_a}{\rho_a}\right]\frac{Q}{u\,u_*^2\,D} = 1.3$$

Figure IV.7. DEGADIS-predicted centerline maximum concentration vs. maximum measured concentration--Welker 298-2.

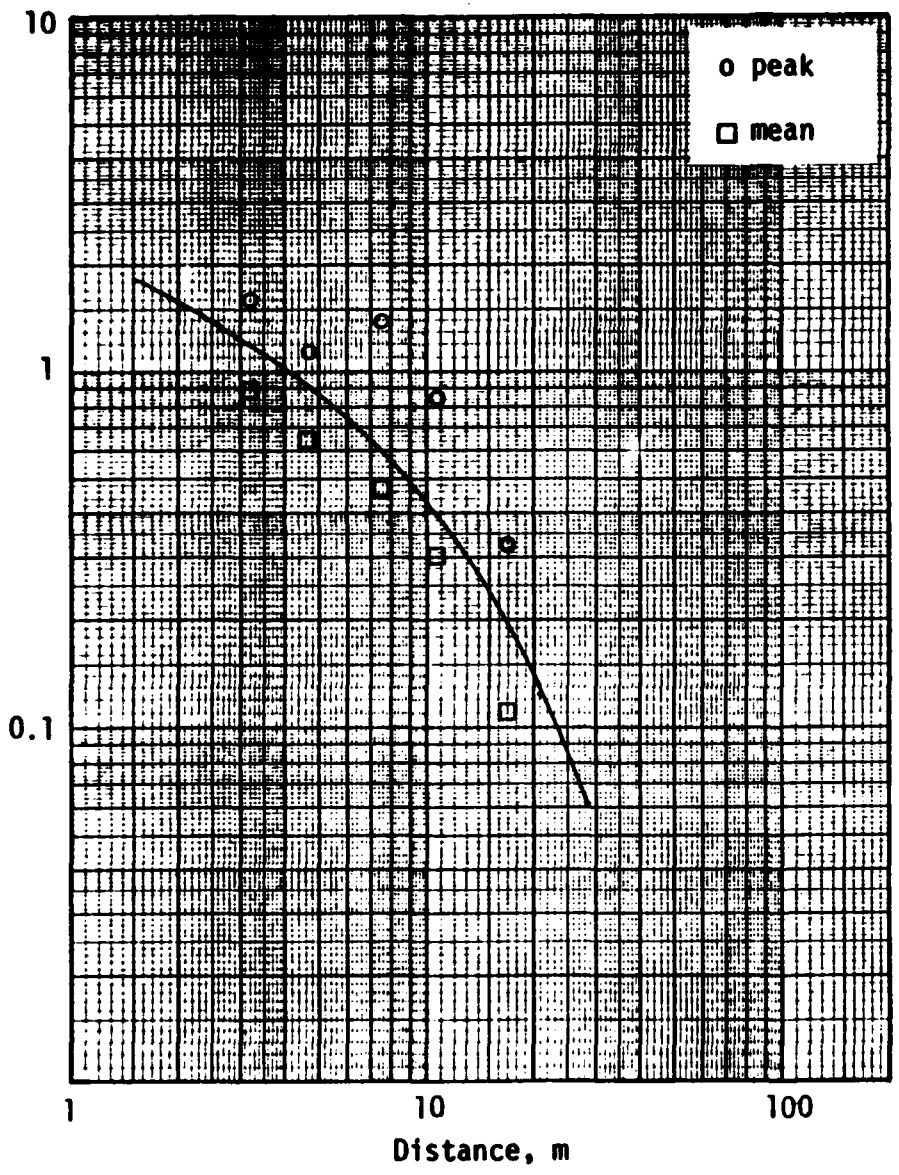

TEST WELKER 302-1

Source Description

Type: Continuous propane

Primary Source Width (m)	:	3.05
Secondary Source Width (m)	:	3.05
Primary Source Flux (kg/m^2 s)	:	7.85 E-3
Rate (kg/s)	:	0.073
Temperature (K)	:	231.0

Meteorological Conditions

Wind Velocity (m/s)	:	7.47
@ Height (m)	:	2.44
Surface Roughness (m)	:	0.01
Pasquill Stability	:	D
Monin-Obukhov Length (m)	:	∞
Air Temperature (K)	:	295
Relative Humidity (%)	:	69
Surface Temperature (K)	:	298

Release Richardson Number

Volumetric Release Rate (m^3/s)	:	.03
Characteristic Width (m)	:	3.05
Estimated Friction Velocity (m/s)	:	0.48

$$Ri_0^C = g\left[\frac{\rho_i - \rho_a}{\rho_a}\right]\frac{Q}{u\,u_*^2\,D} = 0.1$$

Figure IV.8. DEGADIS-predicted centerline maximum concentration vs. maximum measured concentration--Welker 302-1.

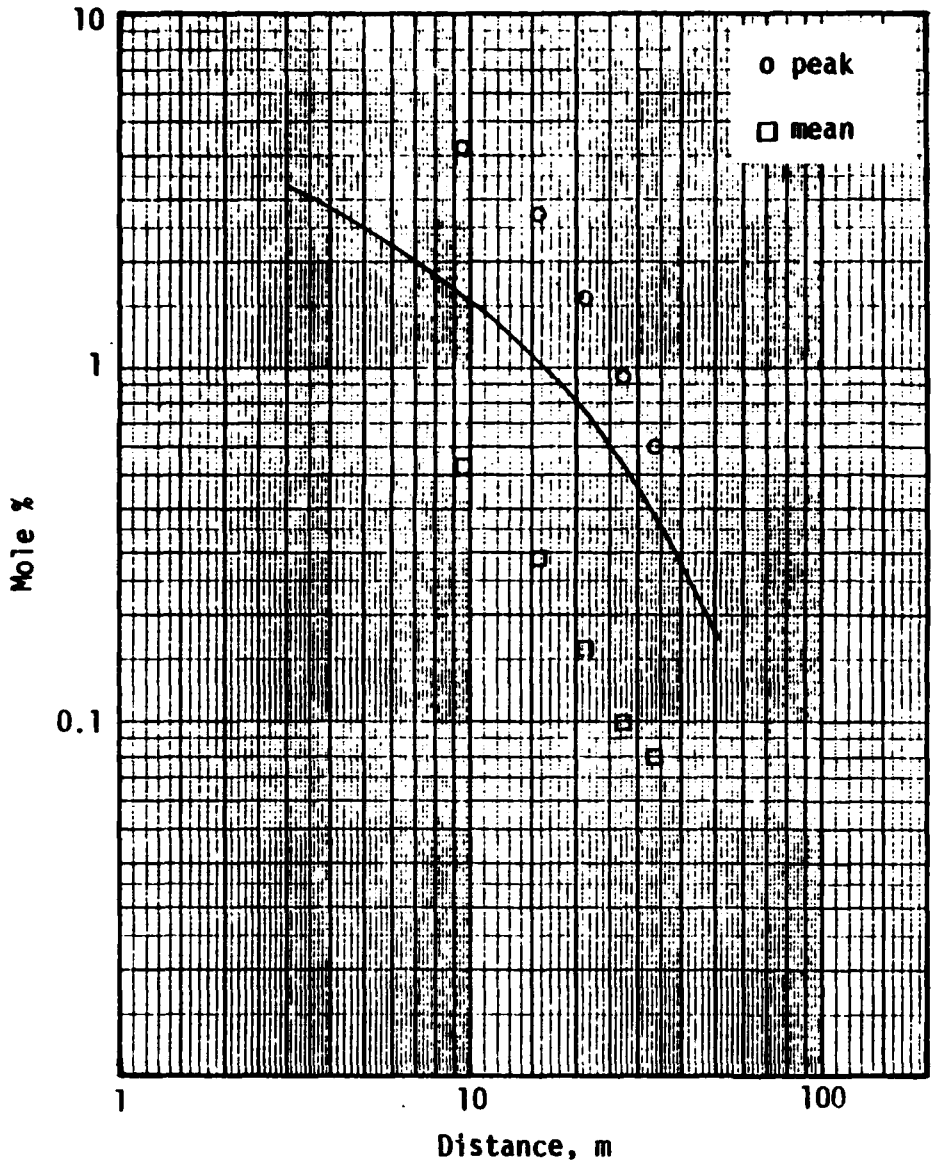

TEST WELKER 334-1

Source Description

Type:	Continuous propane	
Primary Source Width (m)	:	6.10
Secondary Source Width (m)	:	6.10
Primary Source Flux (kg/m^2 s)	:	6.7 E-3
Rate (kg/s)	:	0.249
Temperature (K)	:	231.0

Meteorological Conditions

Wind Velocity (m/s)	:	2.37
@ Height (m)	:	2.44
Surface Roughness (m)	:	0.01
Pasquill Stability	:	C
Monin-Obukhov Length (m)	:	-30.4
Air Temperature (K)	:	279
Relative Humidity (%)	:	~10
Surface Temperature (K)	:	280

Release Richardson Number

Volumetric Release Rate (m^3/s)	:	0.104
Characteristic Width (m)	:	6.10
Estimated Friction Velocity (m/s)	:	0.16

$$Ri_0^C = g\left[\frac{\rho_j - \rho_a}{\rho_a}\right]\frac{Q}{u\,u_*^2\,D} = 3.0$$

Figure IV.9. DEGADIS-predicted centerline maximum concentration vs. maximum measured concentration--Welker 334-1.

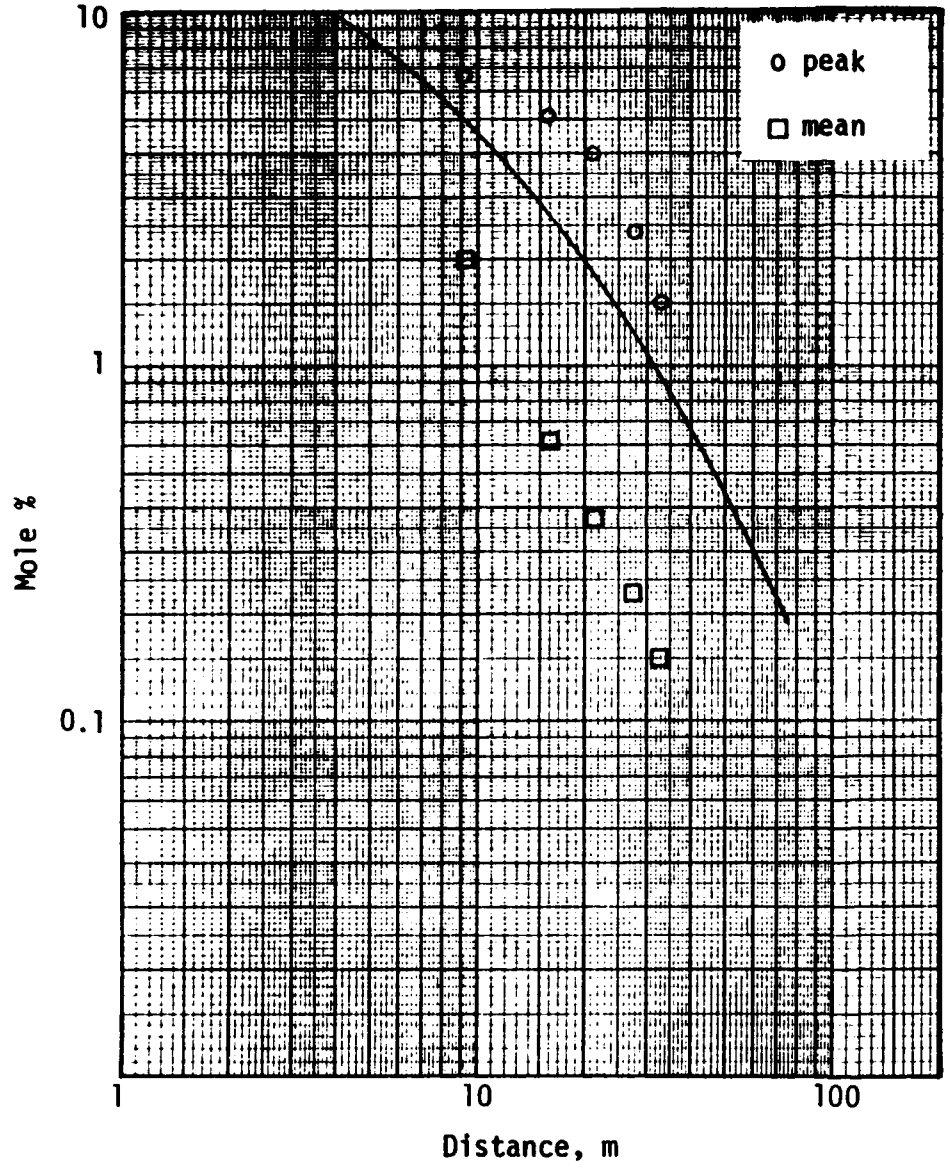

TEST WELKER 334-2

Source Description

Type: Continuous propane		
Primary Source Width (m)	:	6.10
Secondary Source Width (m)	:	6.10
Primary Source Flux (kg/m^2 s)	:	1.48 E-2
Rate (kg/s)	:	0.551
Temperature (K)	:	231.0

Meteorological Conditions

Wind Velocity (m/s)	:	2.77
@ Height (m)	:	2.44
Surface Roughness (m)	:	0.01
Pasquill Stability	:	C
Monin-Obukhov Length (m)	:	-30.4
Air Temperature (K)	:	279
Relative Humidity (%)	:	~10
Surface Temperature (K)	:	279

Release Richardson Number

Volumetric Release Rate (m^3/s)	:	0.23
Characteristic Width (m)	:	6.1
Estimated Friction Velocity (m/s)	:	0.18

$$Ri_0^C = g\left[\frac{\rho_i - \rho_a}{\rho_a}\right]\frac{Q}{u\,u_*^2 D} = 3.5$$

Figure IV.10. DEGADIS-predicted centerline maximum concentration vs. maximum measured concentration--Welker 334-2.

IV.2 LNG Releases on Land from Diked Area Sources

The American Gas Association sponsored a series of more than 30 LNG releases (AGA, 1974) into diked land areas up to 24.4 m diameter in 1973 near San Clemente, California. Releases were made into 1.8 m, 6.1 m, and 24.4 m diameter land areas surrounded by ~0.5 m high, insulated wall dikes. Vapor release rates for the experiments were determined from correlations of experimentally measured liquid boiling rates in the test program, and the LNG vapor source rate used for 1.8, 6.1, and 24.4 m diked areas are shown in Figure IV.11. The measured maximum gas concentration (at a height of 0.5 m) from eleven of the experiments, which included releases in all three dike sizes, were correlated with wind velocity, diked area, and downwind distance as shown in Figure IV.12 (AGA, 1974).

The DEGADIS model has been used to simulate LNG releases with the source rates and dimensions shown in Figure IV.11 and with a wind velocity of 3.6 m/s, representing "typical" releases from 1.8 m, 6.1 m, and 24.4 m dikes respectively. Atmospheric stability C was assumed with ambient and soil surface temperatures 288K and 300K, respectively. The ambient humidity was assumed 45%. The predicted downwind distance to the LFL concentration (5% at ground level) for the three simulations is shown in Figure IV.12 for comparison with the experimental data correlation.

Figure IV.13 shows the DEGADIS-predicted maximum concentration decay (at ground level) with distance from release center compared with reported experimental measurements from AGA Test 44, the largest LNG release of the test series, for which the pertinent test description is given in Table IV.2.

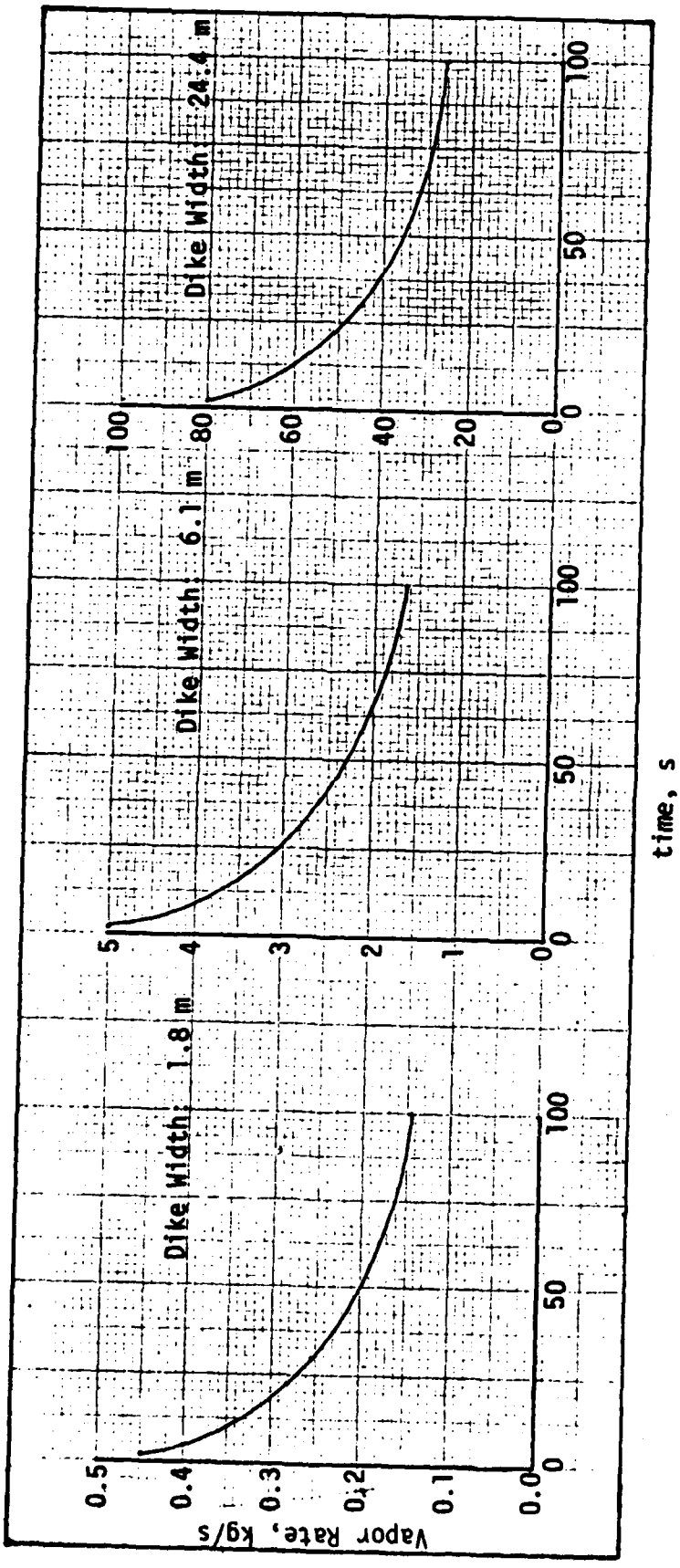

Figure IV.11. Vapor release rates used to simulate AGA LNG releases from diked areas.

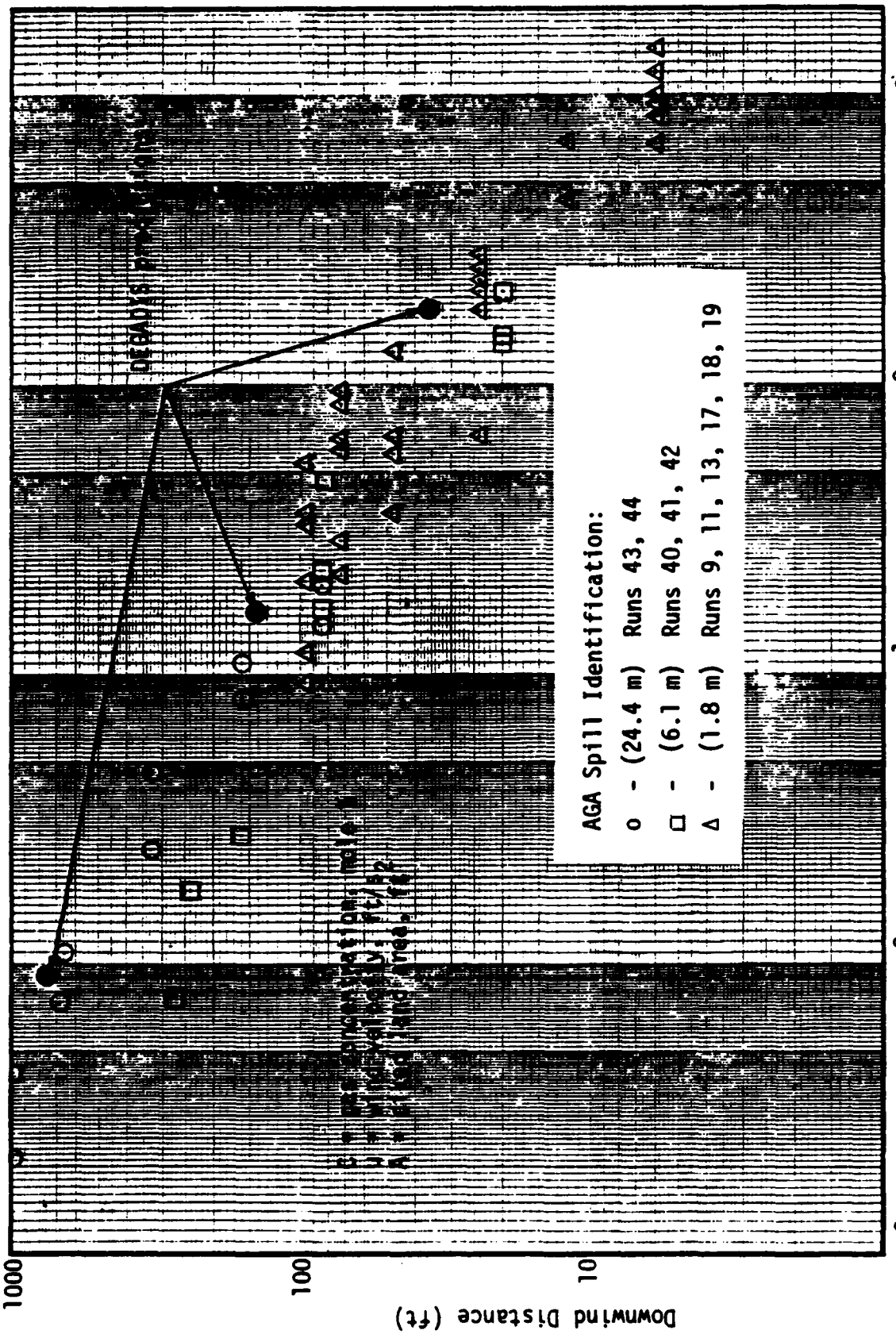

Figure IV.12. DEGADIS predictions for 1.8, 6.1, and 24.4 meter diked land releases compared with Battelle correlation of maximum measured concentrations.

TABLE IV.2
TEST CONDITIONS FOR AGA TEST 44

LNG Volume Spilled: 51 m^3 (liq) in 20-30 s
Diked Area Diameter: 24.4 m
Vapor Release Rate: est. as shown in Figure IV.11
Wind Speed: 3.6 m/s (actual varied 3.6 - 7.2 m/s)
Ambient Temperature: 14.5 C
Surface Temperature: estimated 14.5 C
Atmospheric Stability: estimated Pasquill C
Surface Roughness: estimated 1 cm

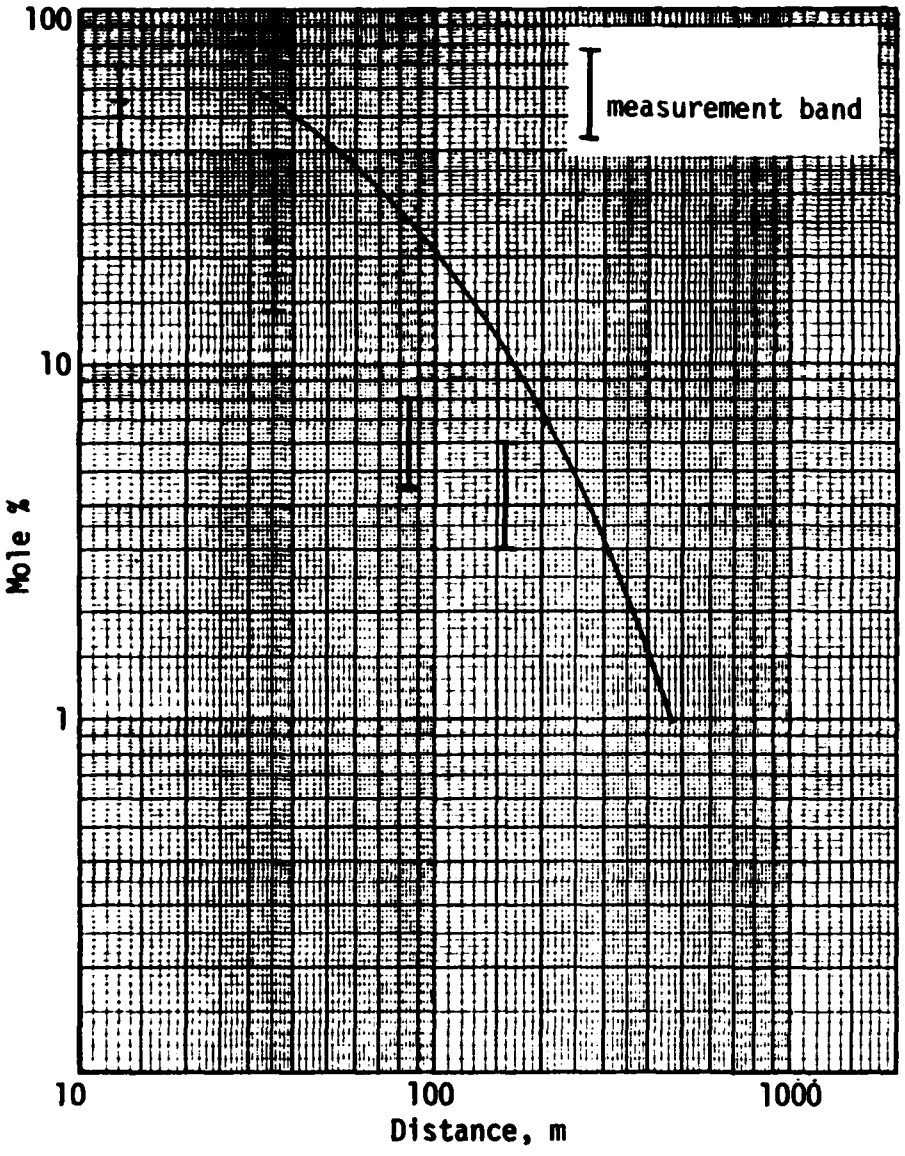

TEST: AGA 44

Source Description

Type: Transient, land
Liquid Volume (m^3): 51.0
Temperature (K) : 112

Meteorological Conditions

Wind Velocity (m/s)	:	3.6
@ Height (m)	:	1.5
Surface Roughness (m)	:	1.0 E-02
Pasquill Stability	:	C
Monin-Obukhov Length (m)	:	-30.4
Air Temperature (K)	:	287.55
Relative Humidity (%)	:	45
Surface Temperature (K)	:	287.8

Figure IV.13. DEGADIS-predicted centerline maximum concentration vs. maximum measured concentration--AGA 44.

IV.3 American Petroleum Institute/ESSO LNG Releases on Water

The American Petroleum Institute sponsored a series of 17 LNG releases conducted by ESSO Research and Engineering Company on Matagorda Bay, Texas, in 1972 (API, 1972). The releases included liquid volumes ranging from about 1 m^3 to 10.2 m^3 with release rates ranging from about 10 m^3/min to about 20 m^3/min. The LNG was discharged from a nitrogen-pressurized ~13 m^3 tank as a jet. The liquid exit point was elevated and about 30° above horizontal. It has been pointed out by Shell Research that a substantial amount of the LNG could have vaporized before hitting the sea surface; estimates of the amount vaporized in the jet range as high as 75%. Since such vaporization would result in an LNG vapor/air mixture denser than pure LNG vapor, the description of the source as input to a vapor dispersion model is uncertain. Predictions for this spill using DEGADIS are consistent with the experimental results when the source is represented as an instantaneous spill of liquid on water with an LNG boiling rate of 0.196 kg/m^2 s. This boiling rate, which is about twice as high as indicated by measurements by Shell (Blackmore, 1982), may be consistent with the experiments because it more closely represents the rapid cloud formation by the jet.

Table IV.3 shows the pertinent test descriptions for tests 11 and 17, which were the two largest LNG releases, simulated with the DEGADIS model. ESSO 11 and ESSO 17 were simulated as instantaneous liquid releases onto water, and the LNG liquid pool growth was estimated using the liquid spread model described by Havens (1982), which incorporated an LNG boiling rate of 0.196 kg/m^2 s.

Figures IV.14 and IV.15 show the DEGADIS model-predicted maximum ground level centerline gas concentration compared with measured maximum concentrations (at ~0.4 m height) as a function of downwind distance from the release center for ESSO 11 and ESSO 17 respectively. The gas concentrations were reportedly measured with a catalytic type hydrocarbon sensor and recorded at 2 Hz.

TABLE IV.3

TEST CONDITIONS FOR ESSO TESTS 11 AND 17

	ESSO 11	ESSO 17
LNG Volume Spilled (m^3)	10.2	8.4
Wind Speed @ 5.6 m (m/s)	8.04	4.1
Atmospheric Stability	D	D
Ambient Temperature (K)	300.2	291.2
Relative Humidity (%)	78	85
Surface Roughness (m) (estimated)	0.0001	0.0001

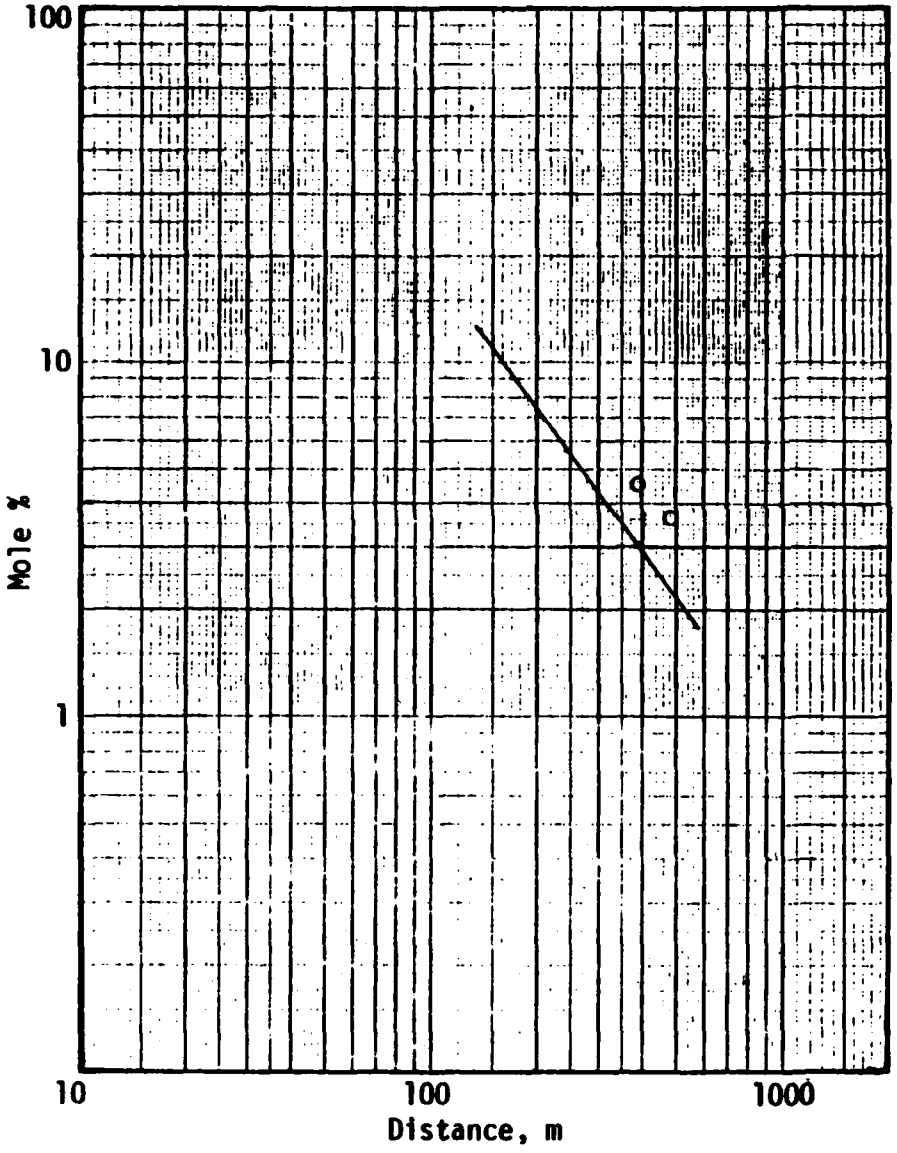

TEST: Esso 11

Source Description

Type: Instantaneous LNG
Liquid Volume (m^3): 10.2
Temperature (K) : 112

Meteorological Conditions

Wind Velocity (m/s)	:	8.04
@ Height (m)	:	5.6
Surface Roughness (m)	:	1.0 E-4
Pasquill Stability	:	D
Monin-Obukhov Length (m)	:	∞
Air Temperature (K)	:	300.15
Relative Humidity (%)	:	78
Surface Temperature (K)	:	301.15
Estimated Friction Velocity (m/s)	:	0.26

Figure IV.14. DEGADIS-predicted centerline maximum concentration vs. maximum measured concentration--Esso 11.

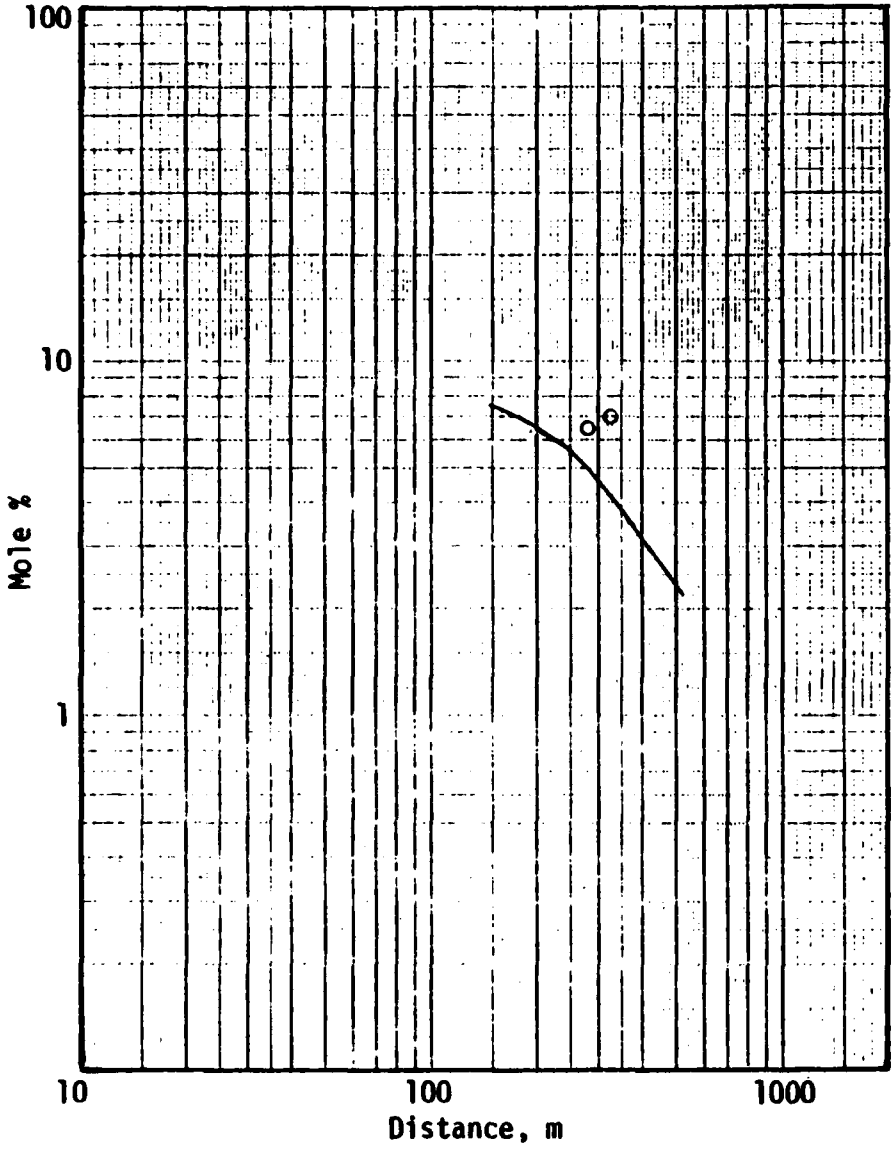

TEST: Esso 17

Source Description

Type: Instantaneous LNG
Liquid Volume (m^3): 8.4
Temperature (K) : 112

Meteorological Conditions

Wind Velocity (m/s)	:	4.1
@ Height (m)	:	5.6
Surface Roughness (m)	:	1.0 E-4
Pasquill Stability	:	D
Monin-Obukhov Length (m)	:	∞
Air Temperature (K)	:	291.15
Relative Humidity (%)	:	85
Surface Temperature (K)	:	291.0
Estimated Friction Velocity (m/s)		0.13

Figure IV.15. DEGADIS-predicted centerline maximum concentration vs. maximum measured concentration--Esso 17.

IV.4 U.S. Department of Energy Burro and Coyote LNG Releases on Water

The U.S. Department of Energy sponsored a series of nine LNG release field experiments conducted in 1980 at China Lake, California. The LNG volumes released on water ranged from 24 to 39 m^3, at rates of 11.3 to 18.4 m^3/min.. with subsequent dispersion over land. The extensive data from the experiments were reported by Koopman et al. (1982), and several analyses of the test data and comparisons with predictions using dispersion models developed by Lawrence Livermore National Laboratories (LLNL) have been published (Cederwell et al., 1981; Ermak et al., 1982; Morgan et al., 1983b; Chan and Ermak, 1983).

The subsequent Coyote test series, designed to study LNG fire and rapid phase transition phenomena also provided test data on atmospheric dispersion of LNG vapors. The test data for the Coyote series are reported by Goldwire et al. (1983), and comparison of the experimental vapor dispersion model predictions using the SLAB and FEM3 models developed by LLNL have been published (Morgan et al., 1983c).

Table IV.4 shows the pertinent test descriptions for Burro 3, 7, 8, 9, and Coyote 5 and 6, which have been simulated with the DEGADIS model. The experiments were modeled as steady, time-limited releases, i.e. Burro 9 was represented as a steady release of 130 kg/s for 79 seconds. The liquid source diameter was determined using an LNG-on-water boiling rate of 0.085 kg/m^2s, suggested by the analysis of the Shell Maplin Sands LNG release experiments (Blackmore et al., 1982). In all cases, LNG is assumed characterized by the properties of methane. The reported measured concentrations are based on a 10 s averaging time; the lowest sensor position was 1 m. Ninety gas sensors were used of which 45 were IST (International Sensor Technology) detectors, 33 were an infrared

absorption detector developed by LLNL, and 12 were MSA (Mine Safety Appliance) catalytic detectors. Figures IV.16 through IV.21 show the DEGADIS model-predicted maximum ground level centerline gas concentration compared with the measured (10 s averaged) maximum concentrations as a function of downwind distance from the release center for these tests.

TABLE IV.4

DOE CHINA LAKE LNG SPILL TEST SCENARIO DATA SUMMARY

Test No.	LNG Comp. % C_1 % C_2 % C_3	Liquid Spill Volume m^3	Liquid Spill Rate m^3/min	Wind Speed, m/s @ 1 m 3 m 8 m	Temp. °C @ 2 m	Atmos. Pressure ATM	Monin Obukhov Length m	Pasquill Stability	Surface Temp. °C	Relative Humidity Upwind / Downwind
Burro 3	Unknown	34.0	12.2	5.1 5.6 5.8	33.8	0.95	-9.06	C	310	-/5.2
Burro 7	92.9 5.8 1.2	39.4	13.6	7.8 8.8 9.6	33.7	0.94	-114	D	310	6.7/7.4
Burro 8	96.5 2.8 0.6	28.4	16.0	1.6 1.9 2.4	33.1	0.94	+16.5	E	310	4.7/4.5
Burro 9	93.6 5.2 0.9	24.2	18.4	5.3 5.9 6.5	35.4	0.94	-140	C	310	11.7/14.4
Coyote 5	74.9 20.5 4.6	28.0	17.1	10.2 10.5 11.9	27.9	0.94	-26.5	C	310	22.1/ --
Coyote 6	81.8 14.6 3.6	22.8	16.6	5.0 5.0 5.9	24.4	0.94	+73.6	D	310	22.8/ --

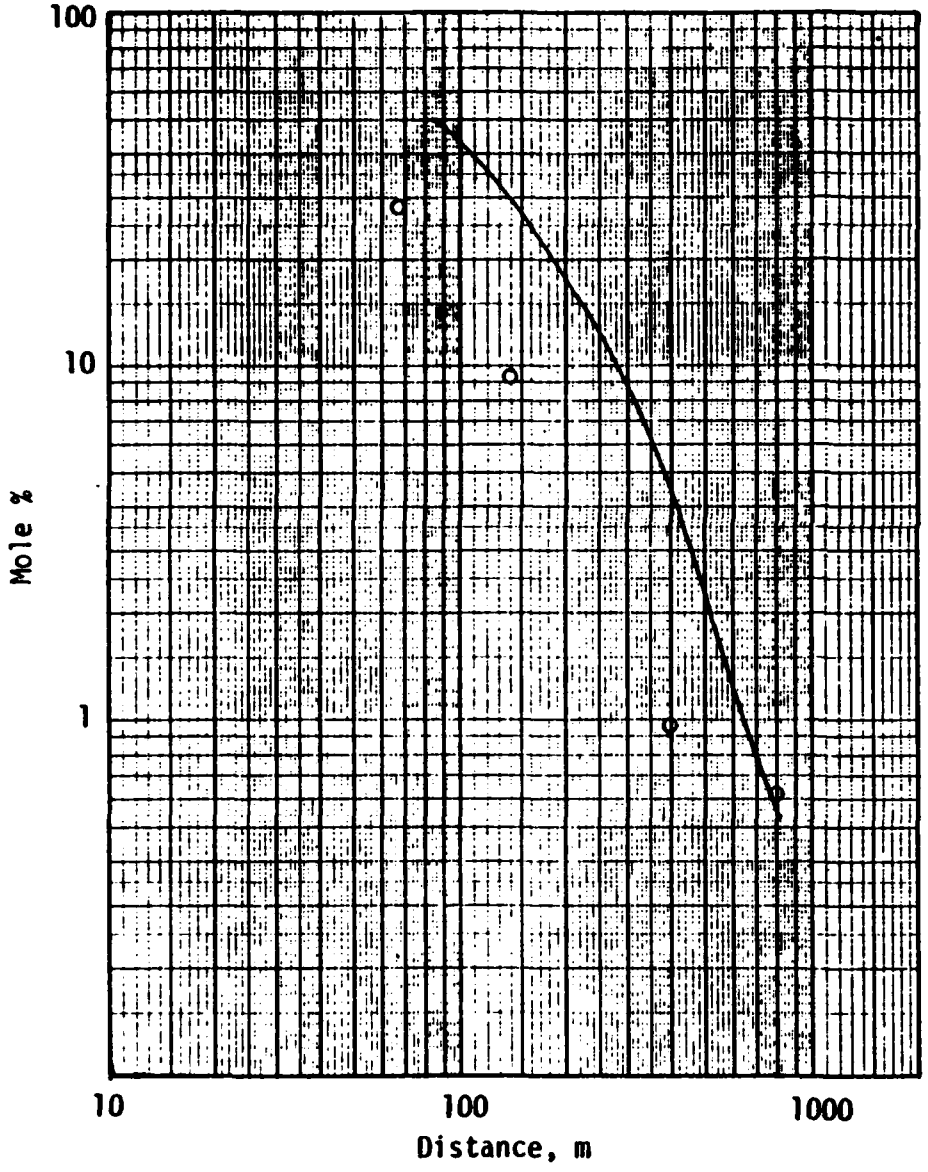

TEST: Burro 3

Source Description

Type:	Steady, time-limited LNG	
Primary Source Radius (m)	:	18.0
Primary Source Flux ($kg/m^2 s$)	:	0.085
Rate (kg/s)	:	86.4 for 167 s
Temperature (K)	:	112

Meteorological Conditions

Wind Velocity (m/s)	:	5.9
@ Height (m)	:	8.0
Surface Roughness (m)	:	2.0 E-4
Pasquill Stability	:	C
Monin-Obukhov Length (m)	:	-9.06
Air Temperature (K)	:	306.95
Relative Humidity (%)	:	5
Surface Temperature (K)	:	310.0

Release Richardson Number

Volumetric Release Rate (m^3/s)	:	48.2
Characteristic Width (m)	:	31.9
Estimated Friction Velocity (m/s)	:	0.22

$$Ri_0^C = g\left[\frac{\rho_i - \rho_a}{\rho_a}\right]\frac{Q}{u u_*^2 D} = 29$$

Figure IV.16. DEGADIS-predicted centerline maximum concentration vs. maximum measured concentration--Burro 3.

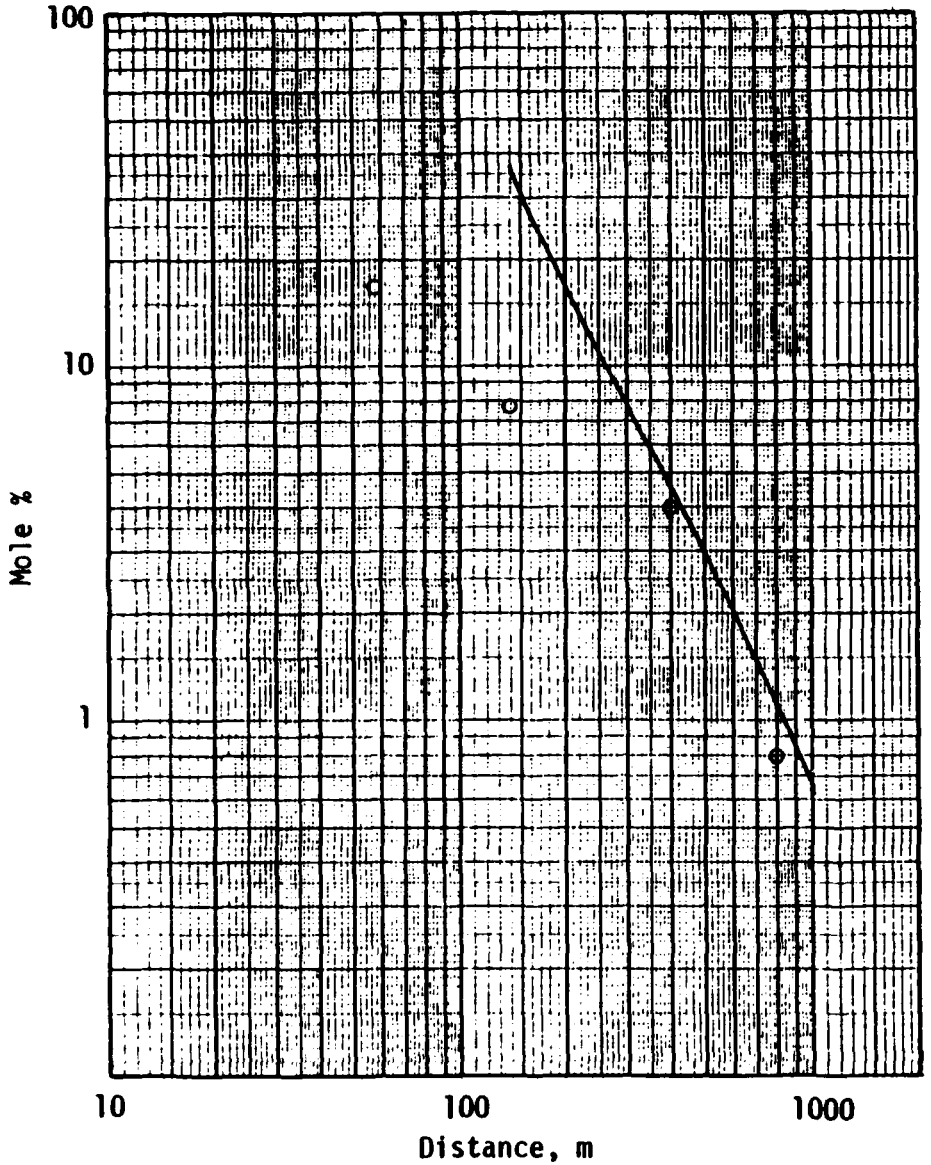

TEST: Burro 7

Source Description

Type:	Steady, Time-Limited LNG	
Primary Source Radius (m)	:	19.0
Primary Source Flux ($kg/m^2 s$)	:	0.085
Rate (kg/s)	:	96.3 for 174 s
Temperature (K)	:	112

Meteorological Conditions

Wind Velocity (m/s)	:	9.6
@ Height (m)	:	8.0
Surface Roughness (m)	:	2.05 E-4
Pasquill Stability	:	D
Monin-Obukhov Length (m)	:	-114.0
Air Temperature (K)	:	306.85
Relative Humidity (%)	:	7
Surface Temperature (K)	:	310.0

Release Richardson Number

Volumetric Release Rate (m^3/s)	:	53.7
Characteristic Width (m)	:	33.6
Estimated Friction Velocity (m/s)	:	0.32

$$Ri_0^C = g\left[\frac{\rho_i - \rho_a}{\rho_a}\right]\frac{Q}{u u_*^2 D} = 8.9$$

Figure IV.17. DEGADIS-predicted centerline maximum concentration vs. maximum measured concentration--Burro 7.

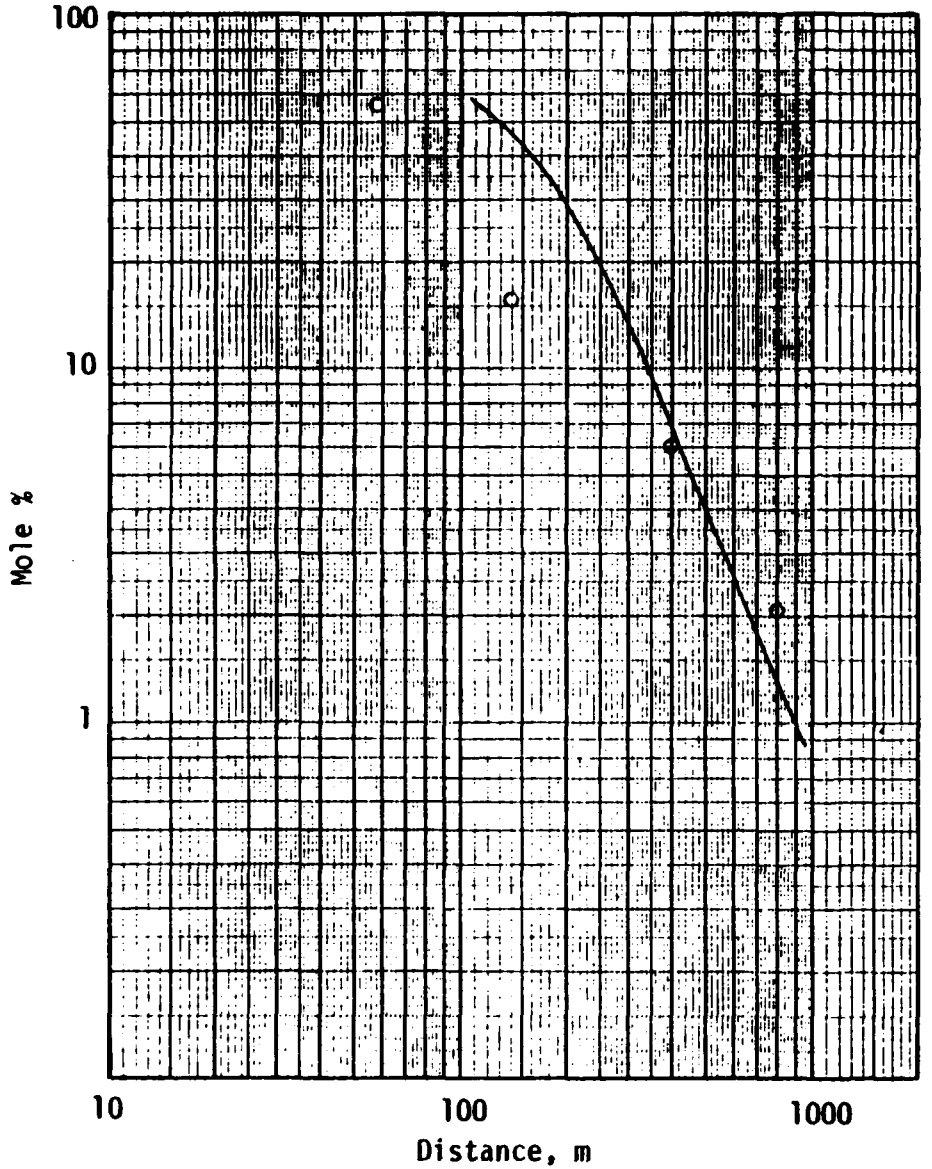

TEST: Burro 8

Source Description

Type: Steady, Time-Limited LNG

Primary Source Radius (m)	:	20.6
Primary Source Flux ($kg/m^2 s$)	:	0.085
Rate (kg/s)	:	113.3 for 106 s
Temperature (K)	:	112

Meteorological Conditions

Wind Velocity (m/s)	:	2.4
@ Height (m)	:	8.0
Surface Roughness (m)	:	2.05 E-4
Pasquill Stability	:	E
Monin-Obukhov Length (m)	:	16.5
Air Temperature (K)	:	306.15
Relative Humidity (%)	:	5
Surface Temperature (K)	:	310.0

Release Richardson Number

Volumetric Release Rate (m^3/s)	:	63.2
Characteristic Width (m)	:	36.5
Estimated Friction Velocity (m/s)	:	0.065

$$Ri_0^C = g\left[\frac{\rho_i - \rho_a}{\rho_a}\right]\frac{Q}{u u_*^2 D} = 930.$$

Figure IV.18. DEGADIS-predicted centerline maximum concentration vs. maximum measured concentration--Burro 8.

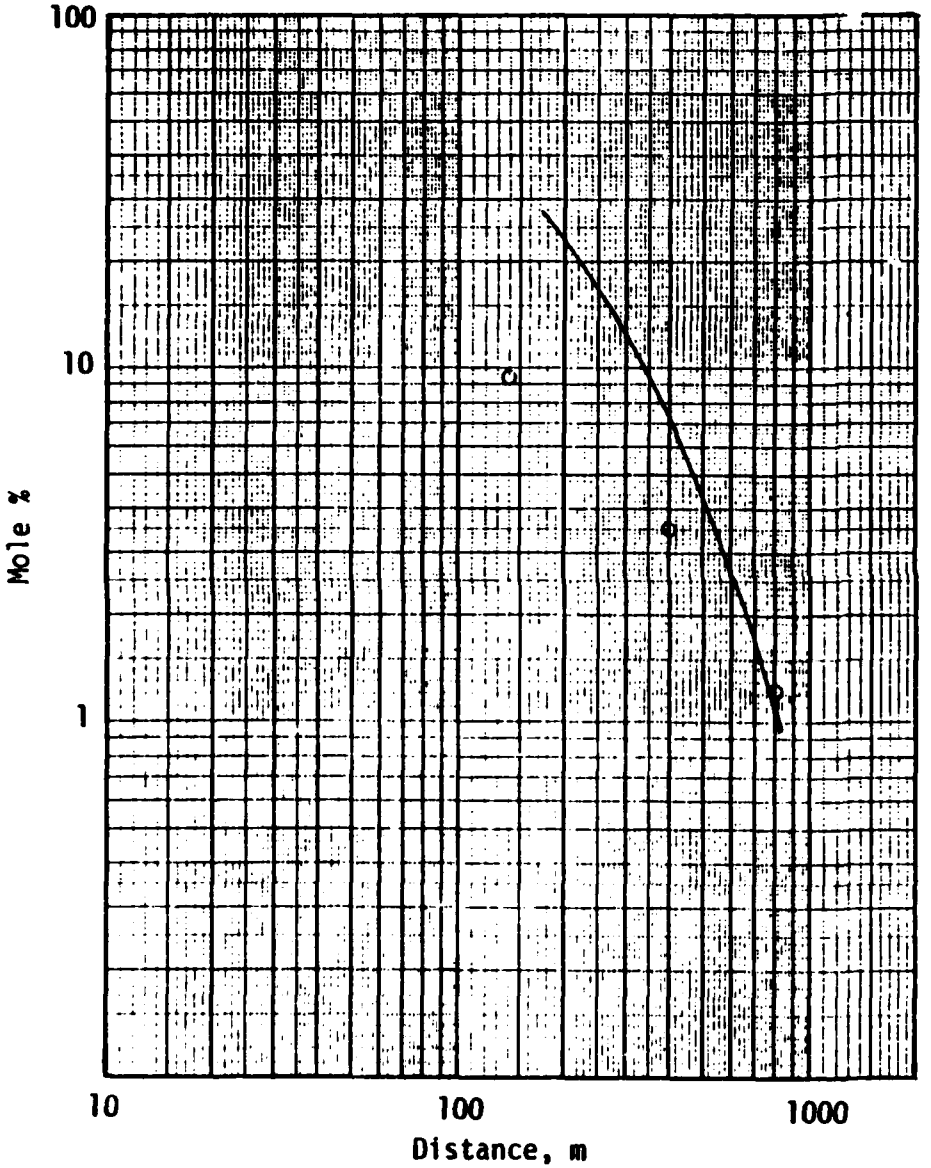

TEST: Burro 9

Source Description

Type:	Steady, Time-Limited LNG	
Primary Source Radius (m)	:	22.1
Primary Source Flux ($kg/m^2 s$)	:	0.085
Rate (kg/s)	:	130 for 80 s
Temperature (K)	:	112

Meteorological Conditions

Wind Velocity (m/s)	:	6.5
@ Height (m)	:	8.0
Surface Roughness (m)	:	2.05 E-4
Pasquill Stability	:	C
Monin-Obukhov Length (m)	:	-140.0
Air Temperature (K)	:	308.55
Relative Humidity (%)	:	13
Surface Temperature (K)	:	310.0

Release Richardson Number

Volumetric Release Rate (m^3/s)	:	72.5
Characteristic Width (m)	:	39.2
Estimated Friction Velocity (m/s)	:	0.22

$$Ri_0^C = g\left[\frac{\rho_i - \rho_a}{\rho_a}\right]\frac{Q}{u u_*^2 D} = 32$$

Figure IV.19. DEGADIS-predicted centerline maximum concentration vs. maximum measured concentration--Burro 9.

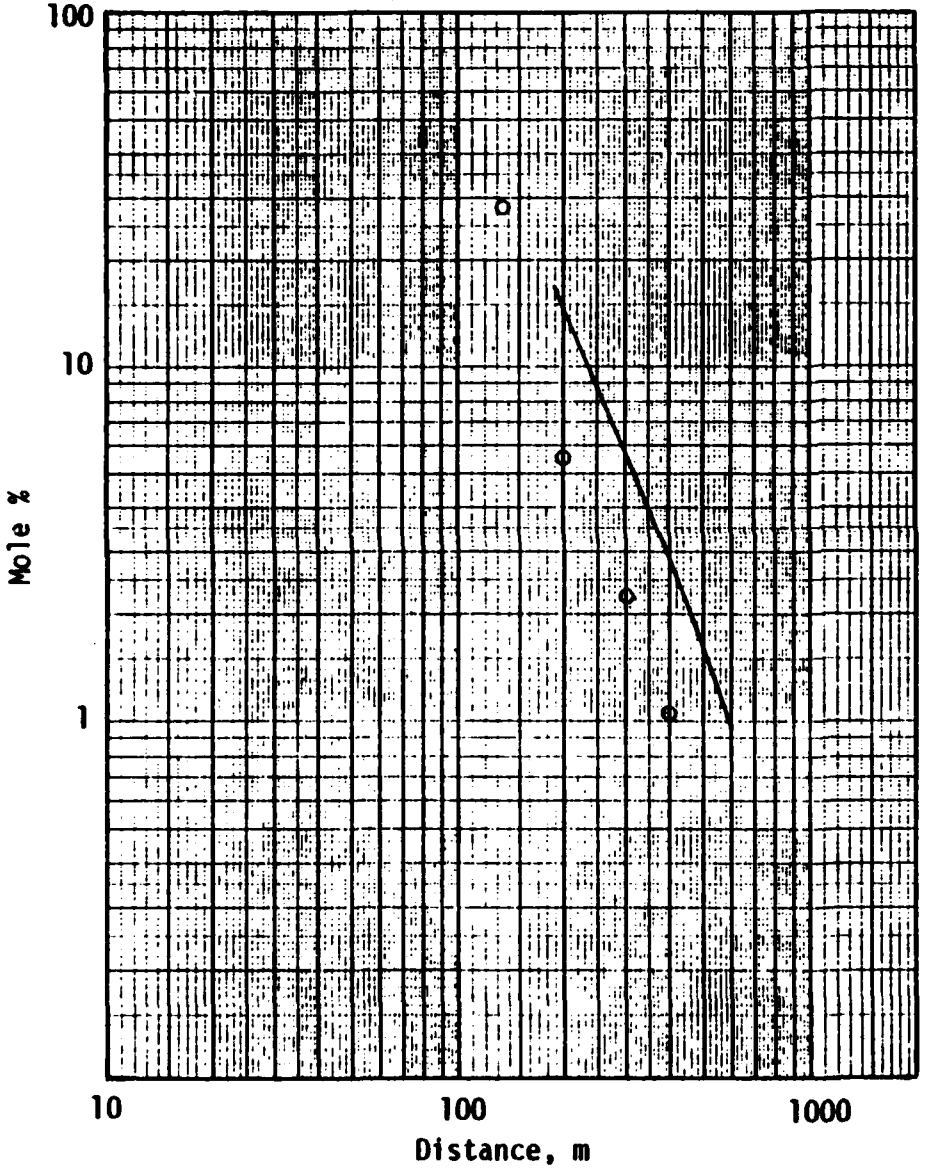

TEST: Coyote 5

Source Description

Type: Steady, Time-Limited LNG

Primary Source Radius (m)	:	21.3
Primary Source Flux ($kg/m^2 s$)	:	0.085
Rate (kg/s)	:	121 for 98 s
Temperature (K)	:	112

Meteorological Conditions

Wind Velocity (m/s)	:	11.9
@ Height (m)	:	8.0
Surface Roughness (m)	:	2.05 E-4
Pasquill Stability	:	C
Monin-Obukhov Length (m)	:	-26.5
Air Temperature (K)	:	301.05
Relative Humidity (%)	:	21
Surface Temperature (K)	:	310.0

Release Richardson Number

Volumetric Release Rate (m^3/s)	:	67.5
Characteristic Width (m)	:	37.8
Estimated Friction Velocity (m/s)	:	0.42

$$Ri_0^C = g\left[\frac{\rho_i - \rho_a}{\rho_a}\right]\frac{Q}{u u_*^2 D} = 4.7$$

Figure IV.20. DEGADIS-predicted centerline maximum concentration vs. maximum measured concentration--Coyote 5.

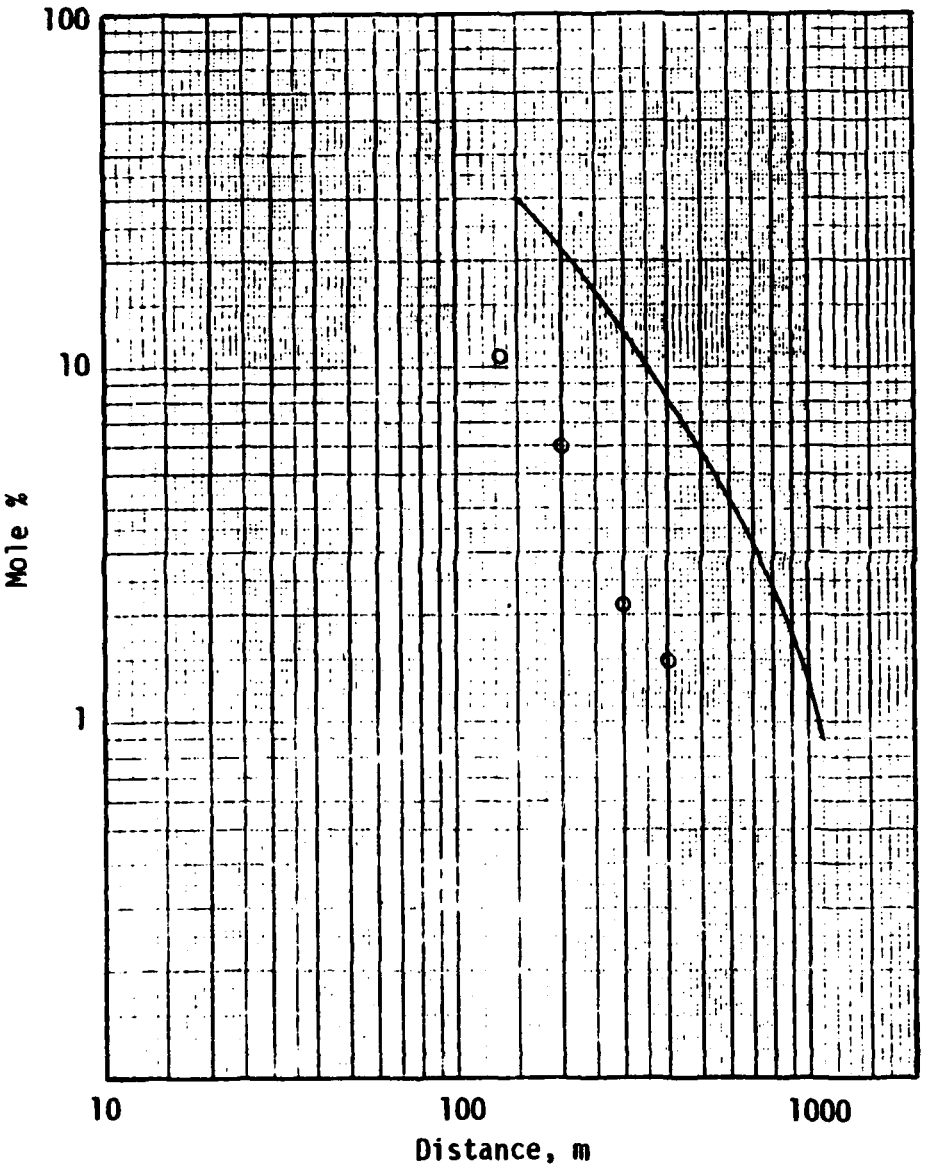

TEST: Coyote 6

Source Description

Type: Steady, Time-Limited LNG

Primary Source Radius (m)	:	21.0
Primary Source Flux ($kg/m^2 s$)	:	0.085
Rate (kg/s)	:	118 for 82 s
Temperature (K)	:	112

Meteorological Conditions

Wind Velocity (m/s)	:	5.9
@ Height (m)	:	8.0
Surface Roughness (m)	:	2.05 E-4
Pasquill Stability	:	D
Monin-Obukhov Length (m)	:	73.6
Air Temperature (K)	:	297
Relative Humidity (%)	:	23
Surface Temperature (K)	:	300.0

Release Richardson Number

Volumetric Release Rate (m^3/s)	:	65.8
Characteristic Width (m)	:	37.2
Estimated Friction Velocity (m/s)	:	0.19

$$Ri_0^C = g\left[\frac{\rho_i - \rho_a}{\rho_a}\right]\frac{Q}{u u_*^2 D} = 47$$

Figure IV.21. DEGADIS-predicted centerline maximum concentration vs. maximum measured concentration--Coyote 6.

IV.5 Shell Research LNG and LPG Releases on Water at Maplin Sands

Shell Research conducted a series of LNG and LPG releases on water at Maplin Sands in 1980-81 in south England. Ten continuous LNG releases, eleven continuous LPG releases, and two instantaneous releases each of LNG and LPG were reported. Some of the releases were ignited to obtain cloud and pool fire heat flux measurements, whereas some experiments were conducted primarily to measure gas concentrations. The volumes of LNG and LPG released ranged from about 6 m^3 to 22 m^3 and 8 m^3 to 27 m^3, respectively. Maximum rates of release in the continuous LNG and LPG spills were about 4.8 m^3/min and 4.3 m^3/min, respectively. Data from these releases have been reported in several papers by Shell personnel (Blackmore et al., 1981; Puttock et al., 1982a, 1982b, 1982c; Colenbrander and Puttock, 1983a), and extensive data digests summarizing the data have been prepared by Shell (Colenbrander et al., 1984). Comparisons of the experimental data with predictions obtained with Shell's HEGADAS model, which was the starting point for the DEGADIS model herein proposed, have also been reported (Colenbrander and Puttock, 1983a).

Table IV.5 shows the test descriptions for six continuous LNG releases, one instantaneous LNG release, and six continuous LPG releases conducted at Maplin Sands which have been simulated with the DEGADIS model. The continuous releases have been simulated as steady state with the liquid-on-water-pool size determined assuming boiling rates for LNG and LPG of 0.085 and 0.12 kg/m^2s, respectively. The simulation of Maplin 22 assumes a steady, time-limited release of 510 kg/s for 10 seconds. All simulations assumed neutral stability with a reported surface roughness of 3.38×10^{-4} m. Figures IV.22 through IV.34 show the DEGADIS model-predicted maximum ground level centerline gas concentration compared

TABLE IV.5

SHELL MAPLIN SANDS LNG/LPG SPILL TEST SCENARIO DATA SUMMARY

	Test No.	Liquid Comp. C_1 C_2 C_3 C_4	Liquid Spill Volume m^3	Liquid Spill Rate m^3/min.	Wind Speed @ 10 m m/s	Air Temp. @ 2 m °C	Relative Humidity @ 10 m %	Surface Temp. °C	Lowest Gas Concentration Sensor m
Continuous LNG	27	93.2 5.4 1.1 0.3	12.6	3.2	5.5	14.9	53	15.6	0.9 - 1.0
	29	98.5 1.4 0.1 --	21.9	4.1	7.4	16.1	52	16.8	0.9
	34	95.9 2.6 0.9 0.6	10.2	3.0	8.6	15.2	72	15.8	0.9 - 1.0
	35	97.8 1.7 0.4 0.1	18.3	3.9	9.8	16.1	63	16.6	0.9 - 1.0
	39	95.2 1.7 0.6 0.2	10.9	4.7	4.1	16.7	63(1)	--	0.9 - 1.3
	56	93.3 4.3 1.5 0.4	6.3	2.5	5.1	10.6	83(1)	11.6	0.6 - 0.7
Instantaneous LNG	22	92.3 4.0 0.9 0.2	12	N/A	5.5	18.9	62	18.6	0.9 - 1.3
Continuous LPG	43	-- 1.22 97.0 1.2	17.2	2.3	5.5	17.0	--	18.9	0.9
	46	0.01 1.05 97.3 1.6	22.2	2.8	8.1	18.7	71(1)	17.3	0.9 - 1.0
	47	0.01 1.78 96.9 1.3	17.6	3.9	5.6	17.4	78(1)	17.1	0.9 - 1.0
	49	-- 2.4 96.5 0.66	8.4	2.0	6.2	13.3	88	13.0	0.9
	50	-- 1.18 97.6 1.2	17.2	4.3	7.9	10.4	79	9.9	0.9 - 1.3
	54	-- 1.1 97.4 1.5	11.7	2.3	3.8	8.4	85(1)	9.4	0.5 - 0.7

(1) Humidity from Foulness Meteorological Station (5 km away and 1 km inland) corrected to Maplin site temperature.

with measured maximum steady state concentrations as a function of downwind distance from the release center. All reported measured concentrations are based on a 3 s moving average. The aspirated concentration sensor used a balanced Wheatstone bridge to measure the heat loss from a sensing element placed in the sample stream. Shaded experimental points represent maximum concentrations which occurred before or following the time interval judged to best delimit the steady release condition.

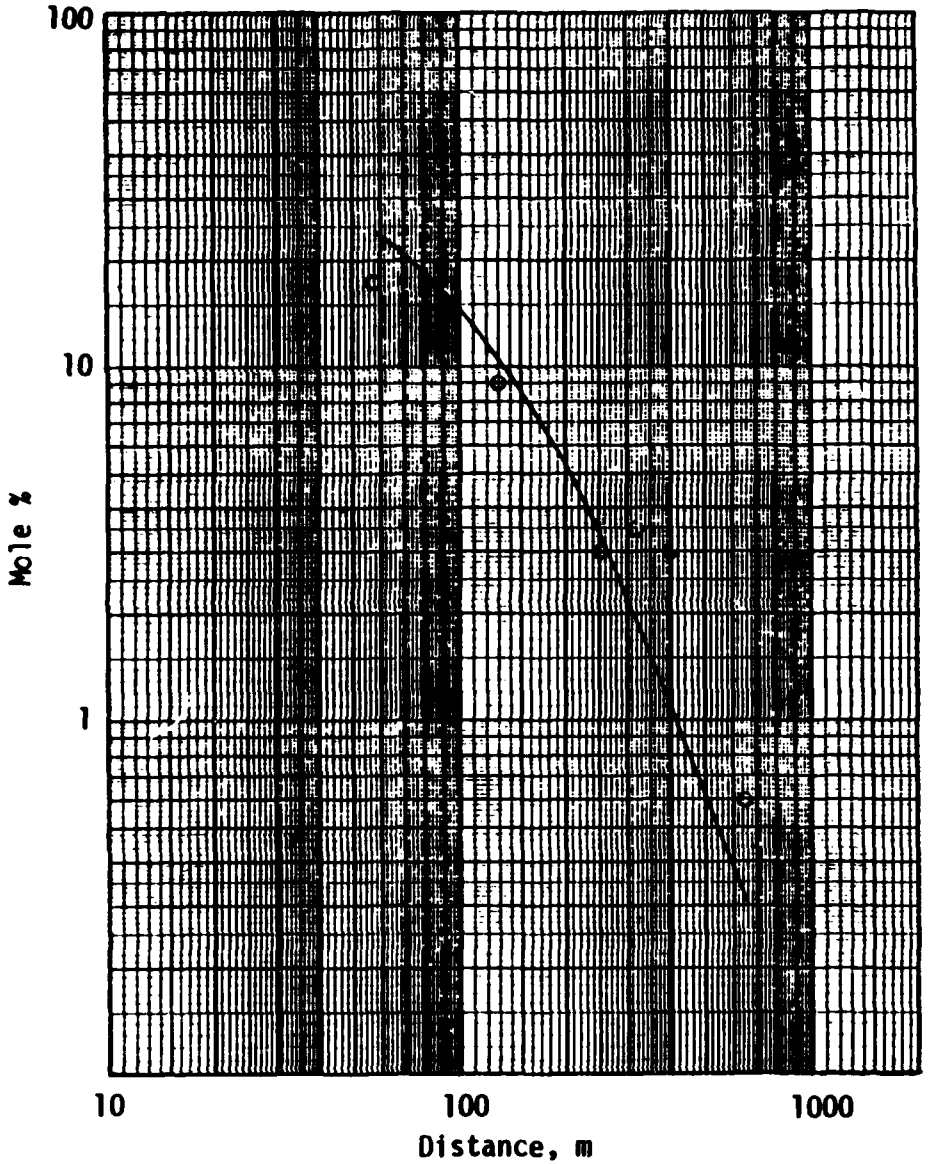

TEST: Maplin 27

Source Description

Type: Continuous LNG

Primary Source Radius (m)	:	9.21
Primary Source Flux ($kg/m^2 s$)	:	0.085
Rate (kg/s)	:	22.67
Temperature (K)	:	111.7

Meteorological Conditions

Wind Velocity (m/s)	:	5.5
@ Height (m)	:	10.0
Surface Roughness (m)	:	3.38 E-4
Pasquill Stability	:	D
Monin-Obukhov Length (m)	:	∞
Air Temperature (K)	:	288
Relative Humidity (%)	:	53
Surface Temperature (K)	:	289

Release Richardson Number

Volumetric Release Rate (m^3/s)	:	12.7
Characteristic Width (m)	:	16.3
Estimated Friction Velocity (m/s)	:	0.19

$$Ri_0^C = g\left[\frac{\rho_i - \rho_a}{\rho_a}\right]\frac{Q}{u u_*^2 D} = 18.$$

Figure IV.22. DEGADIS-predicted centerline maximum concentration vs. maximum measured concentration--Maplin 27.

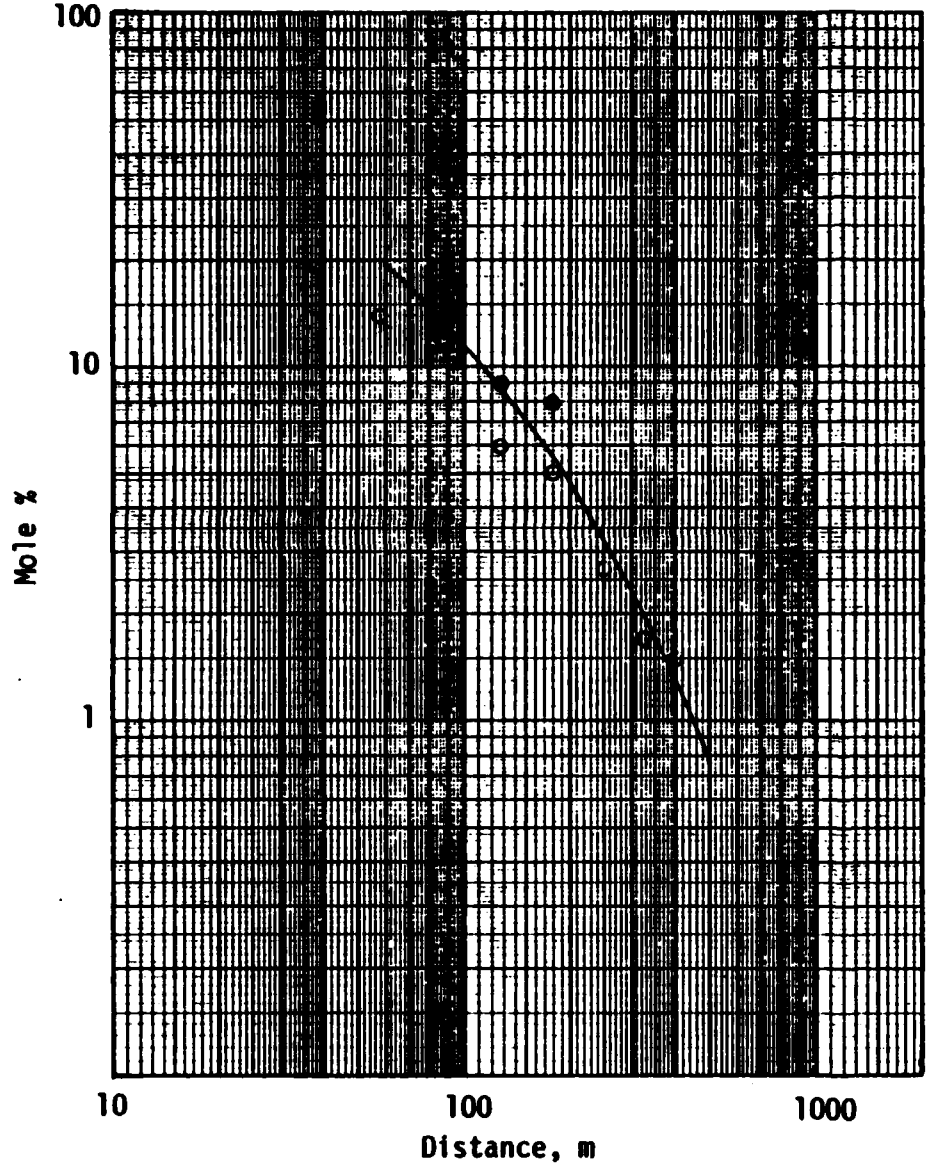

TEST: Maplin 29

Source Description

Type:	Continuous LNG	
Primary Source Radius (m)	:	10.43
Primary Source Flux ($kg/m^2 s$)	:	0.085
Rate (kg/s)	:	29.04
Temperature (K)	:	111.7

Meteorological Conditions

Wind Velocity (m/s)	:	7.4
@ Height (m)	:	10.0
Surface Roughness (m)	:	3.38 E-4
Pasquill Stability	:	D
Monin-Obukhov Length (m)	:	∞
Air Temperature (K)	:	289
Relative Humidity (%)	:	52
Surface Temperature (K)	:	290

Release Richardson Number

Volumetric Release Rate (m^3/s)	:	16.2
Characteristic Width (m)	:	18.5
Estimated Friction Velocity (m/s)	:	0.25

$$Ri_0^C = g\left[\frac{\rho_i - \rho_a}{\rho_a}\right]\frac{Q}{u u_*^2 D} = 8.5$$

Figure IV.23. DEGADIS-predicted centerline maximum concentration vs. maximum measured concentration--Maplin 29.

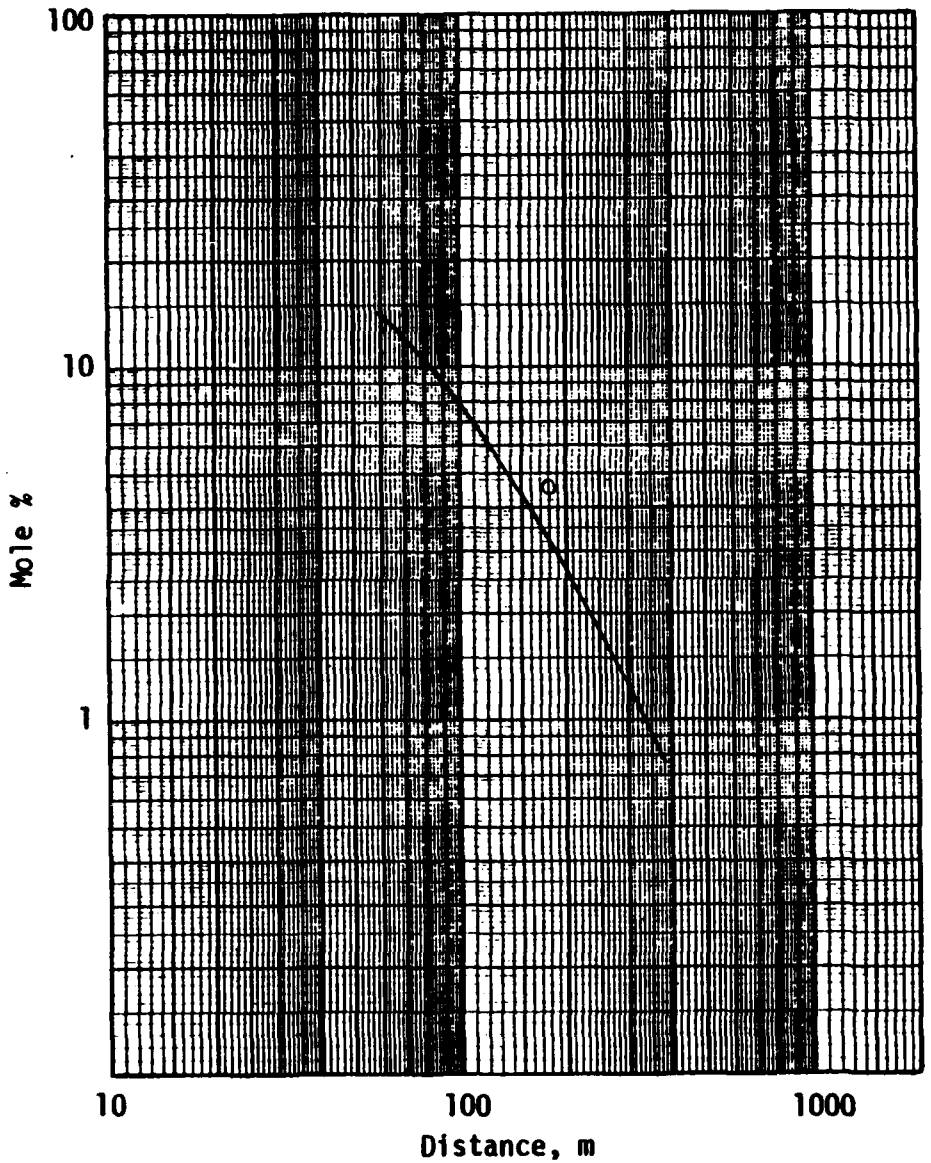

TEST: Maplin 34

Source Description

Type: Continuous LNG

Primary Source Radius (m)	:	8.92
Primary Source Flux ($kg/m^2 s$)	:	0.085
Rate (kg/s)	:	21.25
Temperature (K)	:	111.7

Meteorological Conditions

Wind Velocity (m/s)	:	8.6
@ Height (m)	:	10.0
Surface Roughness (m)	:	3.38 E-4
Pasquill Stability	:	D
Monin-Obukhov Length (m)	:	∞
Air Temperature (K)	:	288
Relative Humidity (%)	:	72
Surface Temperature (K)	:	289

Release Richardson Number

Volumetric Release Rate (m^3/s)	:	11.9
Characteristic Width (m)	:	15.81
Estimated Friction Velocity (m/s)	:	0.29

$$Ri_0^C = g\left[\frac{\rho_j - \rho_a}{\rho_a}\right]\frac{Q}{u u_*^2 D} = 4.7$$

Figure IV.24. DEGADIS-predicted centerline maximum concentration vs. maximum measured concentration--Maplin 34.

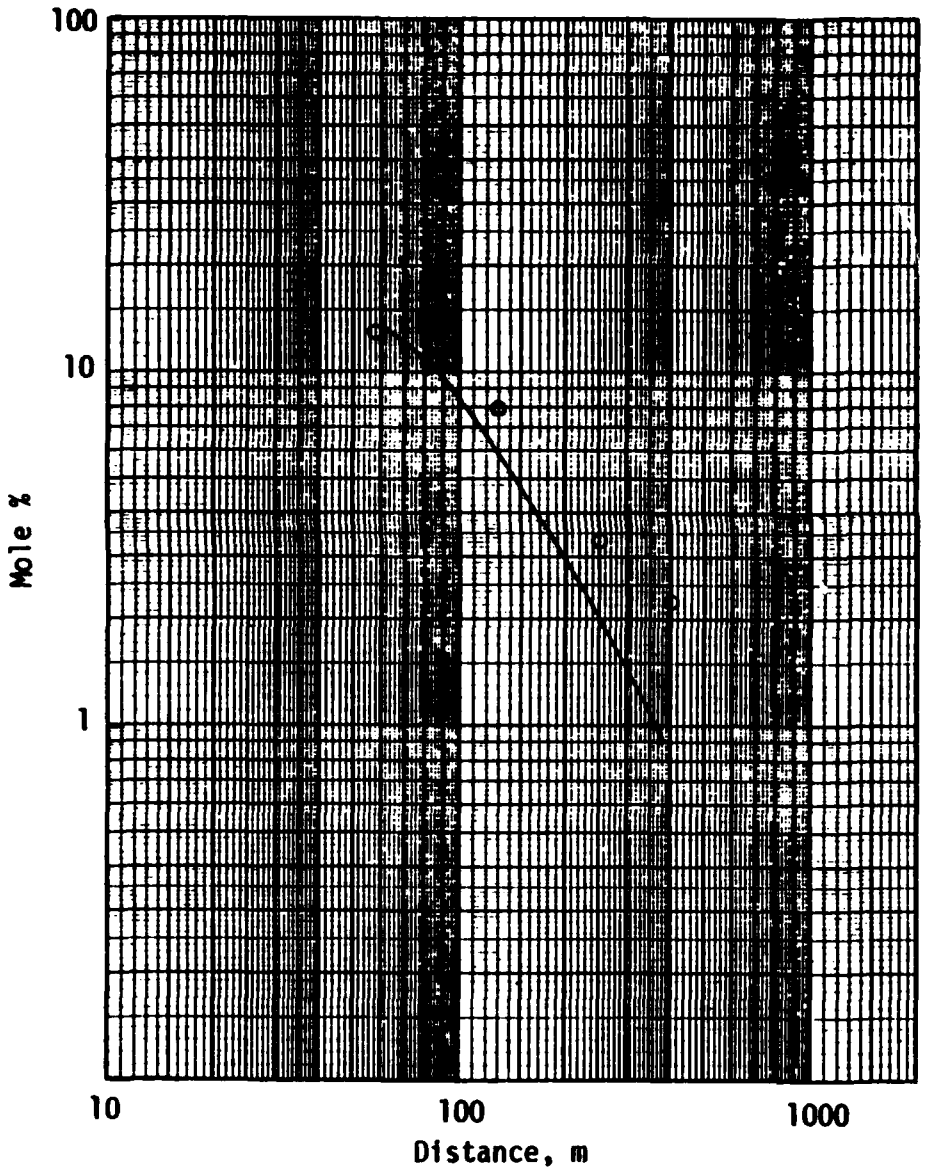

TEST: Maplin 35

Source Description

Type: Continuous LNG

Primary Source Radius (m)	:	10.2
Primary Source Flux ($kg/m^2 s$)	:	0.085
Rate (kg/s)	:	27.60
Temperature (K)	:	111.7

Meteorological Conditions

Wind Velocity (m/s)	:	9.8
@ Height (m)	:	10.0
Surface Roughness (m)	:	3.38 E-4
Pasquill Stability	:	D
Monin-Obukhov Length (m)	:	∞
Air Temperature (K)	:	289
Relative Humidity (%)	:	63
Surface Temperature (K)	:	290

Release Richardson Number

Volumetric Release Rate (m^3/s)	:	15.4
Characteristic Width (m)	:	18.1
Estimated Friction Velocity (m/s)	:	0.33

$$Ri_0^C = g\left[\frac{\rho_j - \rho_a}{\rho_a}\right]\frac{Q}{u u_*^2 D} = 3.6$$

Figure IV.25. DEGADIS-predicted centerline maximum concentration vs. maximum measured concentration--Maplin 35.

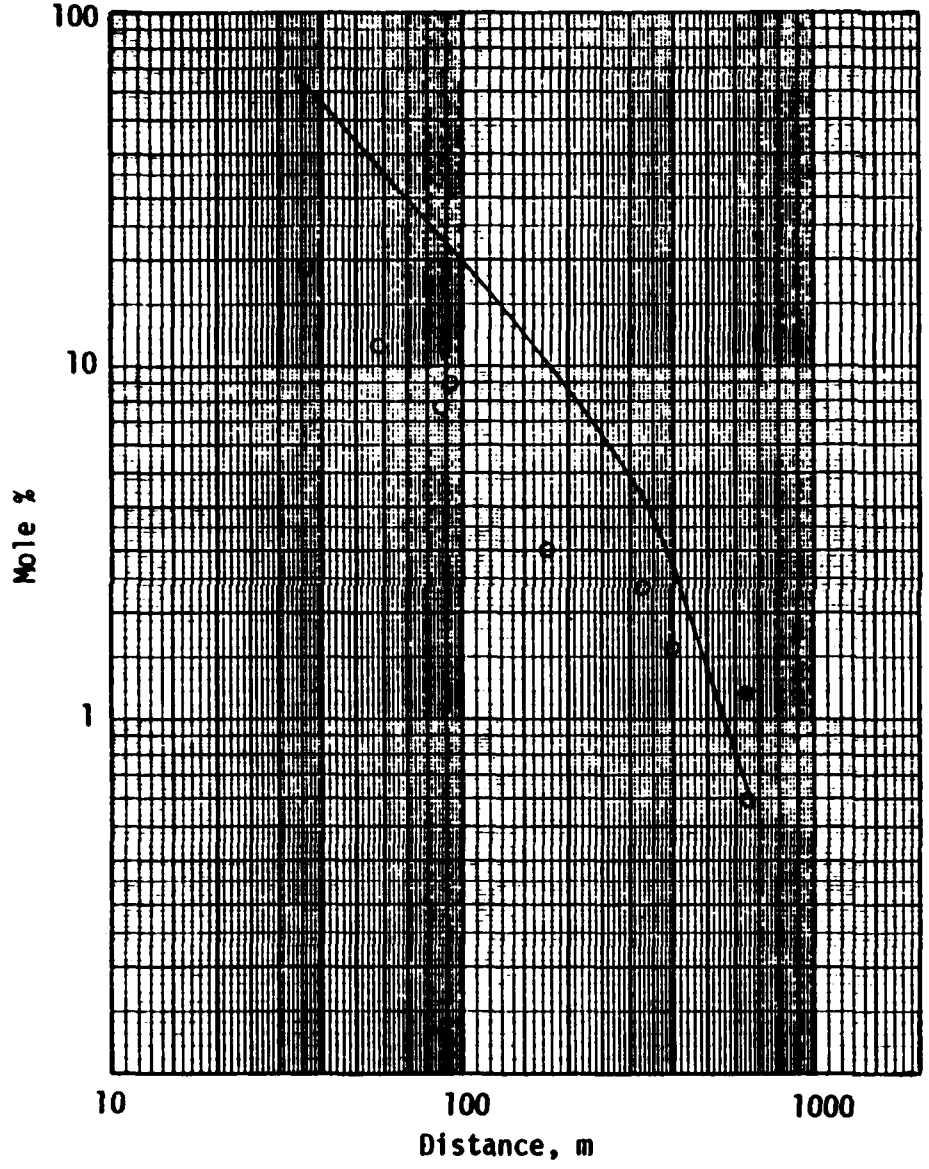

TEST: Maplin 39

Source Description

Type:	Continuous LNG	
Primary Source Radius (m)	:	11.2
Primary Source Flux ($kg/m^2 s$)	:	0.085
Rate (kg/s)	:	33.3
Temperature (K)	:	111.7

Meteorological Conditions

Wind Velocity (m/s)	:	4.1
@ Height (m)	:	10.0
Surface Roughness (m)	:	3.38 E-4
Pasquill Stability	:	D
Monin-Obukhov Length (m)	:	∞
Air Temperature (K)	:	290
Relative Humidity (%)	:	63
Surface Temperature (K)	:	290

Release Richardson Number

Volumetric Release Rate (m^3/s)	:	18.6
Characteristic Width (m)	:	19.9
Estimated Friction Velocity (m/s)	:	0.14

$$Ri_0^C = g\left[\frac{\rho_i - \rho_a}{\rho_a}\right]\frac{Q}{u u_*^2 D} = 54$$

Figure IV.26. DEGADIS-predicted centerline maximum concentration vs. maximum measured concentration--Maplin 39.

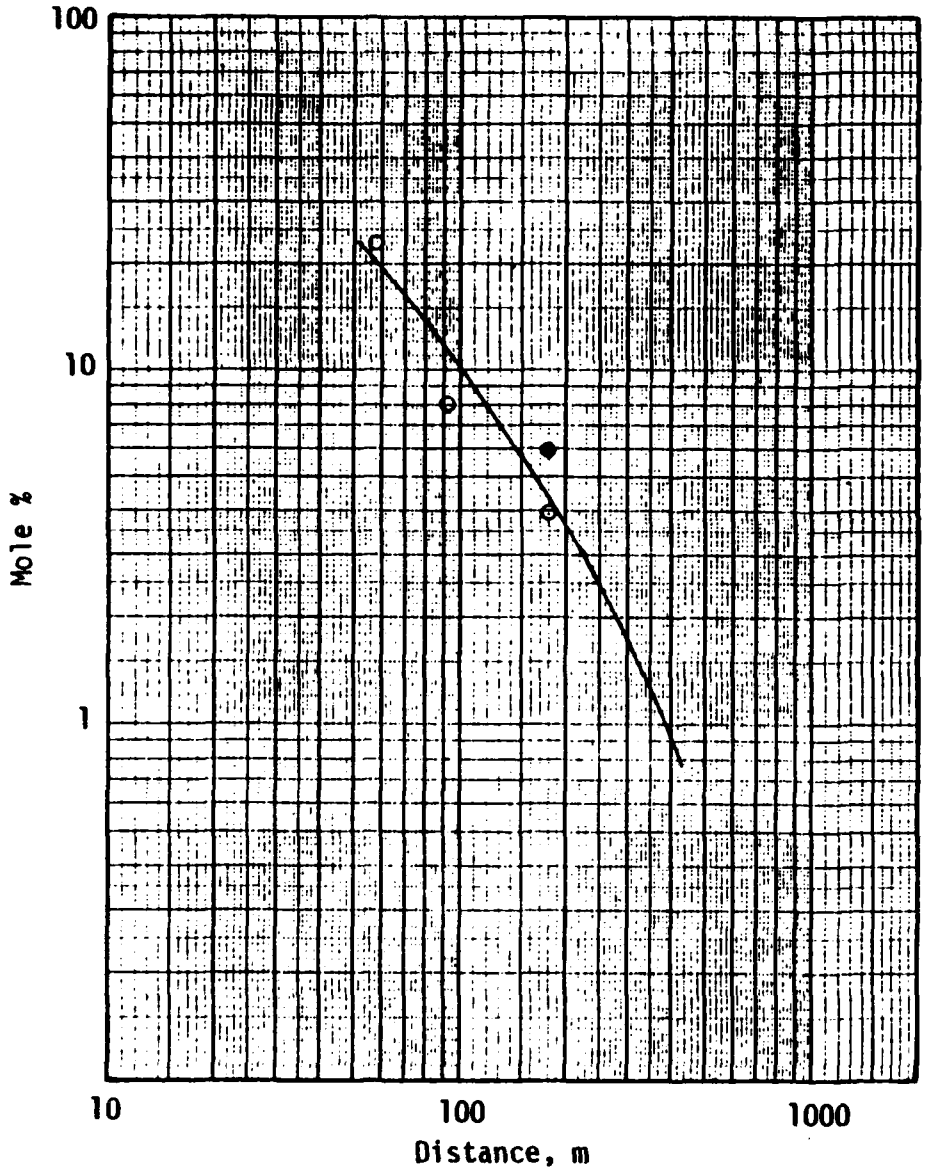

TEST: Maplin 56

Source Description

Type: Continuous LNG

Primary Source Radius (m)	:	8.14
Primary Source Flux ($kg/m^2 s$)	:	0.085
Rate (kg/s)	:	17.71
Temperature (K)	:	111.7

Meteorological Conditions

Wind Velocity (m/s)	:	5.1
@ Height (m)	:	10.0
Surface Roughness (m)	:	3.38 E-4
Pasquill Stability	:	D
Monin-Obukhov Length (m)	:	∞
Air Temperature (K)	:	284
Relative Humidity (%)	:	83
Surface Temperature (K)	:	284

Release Richardson Number

Volumetric Release Rate (m^3/s)	:	9.89
Characteristic Width (m)	:	14.43
Estimated Friction Velocity (m/s)	:	0.17

$$Ri_0^C = g\left[\frac{\rho_i - \rho_a}{\rho_a}\right]\frac{Q}{u u_*^2 D} = 19.7$$

Figure IV.27. DEGADIS-predicted centerline maximum concentration vs. maximum measured concentration--Maplin 56.

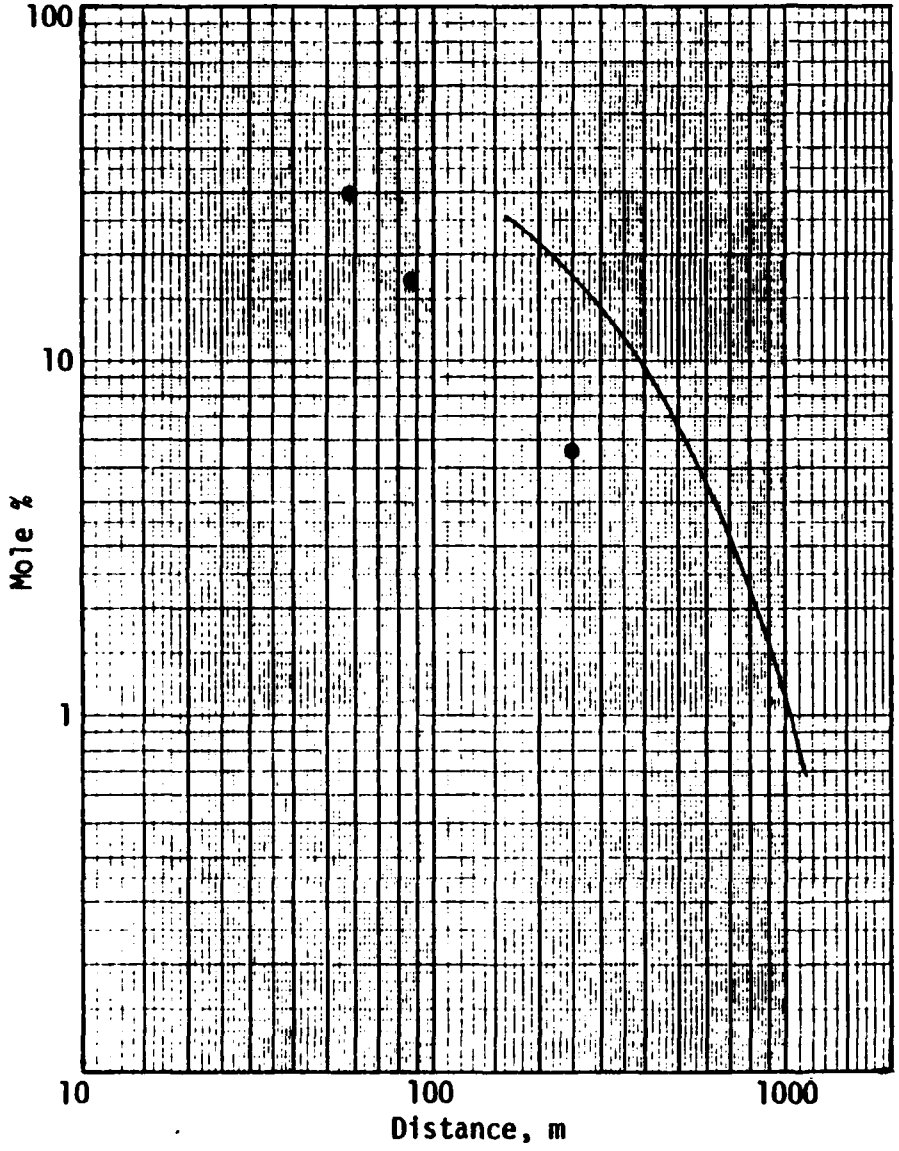

TEST: Maplin 22

Source Description

Type: Instantaneous LNG
Liquid Volume (m^3): 12
Temperature (K) : 112

Meteorological Conditions

Wind Velocity (m/s)	:	5.5
@ Height (m)	:	10.0
Surface Roughness (m)	:	3.38 E-4
Pasquill Stability	:	D
Monin-Obukhov Length (m)	:	∞
Air Temperature (K)	:	292.1
Relative Humidity (%)	:	62
Surface Temperature (K)	:	292.0
Estimated Friction Velocity (m/s)	:	0.19

Figure IV.28. DEGADIS-predicted centerline maximum concentration vs. maximum measured concentration--Maplin 22.

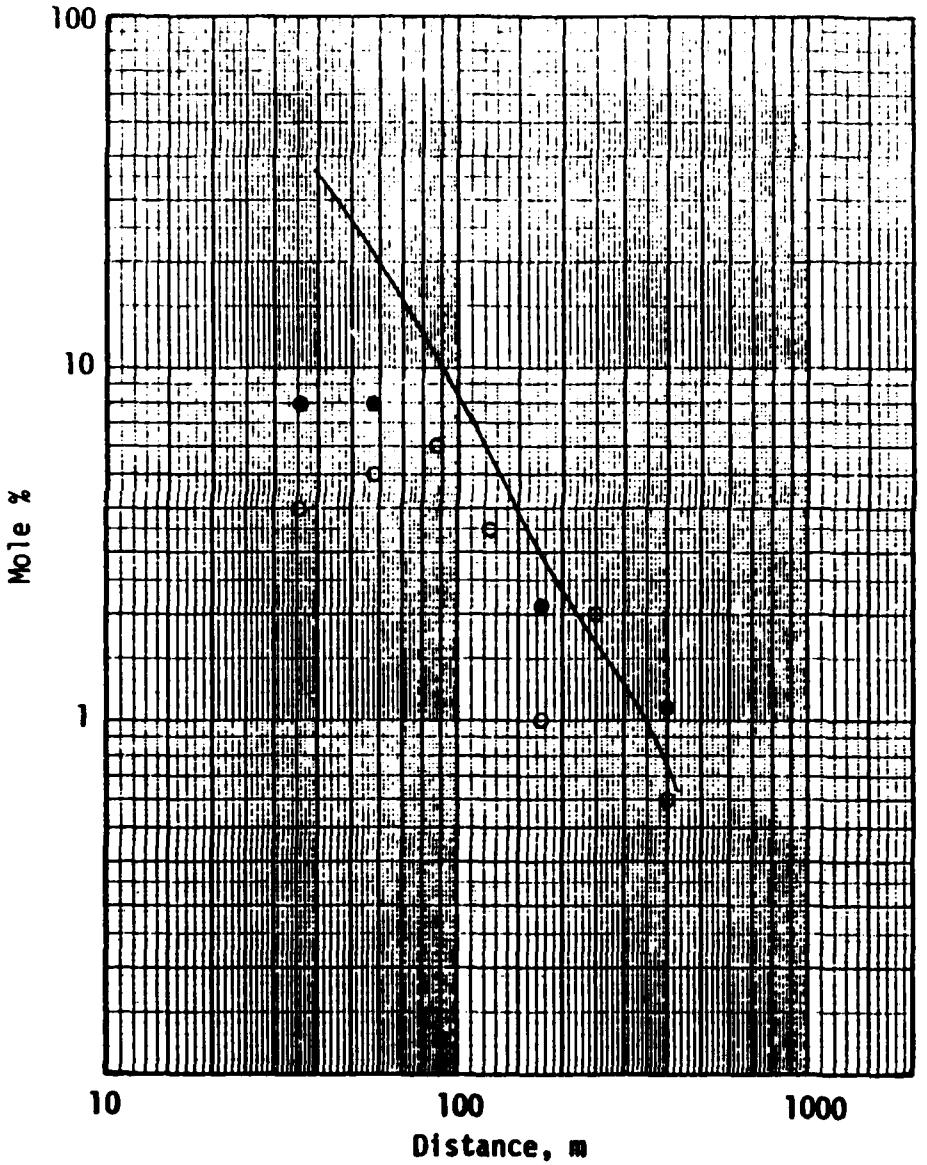

TEST: Maplin 43

Source Description

Type: Continuous Propane

Primary Source Radius (m)	:	7.7
Primary Source Flux ($kg/m^2 s$)	:	0.12
Rate (kg/s)	:	22.31
Temperature (K)	:	231.0

Meteorological Conditions

Wind Velocity (m/s)	:	5.5
@ Height (m)	:	10.0
Surface Roughness (m)	:	3.38 E-4
Pasquill Stability	:	D
Monin-Obukhov Length (m)	:	∞
Air Temperature (K)	:	290
Relative Humidity (%)	:	70 (assumed)
Surface Temperature (K)	:	292

Release Richardson Number

Volumetric Release Rate (m^3/s)	:	9.30
Characteristic Width (m)	:	13.6
Estimated Friction Velocity (m/s)	:	0.19

$$Ri_0^C = g\left[\frac{\rho_j - \rho_a}{\rho_a}\right]\frac{Q}{u u_*^2 D} = 34.1$$

Figure IV.29. DEGADIS-predicted centerline maximum concentration vs. maximum measured concentration--Maplin 43.

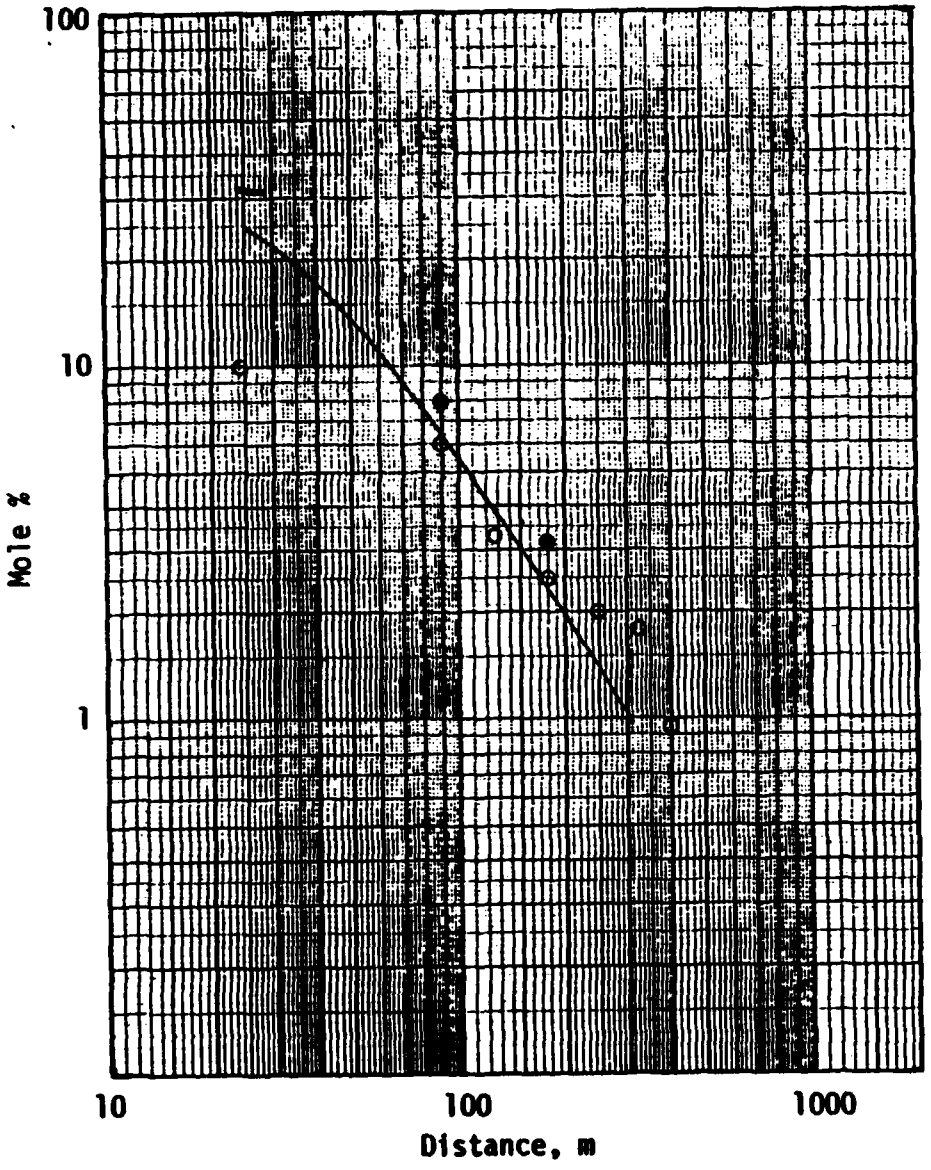

TEST: Maplin 46

Source Description

Type: Continuous Propane

Primary Source Radius (m)	:	8.49
Primary Source Flux ($kg/m^2 s$)	:	0.12
Rate (kg/s)	:	27.16
Temperature (K)	:	231.0

Meteorological Conditions

Wind Velocity (m/s)	:	8.1
@ Height (m)	:	10.0
Surface Roughness (m)	:	3.38 E-4
Pasquill Stability	:	D
Monin-Obukhov Length (m)	:	∞
Air Temperature (K)	:	292
Relative Humidity (%)	:	71
Surface Temperature (K)	:	291

Release Richardson Number

Volumetric Release Rate (m^3/s)	:	11.3
Characteristic Width (m)	:	15.1
Estimated Friction Velocity (m/s)	:	0.28

$$Ri_0^C = g\left[\frac{\rho_i - \rho_a}{\rho_a}\right]\frac{Q}{u u_*^2 D} = 11.9$$

Figure IV.30. DEGADIS-predicted centerline maximum concentration vs. maximum measured concentration--Maplin 46.

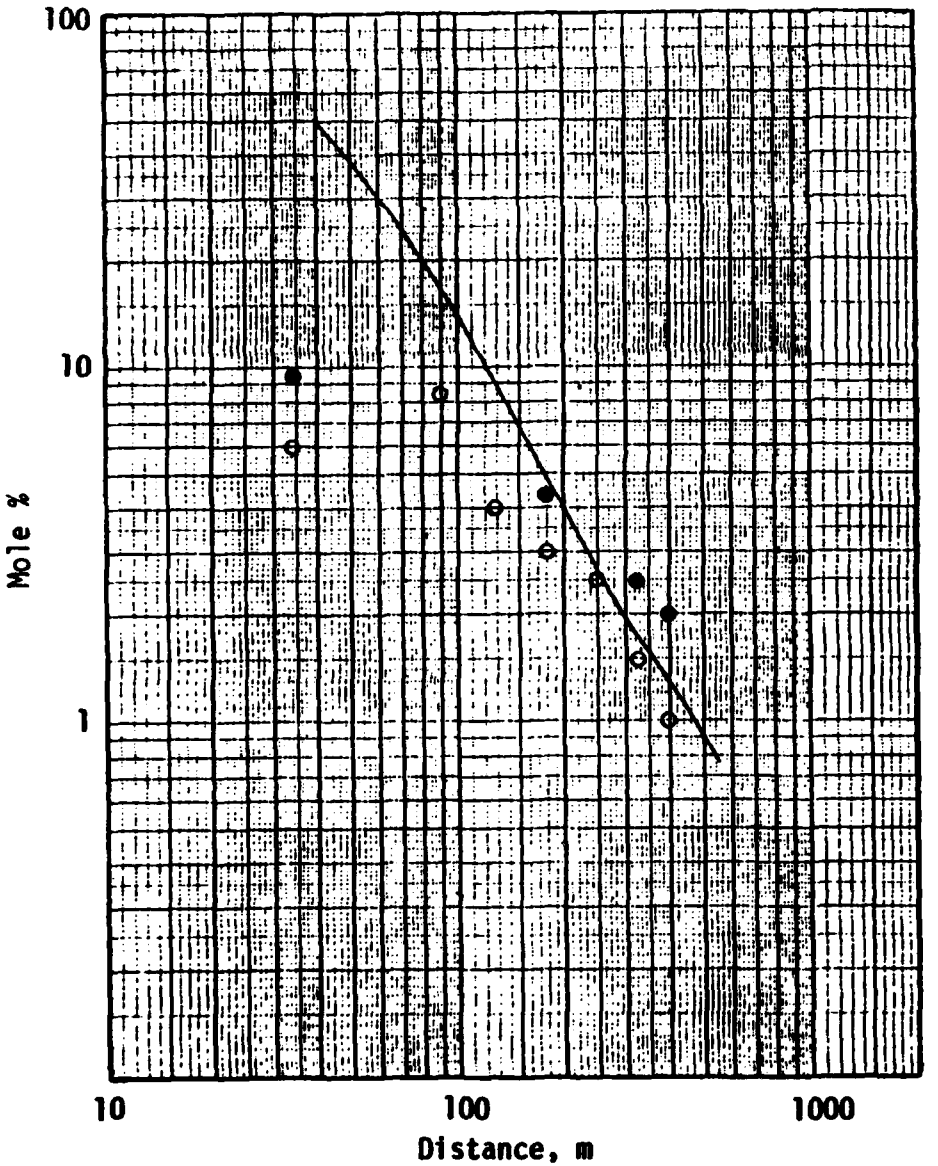

TEST: Maplin 47

Source Description

Type: Continuous Propane

Primary Source Radius (m)	:	10.02
Primary Source Flux ($kg/m^2 s$)	:	0.12
Rate (kg/s)	:	37.83
Temperature (K)	:	231.0

Meteorological Conditions

Wind Velocity (m/s)	:	5.60
@ Height (m)	:	10.0
Surface Roughness (m)	:	3.38 E-4
Pasquill Stability	:	D
Monin-Obukhov Length (m)	:	∞
Air Temperature (K)	:	291
Relative Humidity (%)	:	78
Surface Temperature (K)	:	290

Release Richardson Number

Volumetric Release Rate (m^3/s)	:	15.8
Characteristic Width (m)	:	17.7
Estimated Friction Velocity (m/s)	:	0.19

$$Ri_0^C = g\left[\frac{\rho_i - \rho_a}{\rho_a}\right]\frac{Q}{u u_*^2 D} = 42.2$$

Figure IV.31. DEGADIS-predicted centerline maximum concentration vs. maximum measured concentration--Maplin 47.

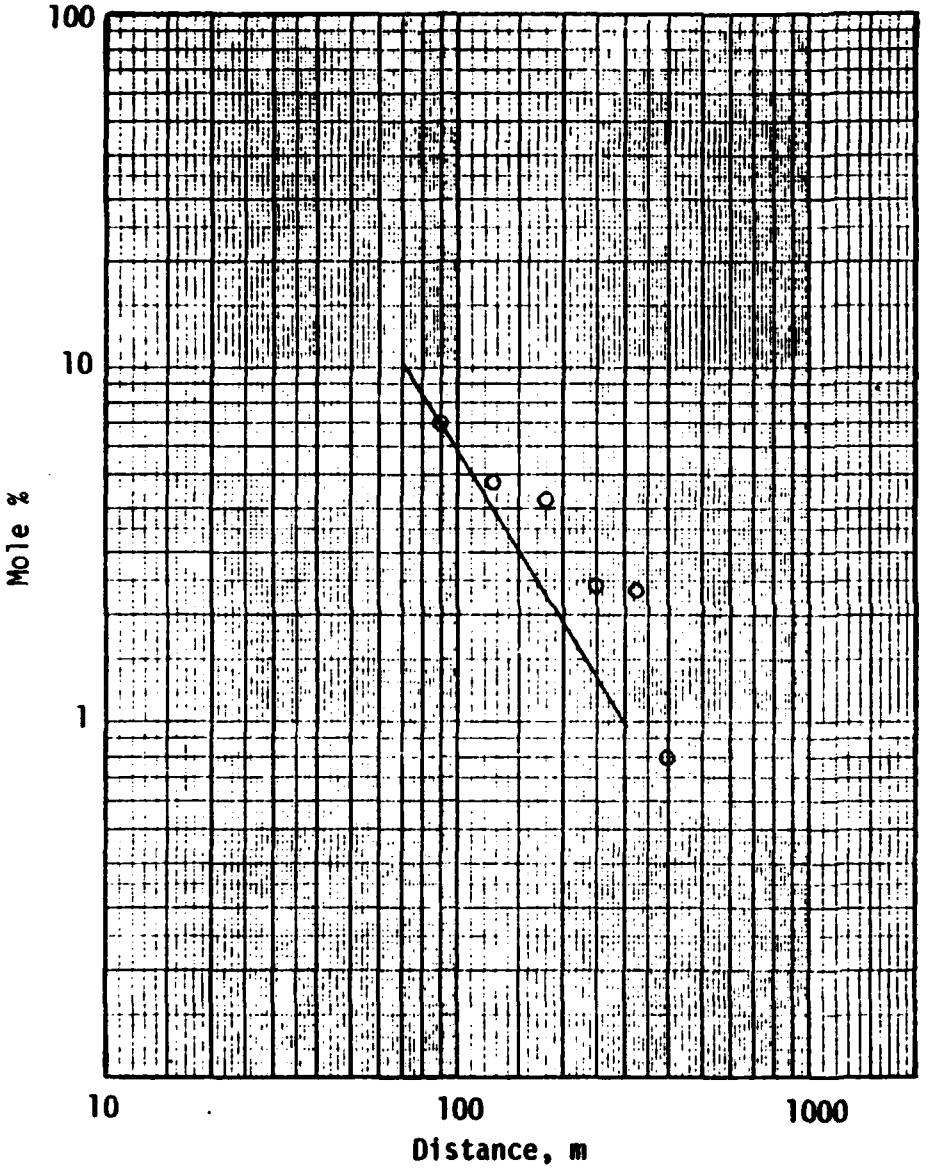

TEST: Maplin 49

Source Description

Type: Continuous Propane

Primary Source Radius (m)	:	7.17
Primary Source Flux ($kg/m^2 s$)	:	0.12
Rate (kg/s)	:	19.40
Temperature (K)	:	231.0

Meteorological Conditions

Wind Velocity (m/s)	:	6.2
@ Height (m)	:	10.0
Surface Roughness (m)	:	3.38 E-4
Pasquill Stability	:	D
Monin-Obukhov Length (m)	:	∞
Air Temperature (K)	:	286.5
Relative Humidity (%)	:	88
Surface Temperature (K)	:	286.0

Release Richardson Number

Volumetric Release Rate (m^3/s)	:	8.08
Characteristic Width (m)	:	12.7
Estimated Friction Velocity (m/s)	:	0.21

$$Ri_0^C = g\left[\frac{\rho_i - \rho_a}{\rho_a}\right]\frac{Q}{uu_*^2 D} = 21.4$$

Figure IV.32. DEGADIS-predicted centerline maximum concentration vs. maximum measured concentration--Maplin 49.

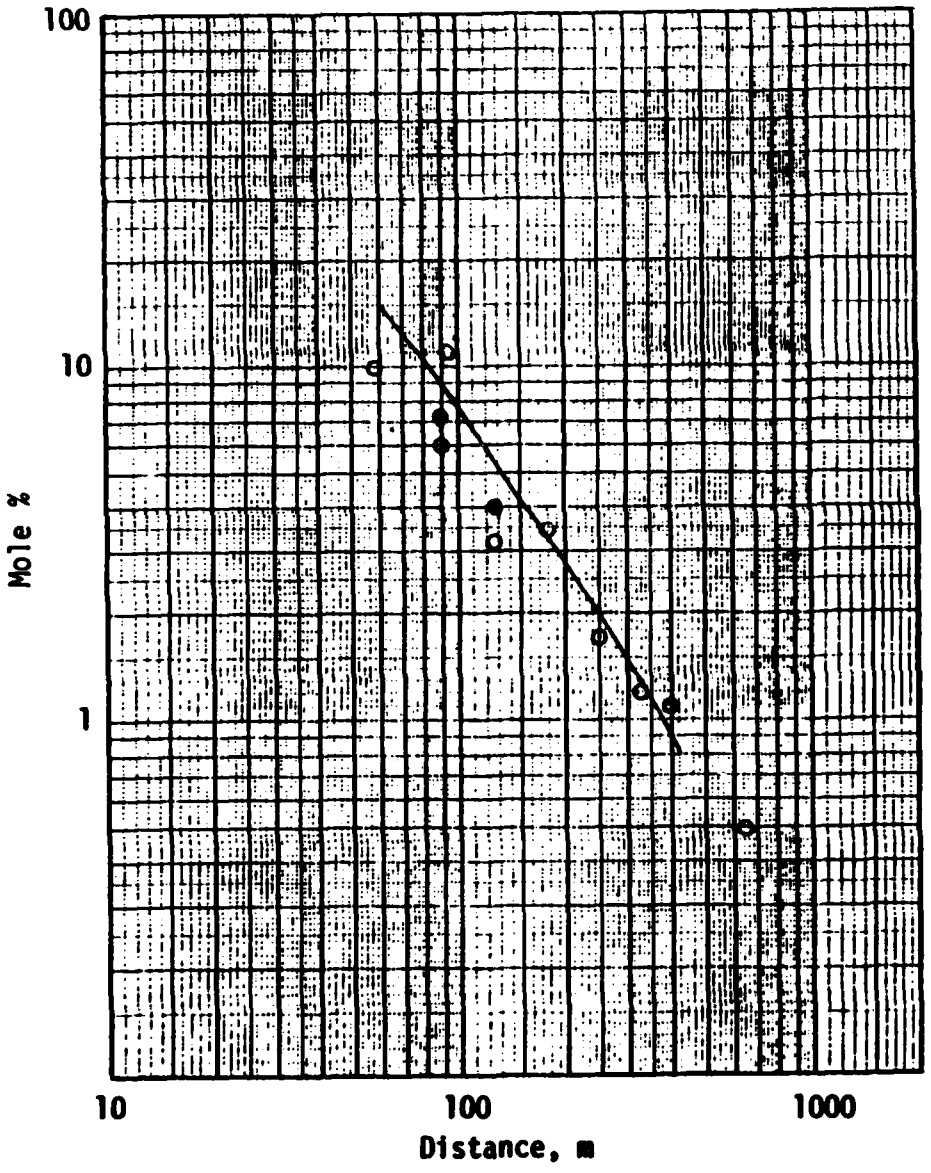

TEST: Maplin 50

Source Description

Type: Continuous Propane		
Primary Source Radius (m)	:	10.52
Primary Source Flux ($kg/m^2 s$)	:	0.12
Rate (kg/s)	:	41.71
Temperature (K)	:	231.0

Meteorological Conditions

Wind Velocity (m/s)	:	7.9
@ Height (m)	:	10.0
Surface Roughness (m)	:	3.38 E-4
Pasquill Stability	:	D
Monin-Obukhov Length (m)	:	∞
Air Temperature (K)	:	283.5
Relative Humidity (%)	:	79
Surface Temperature (K)	:	283.0

Release Richardson Number

Volumetric Release Rate (m^3/s)	:	17.4
Characteristic Width (m)	:	18.7
Estimated Friction Velocity (m/s)	:	0.27

$$Ri_0^C = g\left[\frac{\rho_i - \rho_a}{\rho_a}\right]\frac{Q}{u u_*^2 D} = 15.1$$

Figure IV.33. DEGADIS-predicted centerline maximum concentration vs. maximum measured concentration--Maplin 50.

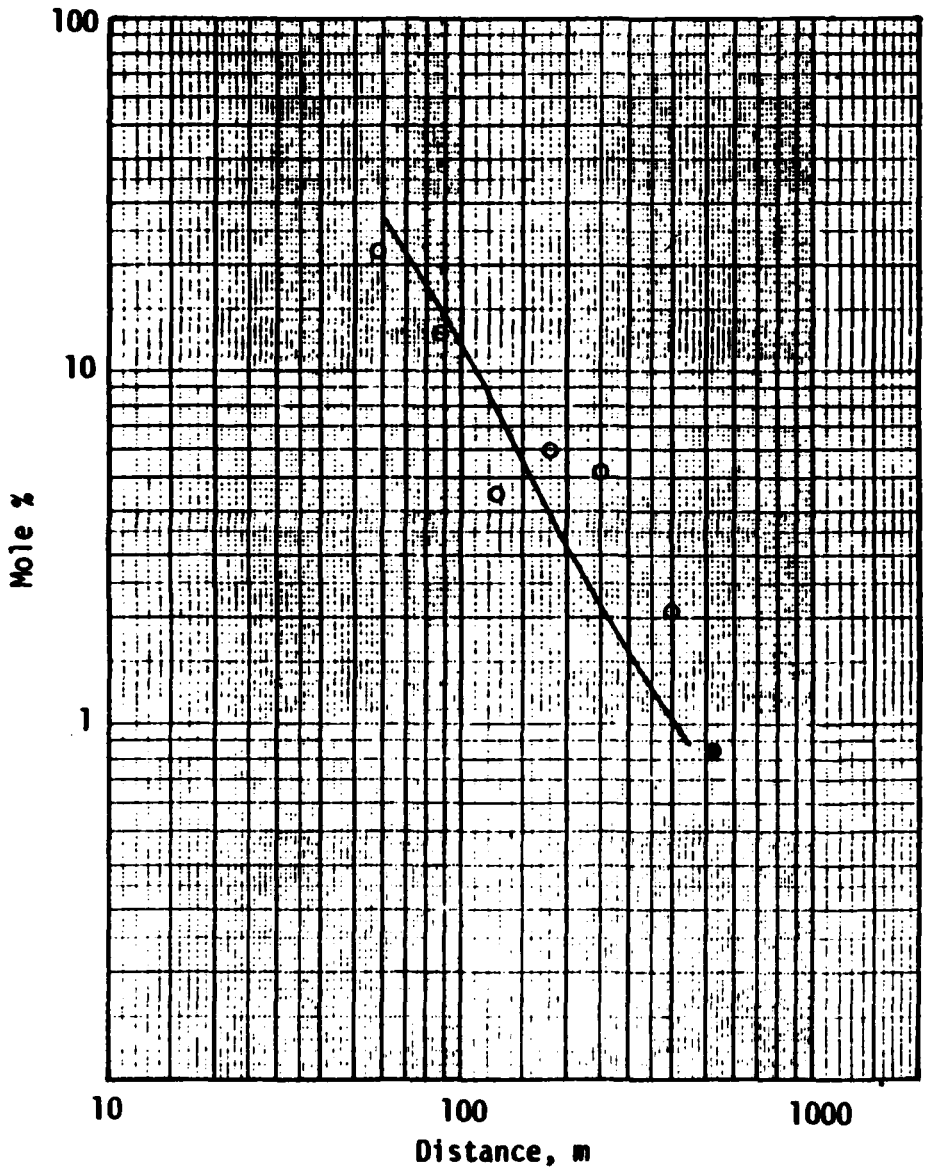

TEST: Maplin 54

Source Description

Type: Continuous Propane

Primary Source Radius (m)	:	7.69
Primary Source Flux ($kg/m^2 s$)	:	0.12
Rate (kg/s)	:	22.31
Temperature (K)	:	231.0

Meteorological Conditions

Wind Velocity (m/s)	:	3.8
@ Height (m)	:	10.0
Surface Roughness (m)	:	3.38 E-4
Pasquill Stability	:	D
Monin-Obukhov Length (m)	:	∞
Air Temperature (K)	:	282
Relative Humidity (%)	:	85
Surface Temperature (K)	:	283

Release Richardson Number

Volumetric Release Rate (m^3/s)	:	9.30
Characteristic Width (m)	:	13.12
Estimated Friction Velocity (m/s)	:	0.13

$$Ri_0^C = g\left[\frac{\rho_j - \rho_a}{\rho_a}\right]\frac{Q}{u u_*^2 D} = 100$$

Figure IV.34. DEGADIS-predicted centerline maximum concentration vs. maximum measured concentration--Maplin 54.

IV.6 British Health and Safety Executive Thorney Island Heavy Gas Trials

An industry-government consortium organized by the British Health and Safety Executive conducted a series of instantaneous releases of nominal 2000 m^3 volumes of Freon-12/nitrogen mixtures on the disused Thorney Island airfield on the southern coast of England from July 1982 - July 1983 (McQuaid, 1983). The releases were conducted in wind speeds (at 10 m) ranging from 1.7 m/s to 7.5 m/s and under different atmospheric stability conditions. In all of the experiments the gas was contained in a twelve-sided, plastic-sheet-walled bag 14 m across and 13 m high. The bag was supported on taut rigging from a central support column with radial guy wires to ground anchors and was fitted with a conical roof, also fabricated from plastic sheeting, which was withdrawn upwards immediately prior to release. The bag was filled by vaporizing liquid Freon-12 and liquid nitrogen and heating the gas mixture to near ambient temperature. The releases were essentially isothermal. The sides of the container collapsed in concertina fashion to ground level in less than two seconds, leaving an upright freestanding cylinder of gas. Detailed descriptions of the experimental design have been published as have complete data digests for all of the trials (HSE, 1982-83). Two gas sensor types were used; the standard gas sensor was an oxygen deficiency meter based on a semipermeable membrane and electrochemical cell. A fast response sensor (10 Hz) basically aspirated a sample past the cell membrane. Reported measured concentrations are based on a 0.6 s time average. The lowest sensors were 0.4 m above ground while the grass was approximately 0.1 m high.

Table IV.6 shows the pertinent test descriptions for Thorney Trials 7, 8, 9, 11, 13, and 15, which have been simulated with the DEGADIS model. Figures IV.35 through IV.40 show thd DEGADIS-predicted average source concentration for shorter distances and the maximum centerline gas concentration for longer distances compared with the maximum measured concentration as a function of downwind distance from the release center for these trials.

TABLE IV.6

BHSE THORNEY ISLAND PHASE I TRIALS--DATA SUMMARY

Test No.	Volume Released (m^3)	Initial Relative Density ρ / ρ_a	Wind Speed @ 10 m m/s	Air Temp. @ 9 m ^oC	Relative Humidity @ 10 m	Pasquill Stability
7	2000	1.75	3.2	17.1	80.7	E
8	2000	1.63	2.4	17.1	87.6	D
9	2000	1.60	1.7	18.6	87.3	E
11	2100	1.96	5.1	12.3	77.1	D
13	1950	2.00	7.5	13.2	74.1	D
15	2100	1.41	5.4	10.3	88.4	C/D

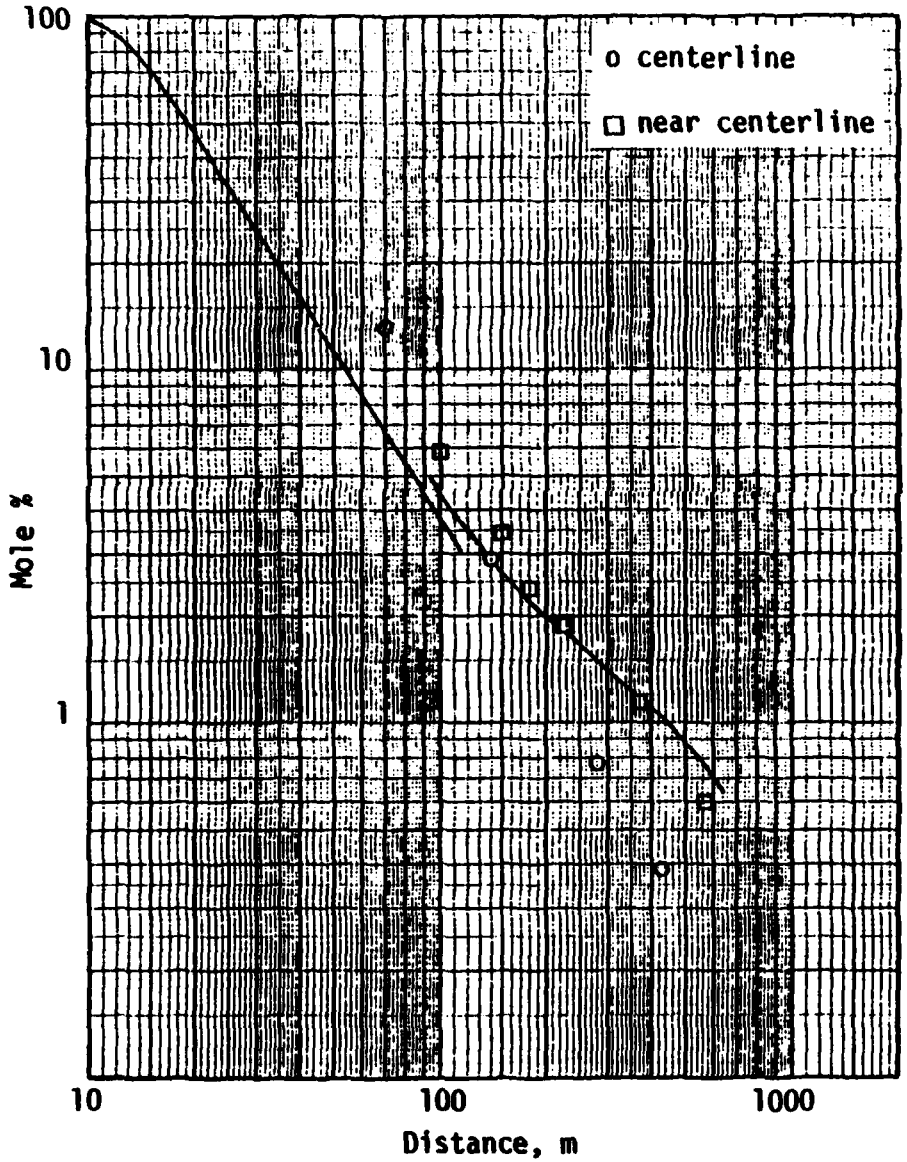

TEST: Thorney 07

Source Description

Type: Instantaneous

Volume (m^3)	:	2000
Initial Relative Density	:	1.75
Temperature (K)	:	Isothermal

Meteorological Conditions

Wind Velocity (m/s)	:	3.2
@ Height (m)	:	10.0
Surface Roughness (m)	:	1.0 E-2
Pasquill Stability	:	E
Monin-Obukhov Length (m)	:	30.4
Air Temperature (K)	:	290.3
Relative Humidity (%)	:	81

Release Richardson Number

Estimated Friction Velocity (m/s): 0.13

$$Ri_0^I = g\left[\frac{\rho_j - \rho_a}{\rho_a}\right]\frac{V_i^{1/3}}{u_*^2} = 5300$$

Figure IV.35. DEGADIS-predicted centerline maximum concentration vs. maximum measured concentration--Thorney 07.

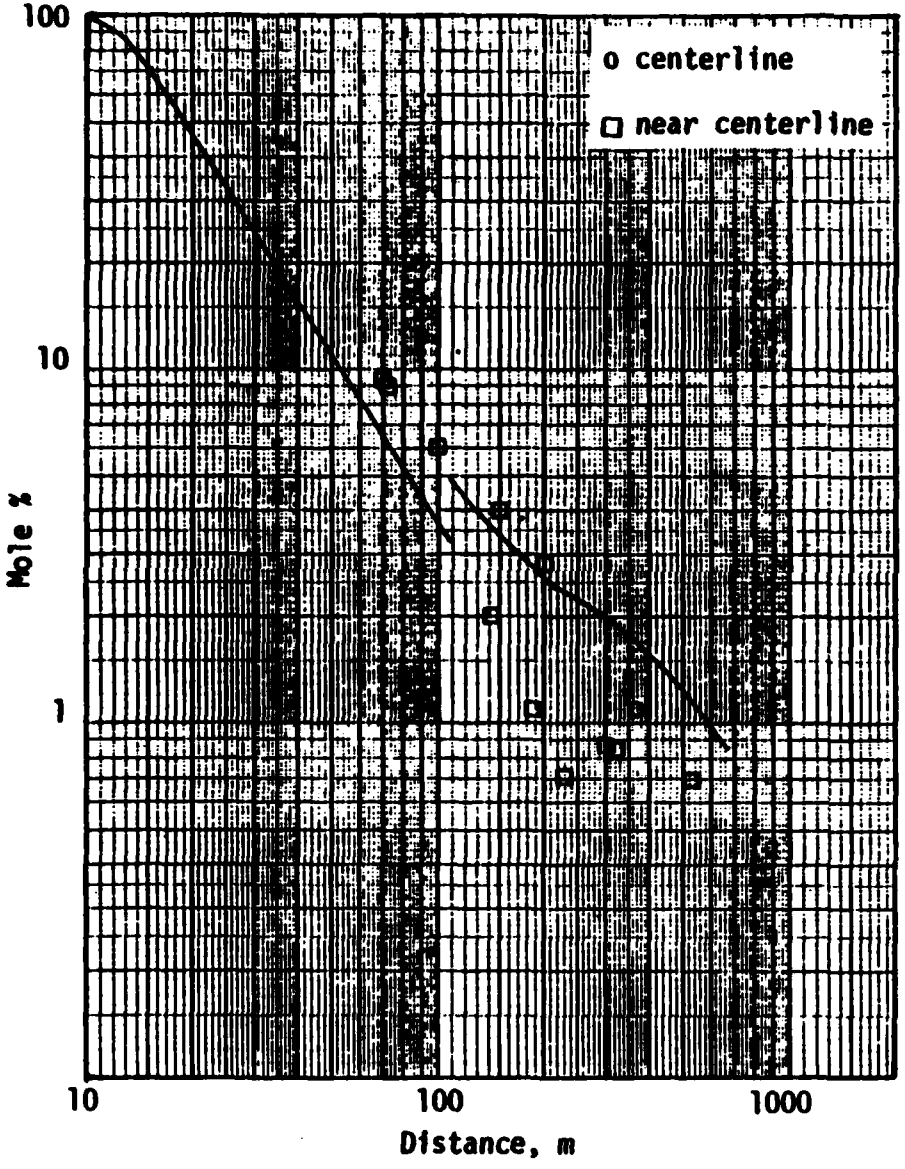

TEST: Thorney 08

Source Description

Type: Instantaneous
Volume (m^3) : 2000
Initial Relative Density: 1.63
Temperature (K) : Isothermal

Meteorological Conditions

Wind Velocity (m/s) : 2.4
@ Height (m) : 10.0
Surface Roughness (m) : 1.0 E-2
Pasquill Stability : D
Monin-Obukhov Length (m): ∞
Air Temperature (K) : 290.25
Relative Humidity (%) : 88

Release Richardson Number

Estimated Friction Velocity (m/s): 0.121

$$Ri_0^I = g\left[\frac{\rho_i - \rho_a}{\rho_a}\right]\frac{V_i^{1/3}}{u_*^2} = 5300$$

Figure IV.36. DEGADIS-predicted centerline maximum concentration vs. maximum measured concentration--Thorney 08.

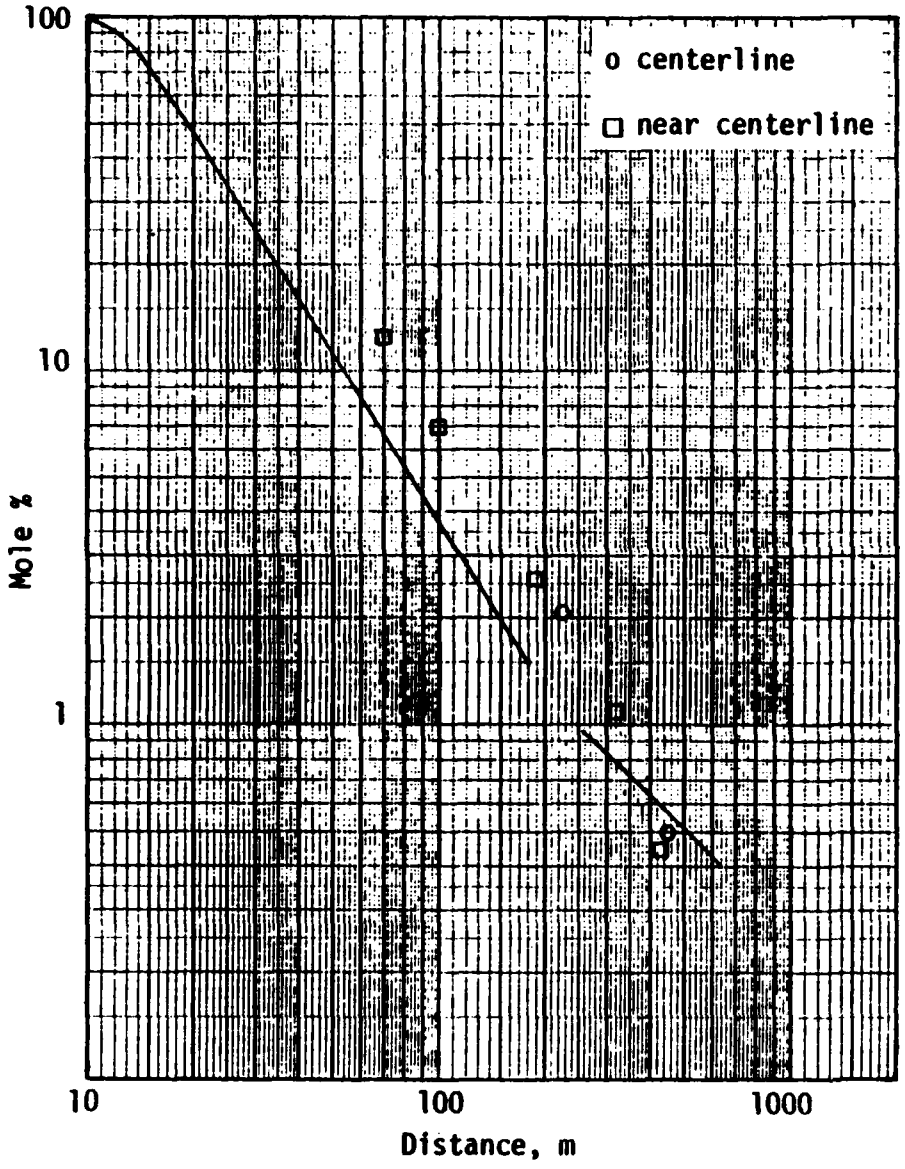

TEST: Thorney 09

Source Description

Type: Instantaneous

Volume (m^3)	:	2000
Initial Relative Density	:	1.60
Temperature (K)	:	Isothermal

Meteorological Conditions

Wind Velocity (m/s)	:	1.7
@ Height (m)	:	10.0
Surface Roughness (m)	:	1.0 E-2
Pasquill Stability	:	E
Monin-Obukhov Length (m)	:	30.43
Air Temperature (K)	:	291.7
Relative Humidity (%)	:	87

Release Richardson Number

Estimated Friction Velocity (m/s): 0.070

$$Ri_0^I = g\left[\frac{\rho_i - \rho_a}{\rho_a}\right]\frac{V_i^{1/3}}{u_*^2} = 15000$$

Figure IV.37. DEGADIS-predicted centerline maximum concentration vs. maximum measured concentration--Thorney 09.

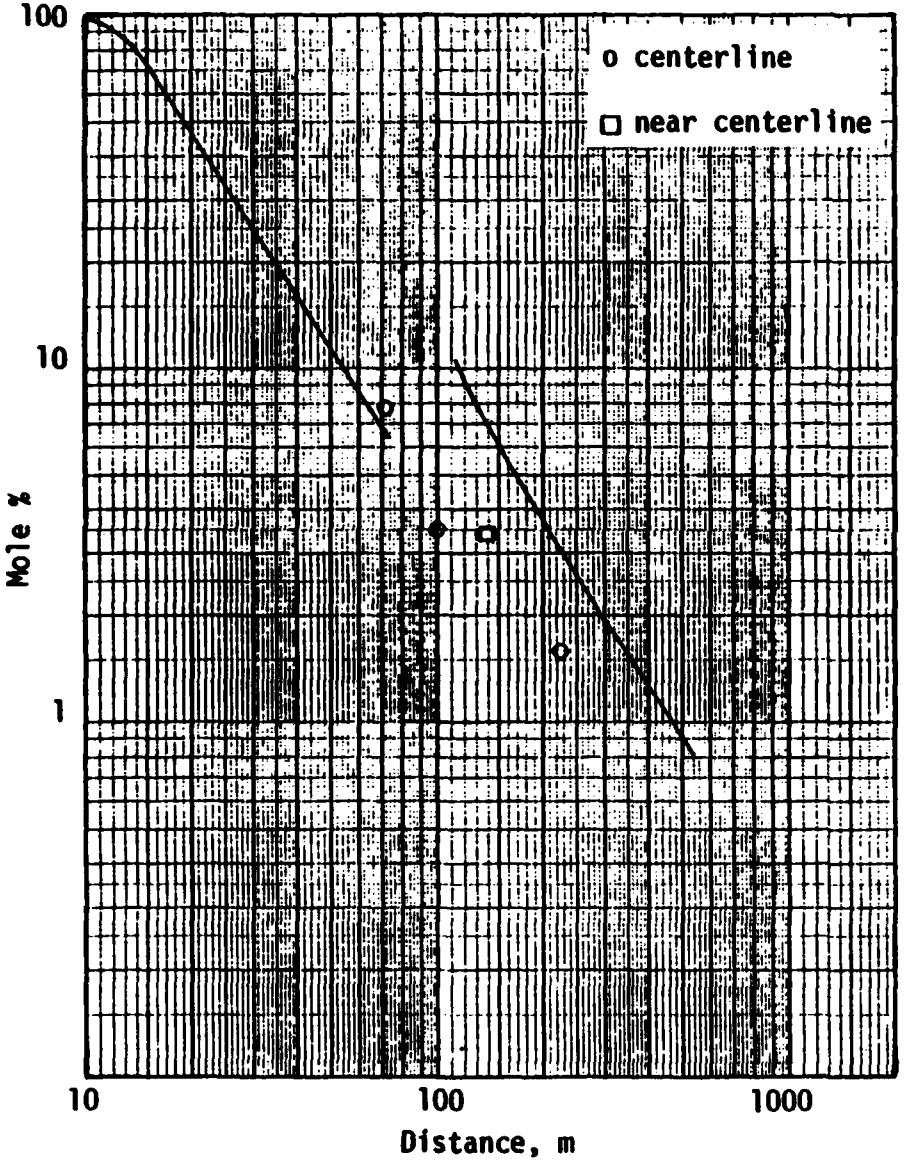

TEST: Thorney 11

Source Description

Type: Instantaneous
Volume (m^3) : 2100
Initial Relative Density: 1.96
Temperature (K) : Isothermal

Meteorological Conditions

Wind Velocity (m/s) : 5.1
@ Height (m) : 10.0
Surface Roughness (m) : 1.0 E-2
Pasquill Stability : D
Monin-Obukhov Length (m): ∞
Air Temperature (K) : 285.5
Relative Humidity (%) : 77

Release Richardson Number

Estimated Friction Velocity (m/s): 0.26

$$Ri_0^I = g\left[\frac{\rho_i - \rho_a}{\rho_a}\right]\frac{V_i^{1/3}}{u_*^2} = 1810$$

Figure IV.38. DEGADIS-predicted centerline maximum concentration vs. maximum measured concentration--Thorney 11.

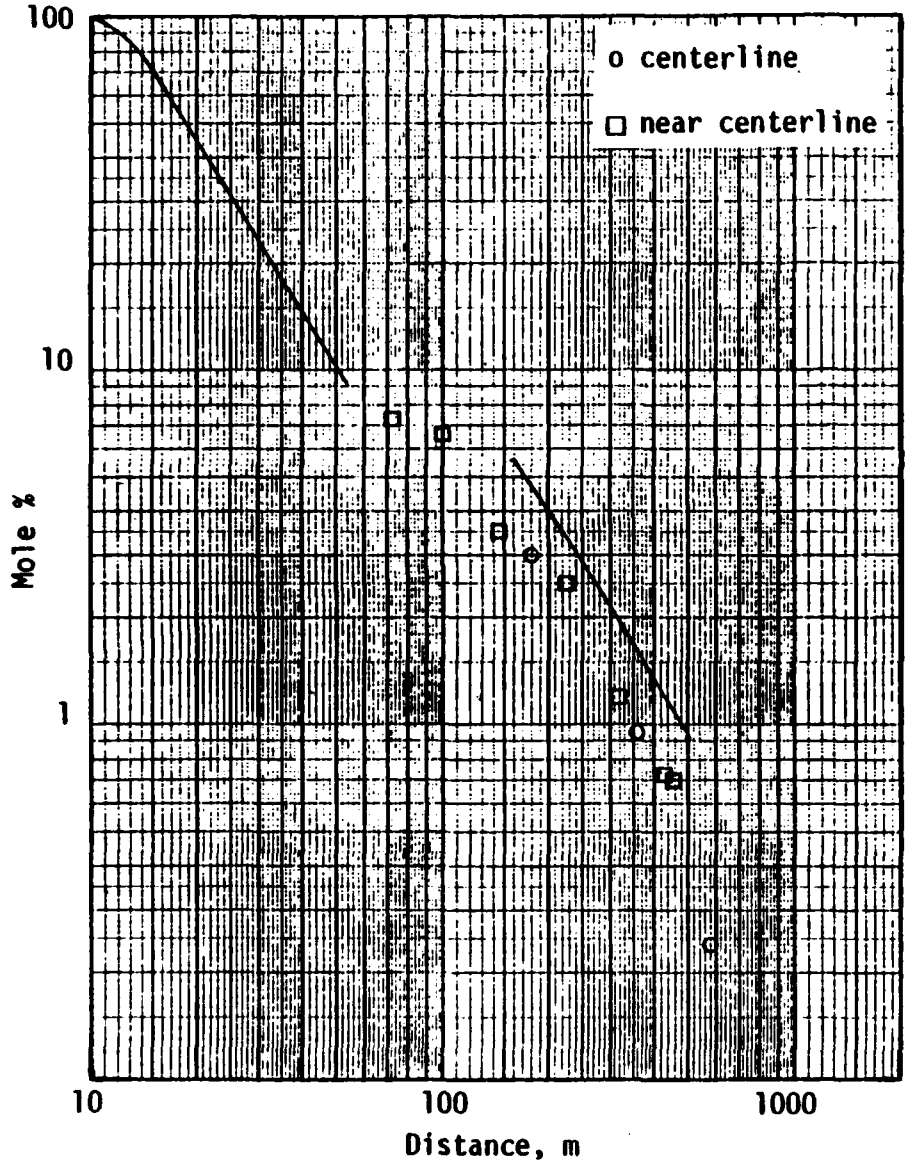

TEST: Thorney 13

Source Description

Type: Instantaneous
Volume (m^3) : 1950
Initial Relative Density: 2.00
Temperature (K) : Isothermal

Meteorological Conditions

Wind Velocity (m/s) : 7.50
@ Height (m) : 10.0
Surface Roughness (m) : 1.0 E-2
Pasquill Stability : D
Monin-Obukhov Length (m): ∞
Air Temperature (K) : 286.4
Relative Humidity (%) : 74

Release Richardson Number

Estimated Friction Velocity (m/s): 0.38

$$Ri_0^I = g\left[\frac{\rho_i - \rho_a}{\rho_a}\right]\frac{V_i^{1/3}}{u_*^2} = 850$$

Figure IV.39. DEGADIS-predicted centerline maximum concentration vs. maximum measured concentration--Thorney 13.

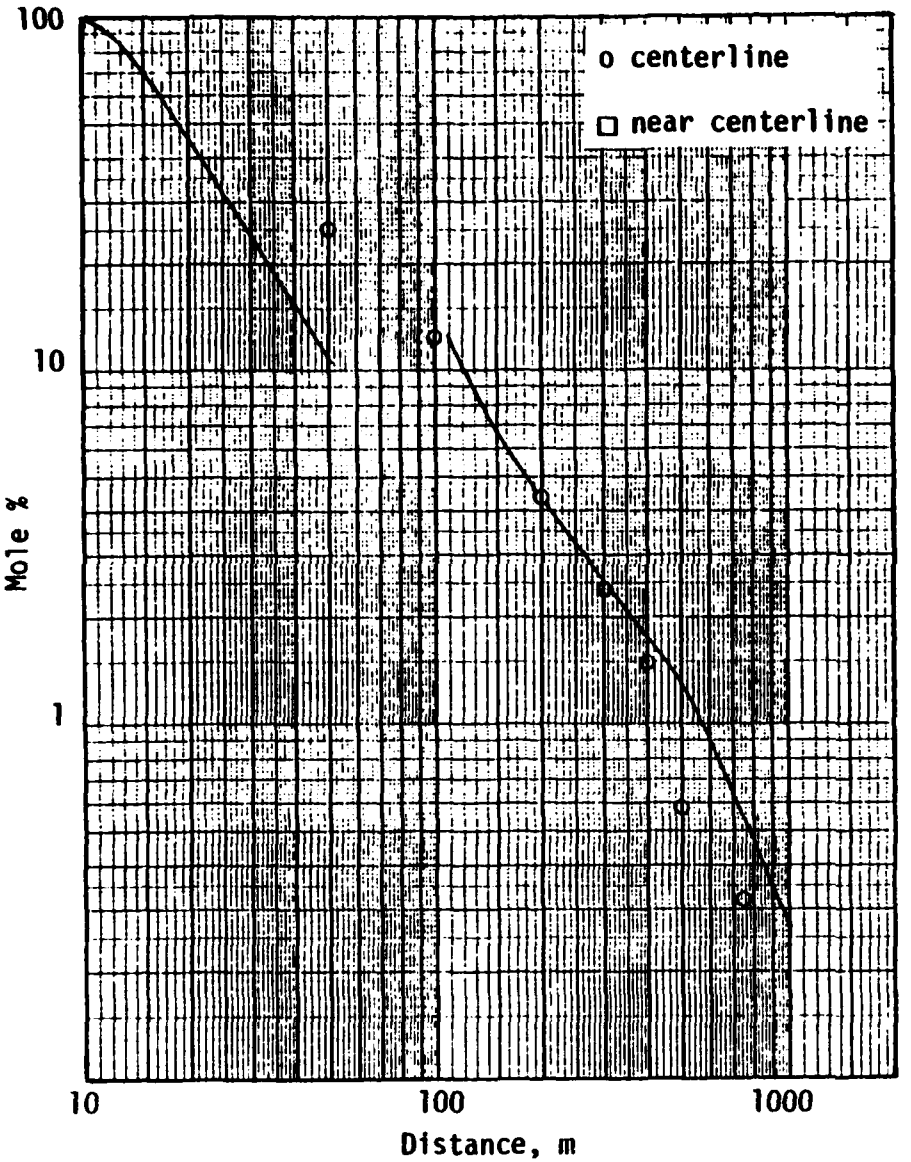

TEST: Thorney 15

Source Description

Type: Instantaneous
Volume (m^3) : 2100
Initial Relative Density: 1.41
Temperature (K) : Isothermal

Meteorological Conditions

Wind Velocity (m/s) : 5.40
@ Height (m) : 10.0
Surface Roughness (m) : 1.0 E-2
Pasquill Stability : D
Monin-Obukhov Length (m): ∞
Air Temperature (K) : 283.45
Relative Humidity (%) : 88

Release Richardson Number

Estimated Friction Velocity (m/s): 0.27

$$Ri_0^I = g\left[\frac{\rho_i - \rho_a}{\rho_a}\right]\frac{V_i^{1/3}}{u_*^2} = 690$$

Figure IV.40. DEGADIS-predicted centerline maximum concentration vs. maximum measured concentration--Thorney 15.

IV.7 Discussion of DEGADIS Simulation vs. Data Comparisons

The thirty-nine field experiments simulated include releases exemplifying a wide range of heavy gas dispersion behavior. The small scale propane releases reported by Welker have been shown to be reasonably well described by a passive dispersion model (Welker, 1982) and were included to demonstrate the applicability of DEGADIS to passive dispersion-dominated heavy gas releases. The Thorney Island instantaneous heavy gas releases are indicated, by comparison with laboratory calm air heavy gas releases (Volume II, this report), to be dominated by buoyancy-driven flow during the period when the cloud concentration decreases to about 5%. The instantaneous releases onto water of LNG, as well as the quasi-continuous releases of LNG and LPG on water, reflect important components of all three flow regimes: buoyancy-dominated flow, stably stratified shear flow, and passive dispersion.

Comparison of the model predictions with experimental observations is facilitated by classification of the tests with a Release Richardson Number which represents the ratio of a buoyancy-driven velocity scale characteristic of the release to a turbulence velocity scale characteristic of the atmospheric flow. Richardson numbers are defined, for this purpose, for continuous and instantaneous releases as follows.

$$\text{Continuous Releases:} \quad Ri_0^c = g\Delta' Q/u\,u_*^2 D$$

$$\text{Instantaneous Releases:} \quad Ri_0^I = g\Delta' V_i^{1/3}/u_*^2$$

where the characteristic buoyancy-driven velocities are

$$\sqrt{g\Delta' H} = \sqrt{g\Delta' Q/uD} \quad \text{and} \quad \sqrt{g\Delta' H} = \sqrt{g\Delta' V_i^{1/3}}$$

for continuous and instantaneous releases respectively, and the friction velocity is assumed characteristic of the atmospheric flow.

Table IV.7 contains a summary of Ri_0^C for the continuous releases considered as well as an indication of whether a secondary gas "blanket" was formed over the primary gas source which occurs when the atmospheric takeup rate is less than the gas evolution rate (i.e. when the atmospheric shear is not sufficient to assimilate the gas as fast as it is being produced by the primary source). A secondary gas blanket was predicted for all of the continuous releases simulated with Richardson numbers above 32. In contrast to the high dilution rates due to frontal air entrainment in the gas blanket for releases such as the Thorney Island trials and this work (Volume II), the secondary blankets formed for these continuous releases are not predicted to be significantly diluted by air. In contrast, the low Richardson number ($Ri_0^C = O(1)$) releases are predicted to have sufficient entrainment of gas by the wind shear to not only preclude the formation of a blanket, but to significantly dilute the gas in the shear layer over the source in agreement with the low Richardson number range indicated above. Between these Richardson number extremes, the source concentration is predicted to decrease with decreasing Richardson number without any upwind spreading.

A summary of the instantaneous release Richardson numbers is given in Table IV.8 for the Thorney Island trials. When scaled to the Thorney Island releases, the laboratory calm air releases presented in Volume II are in good agreement with the maximum observed concentrations for the Thorney Island trials before the time when the average concentration has dropped to about 5%. This suggests the flow and dilutions processes during this period reflect a dominance of buoyancy-driven flow for all six releases (i.e. for $Ri_0^I > 0$ (500)).

In order to quantify the uncertainty associated with a predicted distance to a given concentration level, a quantitative comparison between the predicted and "observed" distance to the 5%, 2-1/2%, and 1% concentration levels was made. The "observed" values were determined from reported maximum concentrations for

TABLE IV.7
SUMMARY OF RICHARDSON NUMBERS FOR CONTINUOUS RELEASES

Test	Ri_0^c	Blanket Formation	Predicted Concentration at Downwind Source Edge (%)
Welker 275-1	0.1	no	1.8
281-2	0.6	no	
296-1	0.3	no	
297-1	0.2	no	
297-3	0.4	no	1.7
298-1	2.1	no	
292-2	1.3	no	2.4
302-1	0.1	no	
334-1	2.5	no	3.2
334-2	3.5	no	
Burro 3	29	no	83
7	8.9	no	55
8	930	yes	
9	32	yes	
Coyote 5	4.7	no	41
6	47	yes	
Maplin Sands 27	18	no	77
29	9	no	57
34	5	no	46
35	4	no	42
39	55	yes	
43	34	yes	
46	12	no	43
47	42	yes	
49	21	no	63
50	15	no	46
54	100	yes	
56	20	no	80

TABLE IV.8
SUMMARY OF RICHARDSON NUMBERS FOR
INSTANTANEOUS RELEASES

Test		R_0^I
Thorney Island	7	5300
	8	5300
	9	15000
	11	1800
	13	850
	15	690

each experiment by drawing a visual best-fit straight line (on the Figures in this Section) through the reported points in the concentration range of interest. All of the measurements used were made at heights at or below 1 m. The predicted distance to a given concentration level was based on the ground level centerline concentration calculated by DEGADIS; for the concentrations and conditions of interest, the predicted concentration level is essentially constant for heights below 1 m. Table IV.9 summarizes the "observed" and predicted distances to the 5%, 2-1/2%, and 1% concentration levels for the Burro, Coyote, Maplin Sands, and Thorney Island releases.

Table IV.9 also includes ratios of the "observed" to predicted distances for the concentration levels of interest. As well, a 90% confidence interval (Conover, 1980) of these ratios is included for each test series and for all of the experiments together. For example, the Maplin Sands comparisons indicate the ratio of the "observed" to the predicted distance to the 2-1/2% concentration level would between 0.91 and 1.20 in nine out of ten realizations. For all of the comparisons, the 90% confidence interval of the ratio of the "observed" to the predicted distance to the 5% level would be 0.73 and 0.96; for the 2-1/2% level, it would be 0.82 and 1.03; and for the 1% level, it would be 0.95 and

TABLE IV.9

COMPARISON BETWEEN "OBSERVED" AND DEGADIS-PREDICTED MAXIMUM DISTANCE TO GAS CONCENTRATIONS IN THE FLAMMABLE CONCENTRATION RANGE

Test	Distance to 5% Concentration $(OBS)^{*}_{5}$ (m)	$(PRE)^{\ddagger *}_{5}$ (m)	$(OBS/PRE)_5$	Distance to 2-1/2% Concentration $(OBS)^{*}_{2.5}$ (m)	$(PRE)^{\ddagger *}_{2.5}$ (m)	$(OBS/PRE)_{2.5}$	Distance to 1% Concentration $(OBS)^{*}_{1}$ (m)	$(PRE)^{\ddagger *}_{1}$ (m)	$(OBS/PRE)_1$
Burro 3	200	380	0.52 6	320	460	0.69 6	540	650	0.83 1
7	240	380	0.63 2	410	550	0.74 5	800	840	0.95 2
8	420	450	0.93 3	740	610	1.21 3	1500	900	1.66 7
9	240	470	0.51 1	480	610	0.78 7	1000	820	1.22 0
Coyote 5	240	320	0.75 0	300	420	0.71 4	420	590	0.71 2
6	210	540	0.38 9	300	790	0.38 0	470	1080	0.43 5
Burro 90% Confidence Interval	$0.46 \leq (OBS/PRE)_5 \leq 0.78$			$0.55 \leq (OBS/PRE)_{2.5} \leq 0.98$			$0.63 \leq (OBS/PRE)_1 \leq 1.31$		
Maplin 22	270	570	0.47 4	500	770	0.64 9	1200	1040	1.15 4
27	200	210	0.95 2	320	290	1.10 3	600	410	1.46 3
29	170	190	0.89 5	280	290	0.96 6	540	450	1.20 0
34	180	140	1.28 6	290	210	1.38 1	600	340	1.76 5
35	180	140	1.28 6	350	220	1.59 1	940	360	2.61 1
39	140	300	0.46 7	260	410	0.63 4	680	560	1.21 4
43	95	130	0.73 1	160	190	0.84 2	320	350	0.91 4
46	120	110	1.09 1	200	170	1.17 6	400	300	1.33 3
47	140	180	0.77 8	240	260	0.92 3	500	470	1.06 4
49	140	110	1.27 3	230	170	1.35 3	440	300	1.46 7
50	120	130	0.92 3	200	220	0.90 9	480	380	1.26 3
54	180	160	1.12 5	280	230	1.21 7	490	410	1.19 5
56	150	160	0.93 8	230	250	0.92 0	400	390	1.02 6
Maplin 90% Confidence Interval	$0.80 \leq (OBS/PRE)_5 \leq 1.10$			$0.91 \leq (OBS/PRE)_{2.5} \leq 1.20$			$1.15 \leq (OBS/PRE)_1 \leq 1.47$		
Thorney Island 7	110	94	1.17 0	180	160	1.12 5	380	440	0.63 6
8	120	110	1.09 1	190	210	0.90 5	390	590	0.66 1
9	130	130‡	1.00 0	190	200‡	0.95 0	320	250	1.28 0
11	95	170	0.55 9	160	260	0.61 5	300	470	0.63 8
13	120	170	0.70 6	190	270	0.70 4	340	480	0.70 8
15	190	180	1.05 6	270	300	0.90 0	440	570	0.77 2
Thorney Island 90% Confidence Interval	$0.71 \leq (OBS/PRE)_5 \leq 1.11$			$0.70 \leq (OBS/PRE)_{2.5} \leq 1.02$			$0.64 \leq (OBS/PRE)_1 \leq 0.99$		
Summary 90% Confidence Interval	$0.73 \leq (OBS/PRE)_5 \leq 0.96$			$0.82 \leq (OBS/PRE)_{2.5} \leq 1.03$			$0.95 \leq (OBS/PRE)_1 \leq 1.24$		
Summary 99% Confidence Interval	$0.64 \leq (OBS/PRE)_5 \leq 1.03$			$0.78 \leq (OBS/PRE)_{2.5} \leq 1.09$			$0.88 \leq (OBS/PRE)_1 \leq 1.33$		

*"Observed" distances to the given concentration level are based on a visual best-fit straight line through the maximum reported concentrations for each of the trials.

**DEGADIS-predicted distances to the given concentration level are based on the ground level centerline concentrations.

‡DEGADIS-predicted distance to the given concentration level based on twice the average concentration of the "source" cloud.

1.24. As an example, if for a given release scenario, the predicted distance to the 2-1/2% concentration level was 120 m, the distance to the 2-1/2% concentration level for nine out of ten realizations would be expected to range between 98 m and 124 m.

In all of these simulations, DEGADIS used correlations for gravity spreading and frontal entrainment during the buoyancy-dominated flow regime based on the laboratory data presented in Volume II. For stably stratified shear flow, the mixing data of McQuaid (1976), Kantha et al. (1977), and Lofquist (1960) were used as discussed in Section I. Heat transfer from the substrate to the cloud was based on correlations for heat transfer from a flat plate as developed in Section III.1. Although field data have been used to describe the crosswind passive dispersion parameter σ_y (Pasquill, 1983) and the along-wind passive dispersion parameter σ_x (Beals, 1971), the model applicability is better justified if no adjustment to laboratory correlations is necessary for simulations to be consistent with observed field data. Accordingly, no such adjustments have been made.

IV.8 Effect of Parameter Variation on DEGADIS Simulations

The steady state base case HTAG dispersion scenario described in Table IV.10 was simulated to provide an illustration of the effect of variation of the important scenario definition parameters: type of gas, wind speed, atmospheric stability, surface roughness, ground-to-cloud heat transfer, and atmospheric humidity.

TABLE IV.10

STEADY STATE BASE CASE DISPERSION SCENARIO

Type of Gas: LNG vapor
Source Rate: 127.5 kg/s (0.3 m^3/s liquid)
Atmospheric Stability: D (Pasquill)
Surface Roughness: 10^{-4} m
Ground-to-Cloud Heat Transfer: DEGADIS correlation
Air Temperature/Surface Temperature: 25°C
Atmospheric Humidity: 50%

Table IV.11 shows the effect of variation of the prescribed parameters from the steady state base case on the predicted maximum distance to the 5% gas concentration level. When changing atmospheric stability class and surface roughness, several default parameter values are changed including the Monin-Obukhov length (which affects α and u_*) as well as the along-wind and crosswind passive dispersion parameters. Noting that the friction velocity is a measure of the ambient turbulent kinetic energy and therefore a measure of the ambient energy available to disperse the contaminant, the downwind LFL distance (5% concentration level) is inversely proportional to the friction velocity for the same wind speed for the D stability cases (i.e. when α is the same value). Therefore, in the absence of obstacles, an increase in surface roughness would result in a concomitant decrease in LFL distance. In comparing the methods of estimating the heat transfer, wind speed and ambient humidity both affect the result. At high wind speeds (10 m/s), the LFL distance is relatively insensitive to how the heat transfer is estimated (or if heat transfer is included at all). For high atmospheric absolute humidities, the LFL distance is insensitive to wind speed under these conditions; this behavior is not observed for propane.

The effect of initial volume and wind speed on the maximum downwind distance to the 5% concentration level for instantaneous LNG releases of 10 m^3, 100 m^3, 1,000 m^3, and 10,000 m^3 is shown in Table IV.12 and Figure IV.41. For the release conditions simulated, there is comparatively little difference between the maximum LFL distance for the 1.25 m/s and 2.5 m/s wind speeds for the initial volumes simulated. For the largest initial volume simulated, there is also little difference between the predicted distance to the 5% concentration level for the 2.5 m/s and 5 m/s wind speeds.

TABLE IV.11

EFFECT OF SOME INPUT PARAMETERS ON THE MAXIMUM DOWNWIND DISTANCE TO THE 5% GAS CONCENTRATION LEVEL FOR A STEADY LNG RELEASE

	Wind Speed: 2.5 m/s Distance (m)*	Wind Speed: 5 m/s Distance (m)*	Wind Speed: 10 m/s Distance (m)*
Base Case	860	600	400
Parameters			
Isothermal Gas (ρ_j = 1.79 kg/m^3)	720	430	220
Atmospheric Stability			
Pasquill B	500	370	230
Pasquill F	1380	--	--
Surface Roughness			
10^{-3} m	700	500	320
10^{-5} m	940	700	490
Substrate Heat Transfer			
None	1370	810	470
Using LLNL Correlation	400	430	400
Atmospheric Humidity			
80%	350	380	300
20%	670	620	410

*Release conditions given in Table IV.10.

TABLE IV.12

EFFECT OF WIND SPEED AND VOLUME ON THE PREDICTED MAXIMUM DOWNWIND DISTANCE TO THE 5% GAS CONCENTRATION LEVEL FOR AN INSTANTANEOUS LNG RELEASE ON WATER

Liquid Volume (m^3)	Wind Speed: 1.25 m/s Distance (m)*	Wind Speed: 2.5 m/s Distance (m)*	Wind Speed: 5 m/s Distance (m)*	Wind Speed: 10 m/s Distance (m)*
10	640	550	480	320
100	1330	1350	1120	800
1,000		3100	2830	2220
10,000		7000	6800	5300

*Release Conditions: Pasquill D stability, air temperature of 298°K, 68% relative humidity, sea temperature of 288°K, LNG boiling rate of 0.085 kg/m^2 s.

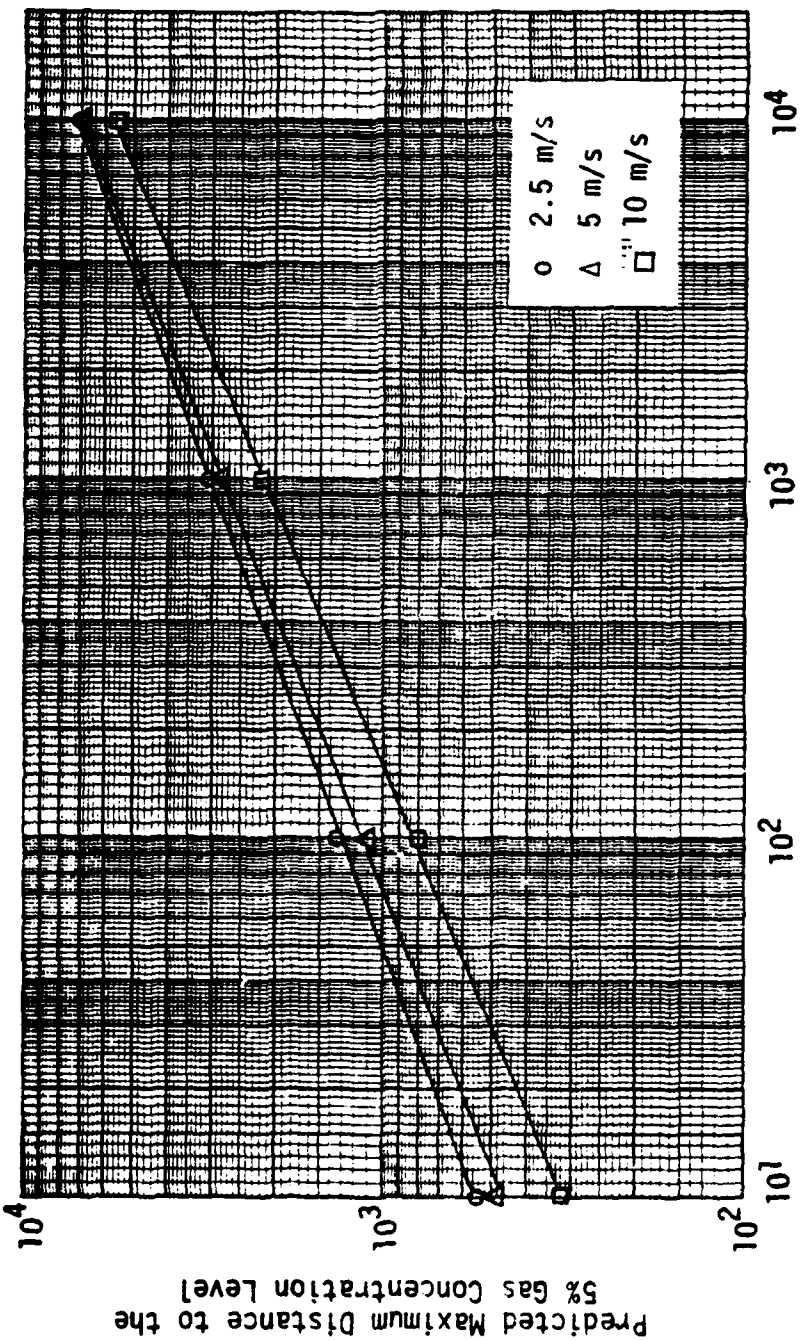

Figure IV.41. Effect of wind speed and volume on the predicted maximum downwind distance to the 5% gas concentration level for an instantaneous LNG release on water.

V. CONCLUSIONS AND RECOMMENDATIONS

Based on review of the phenomenology of heavier-than-air gas (HTAG) dispersion, the following phases are used to describe HTAG dispersion in the atmosphere:

-- Negative buoyancy-dominated dispersion

-- Stably stratified shear flow

-- Passive dispersion due to atmospheric turbulence

Modeling concepts based on investigations of laboratory gravity currents have been used to describe the important HTAG flow and dilution processes that characterize buoyancy-dominated dispersion. Investigation of the gravity spreading and dilution of HTAG volumes released suddenly in calm air demonstrates the applicability of proposed scaling methods; also for these releases, no significant change in measured peak concentration as a function of distance was observed over the tested range of initial height-to-diameter ratio ($0.4 \leq (H/D)_i \leq 1.57$) and initial specific gravity ($2.16 \leq (\rho/\rho_a)_i \leq 4.19$). Scaling of laboratory experimental data from releases of small volumes (35 liters to 530 liters) to similar releases of up to 2000 m^3 in the Thorney Island Trials has been demonstrated.

Laboratory data from stratified shear flow mixing experiments have been used to model the vertical dispersion of HTAG in the atmospheric constant stress layer consistently with the limiting passive dispersion behavior of demonstrated air pollution models.

An interactive computer model for HTAG gas dispersion (DEGADIS), which can simulate a wide variety of HTAG release scenarios, including instantaneous releases, steady releases, and prescribed time-varying releases, has been developed. The model accounts for the three regimes of dispersion described above and for effects due to energy exchange between the dispersing cloud

and the underlying surface. DEGADIS estimates an ensemble-average concentration downwind of a ground level area for flat, homogeneous terrain (i.e. a maximum surface roughness of order 0.01 m).

The DEGADIS model has been used to simulate a wide range of field experimental HTAG releases, including small to intermediate LPG (0.1 to 1 kg/s) and LNG releases (1 - 100 kg/s) on land, large scale releases (10 - 150 kg/s) of LPG and LNG on water, and instantaneous releases of approximately 5000 kg Freon/air mixtures on land. The DEGADIS model predicted downwind gas concentration decay has been shown consistent with data from the field tests considered representing the maximum range of field experimental data currently available. The DEGADIS model-predicted source characteristics have been shown consistent with the continuous water tunnel experiments of Britter (1980a) based on a release Richardson number reflecting the relative importance of the negative buoyancy-driven flow to the ambient shear flow.

Applicability of DEGADIS has been primarily directed to the prediction of concentrations in the lower flammability limit range (~1 to 5%). Even though the relation between the peak and ensemble-averaged gas concentration is uncertain, there is some basis for using 2.0 as an estimate of the peak-to-ensemble-averaged concentration ratio for determining a flammable gas concentration zone; the maximum distance to a flammable gas concentration would then be the distance predicted to one-half the lower flammability limit (LFL/2). Based on comparison with field data, the ratio of observed to calculated distance for the 2-1/2% concentration would be expected to range from 0.78 to 1.09 for 99 out of 100 realizations (i.e. a 99% confidence interval); the 99% confidence interval for this ratio was between 0.64 and 1.03 for the 5% level and between 0.88 and 1.33 for the 1% level. If for a given LNG release scenario, the calculated distance to the 2.5% ensemble-average concentration level was 120 m, the downwind extent of a flammable gas concentration would be expected to range between 94 m and 131 m for 99 out of 100 realizations if the peak-to-ensemble-averaged ratio of 2 is assumed.

The consistency of the model predictions, which reflect small scale laboratory fluid flow and mixing data, with the results of a wide range of field experimental releases, suggests the applicability of the model to prediction of dispersion from much larger releases. The model is recommended on this basis for use in predicting dispersion from very large releases of flammable gas, extending to the largest single container volumes (~25000 m^3) presently in marine use.

The model can readily be modified to incorporate better turbulent mixing and heat transfer sub-models. It is likely that improvements in these two areas, which may result from additional experimental data as well as continuing analysis of the large data base which has become available during this work, can be expected to provide the most important information for improving the confidence level in heavy gas dispersion prediction.

The model has been tested primarily for the prediction of dispersion of heavy gas clouds to concentrations characteristic of the lower flammability limits of hydrocarbon gases, and has not been demonstrated for application to the prediction of dispersion to the ppm concentration range which characterizes the lower limits of toxic gas hazard. However, the model has been developed to be consistent with the existing data base on passive turbulent dispersion in the far field, and it is recommended that the model be evaluated against experimental data which have become available for dispersion of ammonia and nitrogen tetroxide.

REFERENCES

AGA--American Gas Association, "Interim Report on Phase II Work, LNG Safety Program, Project IS-3-1," Battelle Columbus Laboratories, July 1, 1974.

API--American Petroleum Institute--Esso Research and Engineering Report No. EE61E-72, "Spills of LNG on Water--Vaporization and Downwind Drift of Combustible Mixtures," November 24, 1972.

Batchelor, G. K., "Diffusion from Sources in a Turbulent Boundary Layer," Archives Mechaniki Stoswanej, 3, 1964.

Batchelor, G. K., An Introduction to Fluid Dynamics, Cambridge University Press, Cambridge, UK, 1967.

Beals, G. A., "A Guide to Local Dispersion of Air Pollutants," Air Weather Service Technical Report 214, April, 1971.

Benjamin, T. B., "Gravity Currents and Related Phenomena," Journal of Fluid Mechanics, 31, 1968.

Bird, R. B., W. E. Stewart, and E. N. Lightfoot, Transport Phenomena, John Wiley & Sons, Inc. Publishers, New York, 1960.

Blackmore, D. R. et al.,"Refrigerated Gas Safety Research," presented at the AGA Transmission Conference, Atlanta, Georgia, May, 1981.

Blackmore, D. R. et al.,"Dispersion and Combustion Behavior of Gas Clouds Resulting from Large Spillages of LNG and LPG onto the Sea," Transactions, Institute of Marine Engineers, 94, 1982.

Briggs, G. A., "Diffusion Estimates for Small Emissions," ATDL Contribution File No. 79, Atmospheric Turbulence and Diffusion Laboratory (Oak Ridge), 1973.

Britter, R. E., "The Ground Level Extent of a Negatively Buoyant Plume in a Turbulent Boundary Layer," Atmospheric Environment, 14, 1980.

Britter, R. E., unpublished monograph, 1980.

Brown, G. L. and M. R. Rebollo, "A Small, Fast-Response Probe to Measure Composition of a Binary Gas Mixture," AIAA Journal, 10, 1972.

Businger, J. A., J. C. Wyngaard, Y. Izumi, and E. F. Bradley, Flux-Profile Relationships in the Atmospheric Surface Layer," Journal of the Atmospheric Sciences, 28, March, 1971.

Cederwell, R. T. et al., "Burro Series 40-m^3 LNG Spill Experiments," Lawrence Livermore Laboratory Report UCRL-96704, August, 1981.

Chan, S. T., H. C. Rodean, and D. L. Ermak, "Numerical Simulations of Atmospheric Releases of Heavy Gases Over Variable Terrain," Lawrence Livermore National Laboratories Report UCRL-87256, 1982.

Chan, S. T. and D. L. Ermak, "Recent Progress in Modeling the Atmospheric Dispersion of Heavy Gases over Variable Terrain using the Three-Dimensional Conservation Equations," Lawrence Livermore National Laboratories Report UCRL-88495, August, 1983.

Chatwin, P. C., "The Statistical Description of the Dispersion of Heavy Gas Clouds," Report on Contract No. 1189/01.01, Research and Laboratory Services Division, HSE, Sheffield, February 1981.

Colenbrander, G. W., "A Mathematical Model for the Transient Behavior of Dense Vapor Clouds," 3rd International Symposium on Loss Prevention and Safety Promotion in the Process Industries, Basel, Switzerland, 1980.

Colenbrander, G. W., A. E. Evans, and J. S. Puttock, "Spill Tests of LNG and Refrigerated Liquid Propane on the Sea, Maplin Sands, 1980: Dispersion Data Digests," Shell Thornton Research Center, May, 1984 (confidential).

Colenbrander, G. W. and J. S. Puttock, "Maplin Sands Experiments 1980: Interpretation and Modelling of Liquefied Gas Spills onto the Sea," I.U.T.A.M. Symposium on Atmospheric Dispersion of Heavy Gases and Small Particles, Delft, University of Technology, The Netherlands, September, 1983.

Colenbrander, G. W. and J. S. Puttock, "Dense Gas Dispersion Behavior: Experimental Observations and Model Developments," International Symposium on Loss Prevention and Safety Promotion in the Process Industries, Harrogate, England, September, 1983.

Conover, W. J., Practical Nonparametric Statistics, 2nd Ed., John Wiley and Sons, New York, 1980.

Cox, R. A. and R. J. Carpenter, "Further Developments of a Dense Vapor Cloud Model for Hazard Analysis," in S. Hartwig, Heavy Gas and Risk Assessment, D. Reidel, Dordrecht, Holland, 1980.

Eidsvik, K. J., "A Model for Heavy Gas Dispersion in the Atmosphere," Atmospheric Environment, 14, 1980.

Ellison, T. and J. S. Turner, "Turbulent Entrainment in Stratified Flows," Journal of Fluid Mechanics, 6, 1959.

Ermak, D. L. et al., "A Comparison of Dense Gas Dispersion Model Simulations with Burro Series LNG Spill Test Results," Lawrence Livermore National Laboratories Report UCRL 86713, December, 1981.

Fannelop, T., P. A. Krogstadt, and O. Jacobsen, "The Dynamics of Heavy Gas Clouds," Report IFAG B-124, Division of Aero and Gas Dynamics, University of Trondheim, Norway, May, 1980.

Fay, J. A., "Gravitational Spread and Dilution of Heavy Vapor Clouds," 2nd International Symposium on Stratified Flows, Trondheim, Norway, 1980.

Fay, J. A., "Dispersion of Initially Compact Dense Clouds," submitted to Atmospheric Environment, Fall, 1984.

Fay, J. A. and Dale Ranck, "Scale Effects in Liquefied Fuel Vapor Dispersion," Department of Energy Report DOE-EP-0032 UC 11, December, 1981.

Feldbauer, et al., API--Esso Research and Engineering Report No. EE61E-72, "Spills of LNG on Water--Vaporization and Downwind Drift of Combustible Mixtures," November 24, 1972.

Flothmann, D. and H. J. Nikodem, "A Heavy Gas Dispersion Model with Continuous Transition from Gravity Spreading to Tracer Diffusion," in S. Hartwig, Heavy Gas and Risk Assessment, D. Reidel, Dordrecht, Holland, 1980.

Fryer, L. S. and G. D. Kaiser, "DENZ, A Computer Program for the Calculation of the Dispersion of Dense Toxic or Explosive Gases in the Atmospheric," United Kingdom Atomic Energy Authority Report SRD R152, 1979.

General Accounting Office (GAO), "Liquefied Energy Gases Safety," EMD-78-29, July 31, 1978.

Germeles, A. E. and E. M. Drake, "Gravity Spreading and Atmospheric Dispersion of LNG Vapor Clouds," 4th International Symposium on Transport of Hazardous Cargo by Sea and Inland Waterway, Jacksonville, Florida, 1975.

Gifford, F. A., "Use of Routine Meteorological Observations for Estimating Atmospheric Dispersion," Nuclear Safety, 2 (4), 1961.

Gifford, F. A., "Diffusion in the Diabatic Surface Layer," Journal Geophysical Dresearch, 67, 1962.

Gifford, F. A., "An Outline of Theories of Diffusion in the Lower Layers of the Atmosphere," in Meteorology and Atomic Energy--1968. USAEC Report TID-24190 (E. H. Slade, Editor), 1968.

Gifford, F. A., "Turbulent Diffusion Typing Schemes--A Review," Nuclear Safety, 17, 1976.

Goldwire, H. C. et al., "Coyote Series Data Reports, LLNL/NWC 1981 LNG Spill Tests," Lawrence Livermore National Laboratory Report UCID-19953, October, 1983.

Hall, D. J., "Experiments on a Model of an Escape of Heavy Gas," Warren Springs Laboratory, UK, Reports LR 217 (AP), 1976, and LR 312 (AP), 1979.

Hall, D. J. et al., "A Wind Tunnel Model of the Porton Dense Gas Spill Field Trials," LR 394 (AP), Warren Spring Laboratory, Department of Industry, Stevenage, UK, 1982.

Hanna, S. R. et al., Handbook on Atmospheric Diffusion, U.S. DOE/TIC 11223, 1982.

Harris, C., "Analysis of Chlorine Accident Reports," presented at the Chlorine Institute 21st Plant Managers' Seminar, Houston, Texas, February 15, 1978.

Haugen, D. A., "Project Prairie Grass, A Field Program in Diffusion," Geographical Research Paper No. 59, Vol. III, G.R.D.A.F.C., 1959.

Havens, J. A., "Predictability of LNG Vapor Dispersion from Catastrophic Spills onto Water: An Assessment," Department of Transportation--Coast Guard Report CG-M-09-77, April, 1977.

Havens, J. A., "A Description and Assessment of the SIGMET LNG Vapor Dispersion Model," U.S. Coast Guard Report CG-M-3-79, February, 1979.

Havens, J. A., "A Review of Mathematical Models for Prediction of Heavy Gas Atmospheric Dispersion," Institute of Chemical Engineers Symposium Series, No. 71, 1982.

Havens, J. A., "Evaluation of 3-D Hydrodynamic Computer Models for Prediction of LNG Vapor Dispersion in the Atmosphere," Gas Research Institute Contract No. 5083-252-0788 with the University of Arkansas, March, 1983.

Havens, J. A. and T. O. Spicer, "Gravity Spreading and Air Entrainment by Heavy Gases Simultaneously Released in a Calm Atmosphere," Proceedings I.U.T.A.M. Symposium on Atmospheric Dispersion of Heavy Gases and Small Particles, Delft University of Technology, The Netherlands, August 29-September 2, 1983.

HSE--British Health and Safety Executive, Research and Laboratory Services Division, Red Hill, Sheffield, UK--Heavy Gas Dispersion Trials, Thorney Island 1982-83, Data Digests.

Hougen, O. A., K. M. Watson, and R. A. Ragatz, Chemical Process Principles--Part I, 2nd edition, John Wiley and Sons, New York,

Huppert, H. E. and J. E. Simpson, "The Slumping of Gravity Currents," Journal of Fluid Mechanics, 99, 1980.

Kaiser, G. D. and B. C. Walker, "Releases of Anhydrous Ammonia from Pressurized Containers--The Importance of Denser-than-Air Mixtures," Atmospheric Environment, 12, 1978.

Kantha, L. H., O. M. Phillips, and R. S. Azad, "On Turbulent Entrainment at a Stable Density Interface," Journal of Fluid Mechanics, 79, 1977, pp. 753-768.

Koopman, R. P. et al., "Data and Calculations of Dispersion of 5-m^3 LNG Spill Tests," Lawrence Livermore National Laboratories Report UCRL-52876, 1979.

Koopman, R. P. et al., "Description and Analysis of Burro Series 40-m^3 LNG Spill Experiments," Lawrence Livermore National Laboratories Report UCRL-53186, August 14, 1981.

Koopman, R. P. et al., "Burro Series Data Reports, LLNL/NWC 1980 LNG Spill Tests," Lawrence Livermore National Laboratories Report UCID-19075, December, 1982.

Lofquist, Karl, "Flow and Stress Near an Interface Between Stratified Liquids," Physics of Fluids, 3, No. 2, March-April, 1960.

McAdams, W. H., Heat Transmission, McGraw-Hill, New York, 1954.

McQuaid, James, "Some Experiments on the Structure of Stably Stratified Shear Flows," Technical Paper P21, Safety in Mines Research Establishment, Sheffield, UK, 1976.

McQuaid, James, "Large-Scale Experiments on the Dispersion of Heavy Gas Clouds," I.U.T.A.M. Symposium on Atmospheric Dispersion of Heavy Gases and Small Particles, Delft University of Technology, The Netherlands, August 29-September 2, 1983.

Meroney, R. N., "Wind Tunnel Experiments on Dense Gas Dispersion," Journal of Hazardous Materials, 6, 1982.

Meroney, R. N. and A. Lohmeyer, "Gravity Spreading and Dispersion of Dense Gas Clouds Released Suddenly into a Turbulent Boundary Layer," Draft Report CER82-83RNM-AL-7 to Gas Research Institute, Chicago, Illinois, August, 1982.

Monin, A. S., "Smoke Propagation in the Surface Layer of the Atmosphere," in Atmospheric Diffusion and Air Pollution, ed. F. N. Frenkiel, Academic Press, 1959.

Morgan, D. L., L. K. Morris, and D. L. Ermak, "SLAB: A Time-Dependent Computer Model for the Dispersion of Heavy Gases Released in the Atmosphere," Lawrence Livermore National Laboratories Report UCRL-53383, January, 1983.

Morgan, D. L. et al., "Simulations and Parameter Variation Studies of Heavy Gas Dispersion Using the SLAB Model," Lawrence Livermore National Laboratories Report UCRL-88516, August, 1983.

Morgan, D. L. et al., "Phenomenology and Modeling of Heavy Gas Dispersion," Lawrence Livermore National Laboratories Report UCRL 89460, November, 1983.

National Research Council--National Materials Advisory Board (NMAB), "Safety Aspects of Liquefied Natural Gas in the Marine Environment," NMAB Report 354, June, 1980.

Office of Technology Assessment (OTA), "Transportation of Liquefied Natural Gases," U.S. Government Printing Office, Washington, D.C., 1977.

Pasquill, F., "The Estimation of the Dispersion of Windborne Material," Meteorological Magazine, 90, 1961.

Pasquill, F., Atmospheric Diffusion, 2nd edition, Halstead Press, New York, 1974.

Pasquill, F., Chapter 1 in Lectures on Air Pollution and Environmental Impact Analyses, American Meteorological Society, Boston, Massachusetts, 1975.

Pasquill, F., Atmospheric Diffusion, 3rd edition, Halstead Press, New York, 1983.

Picknett, R. G., "Field Experiments on the Behavior of Dense Clouds," Chemical Defence Establishment Report PTN, IL 1154/78/1, Porton Down, UK, September, 1978.

Picknett, R. G., "Dispersion of Dense Gas Puffs Released in the Atmosphere at Ground Level," Atmospheric Environment, 15, 1981.

Puttock, J. S. et al., "Maplin Sands 1980: Dispersion Results from Continuous Releases of Refrigerated Liquid Propane," Symposium on Heavy Gas and Risk Analysis, Battelle Institute, Frankfurt, Germany, May, 1982.

Puttock, J. S. et al., "Maplin Sands Experiments 1980: Dispersion Results from Continuous Releases of Refrigerated Liquid Propane and LNG," NATO/CCMS 13th International Technical Meeting on Air Pollution Modeling, Cannes, France, September, 1982.

Puttock, J. S. et al., "Field Experiments on Dense Gas Dispersion," Journal of Hazardous Materials, 6, 1982.

Rosenzweig, J. J., "A Theoretical Model for the Dispersion of Negatively Buoyant Vapor Clouds," Ph.D. Dissertation, M.I.T., 1980.

Schmidt, W., "Zur Mechanik Der Boen," Meteorologisches Zeitschrift, August, 1911.

Simpson, J. E., "Gravity Currents in the Laboratory, Atmosphere, and Ocean," Annual Review of Fluid Mechanics, 14, 1982.

Simpson, J. E. and R. E. Britter, "The Dynamics of the Head of a Gravity Current Advancing over a Horizontal Surface," Journal of Fluid Mechanics, 94, Part 3, 1979.

Smith, M. E., "Atmospheric Dispersion at Brookhaven Laboratories," Air and Water Pollution International Journal, 10, 1966.

Smith, M. E., "Recommended Guide for the Prediction of the Dispersion of Airborne Effluents," 1st Edition, American Society of Mechanical Engineers, New York, 1968.

Spicer, T. O. and J. A. Havens, "Modeling the Phase I Thorney Island Experiments," Symposium on the Thorney Island Heavy Gas Trials, sponsored by the British Health and Safety Executive, Sheffield, UK, April, 1984.

Taylor, R. J., J. Warner, and N. E. Bacon, "Scale Lengths in Atmospheric Turbulence as Measured from an Aircraft," Quarterly Journal Royal Meteorological Society, 96, 1970.

te Reile, P. H. M., "Atmospheric Dispersion of Heavy Gases Emitted at or near Ground Level," Second International Symposium on Loss Prevention and Safety Promotion in the Process Industries, Heidelberg, Germany, 1977.

Treybal, R. E., Mass Transfer Operations, 3rd edition, McGraw-Hill, New York, 1980.

Turner, J. S., Buoyancy Effects in Fluids, Cambridge University Press, Cambridge, UK, 1973.

van Ulden, A. P., "On the Spreading of a Heavy Gas Released Near the Ground," 1st International Loss Symposium, The Hague, Netherlands, 1974.

van Ulden, A. P., "The Unsteady Gravity Spread of a Dense Cloud in a Calm Environment," 10th International Technical Meeting on Air Pollution Modeling and its Applications," NATO-CCMS, Rome, Italy, October, 1979.

van Ulden, A. P., "A New Bulk Model for Dense Gas Dispersion: Two-Dimensional Spread in Still Air," I.U.T.A.M. Symposium on Atmospheric Dispersion of Heavy Gases and Small Particles, Delft University of Technology, The Netherlands, August 29-September 2, 1983.

Webber, D. M., "The Physics of Heavy Gas Cloud Dispersal," United Kingdom Atomic Energy Authority Report SRD R243, March, 1983.

Welker, J. R., "Vaporization, Dispersion, and Radiant Fluxes from LPG Spills," U.S. Department of Energy Report DOE/EV/07020-1, May, 1982.

Wilson, D. J. and D. D. J. Netterville, "A Fast Response Heated Element Concentration Detector for Wind Tunnel Applications," Journal of Industrial Aeronautics, 1981.

Zeman, O., "The Thermodynamics and Modeling of Heavier-than-Air, Cold Gas Releases," Lawrence Livermore National Laboratories Report UCRL-15224 S/C 4424509, April 17, 1980.

Zeman, O. and H. Tennekes, "Parameterization of the Turbulent Energy Budget at the Top of the Daytime Atmospheric Boundary Layer," Journal of the Atmospheric Sciences, January, 1977.

APPENDIX A

CLOUD ENTHALPY AND DENSITY CALCULATIONS

The estimation of cloud density is an important part of the DEGADIS model, especially for releases of a cryogenic gas with molecular weight lower than that of air. With regard to the density/enthalpy calculations, DEGADIS can be run in one of three modes.

If no heat transfer is to be included in the calculations, the density can be specified as a function of concentration in two different ways. When either the release is isothermal (Thorney Island Trials) or the user needs to take into account some chemical reaction (nitrogen tetroxide) or phase change (ammonia) of the contaminant, the density as a function of concentration is input as a list of data triplets consisting of mole fraction, concentration (kg/m^3), and mixture density (kg/m^3). Linear interpolation is used between points.

For cryogenic gas simulations without heat transfer, the enthalpy and density relationships are determined by adiabatic mixing. For ideal solutions of ideal gases with the same constant molal heat capacity, adiabatic mixing gives

$$\left[\frac{\rho - \rho_a}{c_c}\right] = \gamma = \text{constant} \qquad \text{(A-1)}$$

where ρ is the mixture density and c_c is the concentration of contaminant. Since any possible condensation of ambient humidity is not included in Equation (A-1), a more general procedure is used. For ideal solutions of mixtures of contaminant/air/water, the mixture enthalpy h(T) can be expressed by

$$h(T) = w_c C_{p_c}(T)(T - T_R) + w_A (1 + \text{Hum}(T)) C_{p_a}(T - T_R) + (w_w - w_A \text{Hum}(T)) [C_{p_w}(T - T_R) - \lambda'] \qquad \text{(A-2)}$$

where w_c, w_A, and w_w are the mass fractions of contaminant, air, and water, respectively. The heat capacities of air and water are assumed constant at 1006 and 1865 J/kg°K, respectively, while the heat capacity of contaminant is described (after Hougen et al., 1967) by a mean molal heat capacity given by

$$C_{p_c}(T) = MW_c\, C_{p_{c,m}}(T) = MW_c \left[3.33 \times 10^4 + q_1 \left(\frac{T^{p_1} - T_0^{p_1}}{T - T_0} \right) \right] \tag{A-3}$$

where T_0 is the contaminant storage temperature (K) and values of q_1 and p_1 are given in Table A-1 for the range 90 K $\leq T \leq$ 360 K. Note that a constant mean molal heat capacity can be used by setting $p_1 = 1$ and q_1 to the necessary value. The latent heat given in Equation (A-2) is modeled as a ramp function around the freezing point of water by

$$\begin{aligned} \lambda' &= \lambda_{vap} && \text{for } T \quad 273.15 \text{ K} \\ &= \lambda_{vap} + \lambda_{fus}\left(\frac{T - 263.15}{10}\right) && \text{for } 263.15 \leq T \leq 273.15 \\ &= \lambda_{vap} + \lambda_{fus} && \text{for } T < 263.15 \end{aligned} \tag{A-4}$$

In order to determine the absolute humidity to be used in Equation (A-2), the saturation conditions are first determined. The saturation vapor pressure of water p_w^* is estimated with

$$p_w^* = 6.0298 \times 10^{-3} \exp\left[5407 \left(\frac{1}{273.15} - \frac{1}{T} \right) \right] \tag{A-5}$$

where p_w^* is in atmospheres. The saturation conditions are then given by

$$H_{sat} = \frac{0.622\, p_w^*}{(p - p_w^*)} \tag{A-6}$$

where p is the total pressure. The absolute humidity in Equation (A-2) is the minimum of the saturated humidity and the ambient humidity, i.e. Hum = min (H_{sat}, H_a). Finally, the reference temperature is chosen as the ambient air temperature.

The sum of the pure component enthalpies in a particular mixture then determines the enthalpy of the mixture under the assumption of adiabatic mixing. Due to the choice of reference temperature, the enthalpy associated with any entrained air is zero. A trial and error procedure calculates the mixing temperature from its enthalpy.

For cryogenic gas simulations with heat transfer, the amount of heat added to the mixture (D_h) is calculated by the model. This determines the enthalpy of a given mixture by

$$h(T) = h_{AM} + D_h \tag{A-7}$$

where h_{AM} is the adiabatic mixing enthalpy of a given mixture. A similar trial and error procedure then determines the mixture temperature T from the new value of enthalpy.

With the mixture temperature known, the density of the mixture is calculated assuming Amagat's law of additive volumes for the vapor phase given by

$$\rho = [\bar{V}_a + \bar{V}_{w,vapor} + \bar{V}_c]^{-1} \tag{A-8}$$

where $\bar{V}_a + \bar{V}_{w,vapor}$ is the volume of air and water in the vapor phase given by

$$\bar{V}_a + \bar{V}_{w,vapor} = w_a(0.00283 + 0.00456\ \text{Hum})\ T/p \tag{A-9}$$

The volume of contaminant in the vapor phase is

$$\bar{V}_c = w_c \left(\frac{T}{\rho_0 T_0}\right) \tag{A-10}$$

where ρ_0 is the density of the saturated vapor at the storage temperature T_0 and ambient pressure p.

TABLE A-1

VALUES FOR MEAN MOLAL HEAT CAPACITY CONSTANTS

Species	p_1	q_1
methane	5.00	5.6×10^{-8}
ethane	2.79	0.266
propane	2.25	15.4

END

10-86

DTIC